Dissertation

Bastian Eder

14. Feb. 2017

A D A M Absolute Distance Accurately Measured

E V A External Vehicle Adjustment

Physik-Department

Technische Universität München

Technische Universität München

Physik-Department

Lehrstuhl für Laser- und Röntgenphysik E11

ADAM & EVA

Absolute Distance Accurately Measured
&
External Vehicle Adjustment

Bastian Eder

Vollständiger Abdruck der von der Fakultät für Physik der Technischen Universität München zur Erlangung des akademischen Grades eines

Doktors der Naturwissenschaften

genehmigten Dissertation.

Vorsitzende(r) : Prof. Dr. Michael Knap

Prüfer der Dissertation : 1. Prof. Dr. Reinhard Kienberger

2. Prof. Dr. Peter Fierlinger

Die Dissertation wurde am 28.02.2017 bei der Technischen Universität München eingereicht und durch die Fakultät für Physik am 23.05.2017 angenommen.

Wenn ma an Frosch fragt, "wia schaut'n der Himmel aus?".
Der sitzt ja in seim Brunnenschacht drin, und da is stockfinster.
Aber oben an der Abdeckung kommt, durch an bissl an Spalt, a Licht rei.
Und des is für'n Frosch der Himmel.

Wenn ma jetzt an Vogel fragt, "wia schaut'n der Himmel aus?",
sagt der Vogel, "ja, unendlich weit, bis zum Horizont. Und wenn ma dahin fliegt, geht's nummoi weiter".

Und beide ham's Recht, obwohl's so unterschiedlich klingt.

Deswegn möcht i a Frosch sei, der an Vogl hat!

Fredl Fesl

Contents

1 Introduction and Motivation

Time is a fundamental unit in Physics. To understand time, humanity has developed clocks in order to see it (watch), to hear it ('tick tock') and to feel it (stress).
Reciprocal connected to time is frequency. The definition of time is a purely human construct and has received multiple steps of development. In the very beginning there was the simple looking up to the sun and the stars, then sun clocks, water clocks, pendulums and quartz clocks to finally the current stage of time and frequency definition: the atomic clock.

Now, at the edge of a new time standard, in all parts of the world scientists make huge efforts in this development.
Until now (year 2017) the definition of the second is as follows.

> *The second is the duration of 9 192 631 770 periods of the radiation corresponding to the transition between the two hyperfine levels of the ground state of the caesium 133 atom.* [1]

This definition is valid since the year 1967. Current ^{133}Cs clocks have stabilities in the area of $\sigma_y(\tau) \approx 10^{-13}\tau^{-1/2}$ and an uncertainty at the 10^{-16} level [2].
The next definition of a second may be:

> *The second is the duration of 642 121 496 772 646.22 periods of the radiation corresponding to the octupole transition* $^1S_{1/2}$ *and* $^1F_{7/2}$ *of the single ionized Ytterbium 171 isotope* [3]

But further development of time/frequency is directly connected with the transport of this information from one spot to another. The best clock is useless, if its information is hidden within.
Without the help of our standard electronic equipment, e.g. Global Navigation Satellite System (GNSS) synchronized smartphones, the transport is actually very difficult in our daily life.

A simple example is the 100 m run in school. One person with the starting pistol gives the commando to start the race. Another person at the finishing line waits for the signal to start measuring the time until the sprinters arrive. If the acoustic signal is taken, a time delay of about 0,3 s is included due to the velocity of sound in the air. Nevertheless humans react within a few milliseconds on sound information.
If the information is transported optically (seeing the explosion at the top of the pistol) it reaches the measuring person with the speed of light propagating through the air (in no-time compared to acoustic signals). But the reaction of human eye on light has also a delay of about 40 ms.
With this precision of time distribution over 100 m, some athletic championships would score even. Also a global synchronization of the results would be most complicated. Fortunately the distribution of time nowadays ensure that even time measurements for Formula One races can be done without highest complexity.

As the example shows, time transport is connected to the distance. The information should be transported from a spot A to a spot B without loss of information, no matter how far away the spots are. To ensure that every spot has the same time 't_0' at the same moment, includes the

information of how large the distance of the time distribution is. The better the performance of a clock, the better must be the performance of distance resolution to guarantee the transportation of 't_0'.

Other examples which require highest complexity of time distribution would be:
- High frequency trading in the stock exchange
- Detection of new particles at Large Hadron Collider
- High precision of localization determination using GNSS

Within this thesis a new approach is shown for time and frequency synchronization between to locations in space relevant distances (10^4km). This time and frequency synchronization is possible in static as well as in dynamic systems. The new method covers even newest/future time standards, which enables a long duration of application. Its simplicity and compactness in function results in a most handy system. Applications on ground or space can equally profit from the new system.

In Section 2 the theory is presented in order to give an overview over every important aspect of time and frequency synchronization. The new approach is explained in detail and applications are shown.
The definition of the measurement systems and setup is presented in Section 3 in order to explain how the theory is proven.
The measurements are shown in Section 4 with the proof of concept and compares it to an already existing system, which promises high performances.
In Section 5 there is given a summary of the executed work.
Finally there will be given an outlook in Section 6 on the possibilities of further developments.

2 Theory

In this section the theory of all necessary topics is given. Some sections are mentioned to give a rough overview since most of the theories are published already in more detail. The purpose is that the reader is capable of understand the context between different systems and their application. Also interfaces and their requirements result from the connection between the different theories. References help the reader if more detail in some topics is requested. However the theory of the new approach is (as to the knowledge of the writer) described the first time within this thesis. The description of the new theory is limited to the content which is necessary for the setups and measurements within this thesis. It is expected, that further development of the new approach increases the theoretical input and creates more possibilities and applications.

A description of frequency and time is given in Section 2.1 which implies characterization and meaning of time and frequency transfer.
An overview of current and future time standards can be seen in Section 2.2.
Optical Frequency Comb as an essential part for future time distribution and its interaction with future time standards is explained in Section 2.3.
Precise distance measurement and/or time and frequency distribution are applicable for multiple scenarios. Within this thesis three space scenarios are considered. The requirements of distance resolution and time and frequency transfer result from these mission scenarios. These topics are summarized in Section 2.4.
Afterwards follows the Frequency Domain Distance Measurement (FDDM) method in Section 2.5.
For time and frequency synchronization two Cross Correlations are shown in Section 2.6. This section includes the new approach FDDM Cross Correlation (FDDM CC) and the system to compare it, the Balanced Optical Cross Correlation (BOCC).

2.1 Frequency & Time

A clock is defined by two essential characteristics: Stability and Accuracy [4].
Each clock creates a frequency which should be constant over long time.
This 'frequency' can be generated by a sun clock (period over one day), a water clock (period of one drop of water followed by the next drop) or the current technologies of atomic clocks (transmission between two hyper fine levels of an atom).
No matter which oscillator is used, the constance of the period defines the stability and the accuracy of each clock type.
A visualization of the difference between stability and accuracy is shown in Figure 1

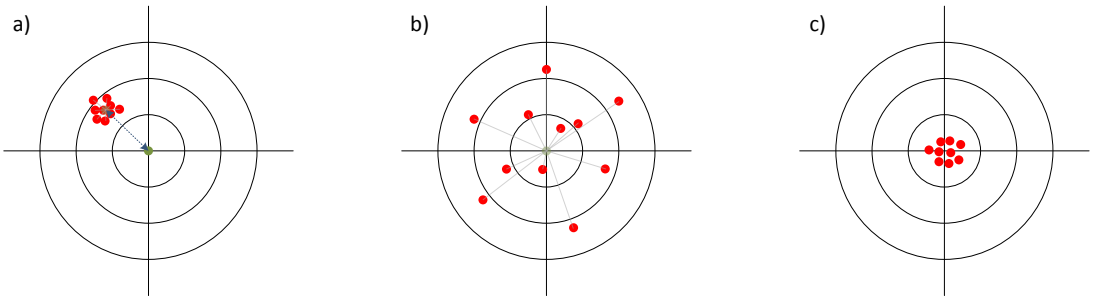

Figure 1: Visualization of stability and accuracy

The system in Figure 1 a) has a good stability, but a bad accuracy. All shots are about in the same region, but the focal point of the shots is not the required centre.
The system in Figure 1 b) has a good accuracy, but a bad stability. The focal point of all shots is at the required centre, but they are spread around within a large divergence. It takes longer time to calculate the focal point.
The system in Figure 1 c) has a good stability and a good accuracy. The shots are about in the required centre and it takes short time to create the focal point in the right area.

Stability is a factor which implies how accurate an oscillator can be dependent on the integrated time.
The accuracy is a limit of the stability. At a specific integrated time the accuracy (time resolution) is reached. Further time integration results in the same accuracy.

The characteristic of the stability is expressed by the Allan Deviation [4]. The squared Allan Deviation is the Allan Variation.
Target of typical clocks is to create a perfect frequency with lowest Allan Deviation and highest accuracy. Therms like thermal noise, mechanical imperfection, voltage jitter or statistical limitation are responsible for their imperfection.

Clocks generally consist of a resonator/cavity and a norm.
The cavity is responsible for the frequency generation. The norm is a control unit that the created frequency can always be compared with.
Cavities are different from one clock to another. Therefore they create different frequencies. The norm is equal to each clock.
Water clocks use defined water pots with defined water flow as a cavity. The norm is the position of the sun to earth.
The lengths of a pendulum is its cavity. Again, the position of the sun is the norm.
New time standards use a gas cylinder as cavity and a hyperfine transition of an atom as a norm.

It is indispensable for further development that they result in higher frequencies. The higher the created frequency the better the statistic to measure time, e.g. one second. But faster frequencies also require norms with adequate frequency response. Control of faster frequencies implies more

technological development.

For absolute and highly precise distance measurements the frequency of an oscillator must be known precisely. The better the frequency can be measured or stabilized, the better the functionality of the complete system. A characterization of frequency is shown in this section.

The frequency stability of each oscillator is defined by its own phase noise characteristic. This characteristic defines the precision of each oscillator thus the preciseness to generate a constant oscillation. The phase noise $S_\Phi(f)$ [5] depending on frequency is characteristic for each oscillator. The higher the phase noise, the less stable is an oscillator. Unstable oscillator change their frequency which results in a less precise measurement of time and therefore all units which are connected to time (e.g. distance measurements).

The frequency can be illustrated as a circulation in the complex area with a defined frequency $\phi = i\omega t = i2\pi f_0 t$. The imperfection ('jitter') of the circulation is the phase noise of the oscillator. The phase noise can be expressed by power spectral density $S_\Phi(f)$ or in spectral density in frequency fluctuations $S_y(f)$ [6]. Both are equally measured by spectrum analysis. The difference is the main frequency: Whereas S_Φ is defined for the whole frequency area, S_y has its focus on the oscillator frequency f_0.

An illustration of frequency instability is shown in Figure 2.

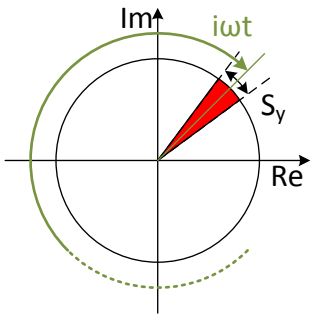

$$S_y(f) = \left(\frac{f}{f_0}\right)^2 S_\Phi(f)$$

$$S_y = \int_{f_{min}}^{f_{max}} df\, S_y(f)$$

Figure 2: Integrated phase noise results in frequency instability

Figure 2 shows also the relation between S_y and S_Φ. The centre frequency f_0 creates a constant oscillation in the complex area. The phase noise is the jitter around the current complex vector.

Phase noise S_y is measured using spectrum analysers. Within these devices two frequencies are shifted against each other. Fourier transformation of the interference signal results in the power density and therefore in the phase noise.
The phase noise correlates with the Allan Variance directly with [6]

$$\sigma_y^2 = S_y = \int_{f_{min}}^{f_{max}} df\, S_y(f) \tag{1}$$

Therefore an oscillator can be characterized within different frequency/time areas. The integration area can be defined as what suits best to the current measurement. Within this thesis the integration area is defined by 1 second. This means that all stability values (Allan Deviation) are calculated to the measurement time of 1 s.

The phase noise measurement of 1 s is defined by the integration within the frequency area $f_{int} = [1\,\text{Hz}, f_0/2]$. Measurements with a spectrum analyser result in a spectral density of the phase noise, which can be characterized. Different frequency areas result in different frequency dependencies as illustrated in Figure 3.

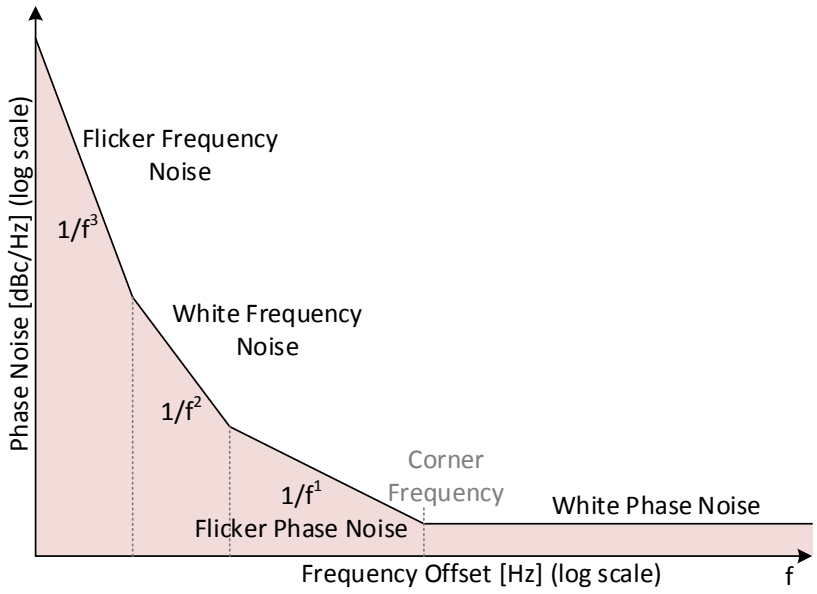

Figure 3: Phase noise characteristic of an oscillator [7]

The higher the frequency offset of the centre frequency the lower the frequency/phase noise. Different phase noises are defined by order of attenuation dependent on offset frequency:
Flicker Frequency Noise, White Frequency Noise, Flicker Phase Noise and White Phase Noise.
A 'simple' integration over the measured phase noise spectrum yields to the phase noise of an oscillator. The Random walk is not illustrated in this diagram, but would be found in lower frequencies than Flicker Frequency Noise. Using a Phase Lock Loop (PLL), locking an oscillator to another oscillator, the phase noise can be lowered (in case that the reference oscillator has a better stability). The limit for stabilization is the Corner Frequency. Any PLL has a frequency range within the oscillator can be locked. If the range of the PLL is higher than the Corner Frequency

there is no improvement of the phase noise.
Generally the higher the modulation frequency f_{mod} of a PLL, the higher the noise of the PLL itself.

Low noise oscillators have (compared to not-low noise oscillators) a lower Corner Frequency and a lower White Phase Noise. Since low phase noise is correlated to low frequency variability, most of the time a compromise must be found between flexibility and performance.

The time stability of an oscillator is different to its frequency stability but they are related to each other. The time stability can be expressed by the Allan Deviation/Variation which is connected to the phase noise of an oscillator. Therefore the time/frequency integration area is the difference between the two expressions.

Time stability is used to measure a random walk of an oscillator (which is not illustrated in Figure 3). The random walk is also a characteristic of an oscillator. If the oscillator is not stabilized to a norm, the frequency of the oscillator would drift to a not-known (random) frequency.

For time characterization of larger time scales (days, months) usage of phase noise is not preferable, because it causes a huge measurement effort and much data. Each measurement of phase noise includes the whole spectrum of the integrated frequency area. This spectrum is important for oscillator or PLL characterization and for their improvements, but is constant over long time.

However frequency measurements imply a complete integrated phase measurement. The resulting frequency output includes its uncertainty indicated by frequency fluctuation between one measurement and the other. A frequency counter with a defined gate time τ_0 is the result of the integration of the phase noise. The calculation of a time stability dependent on a time slot is illustrated in Figure 4.

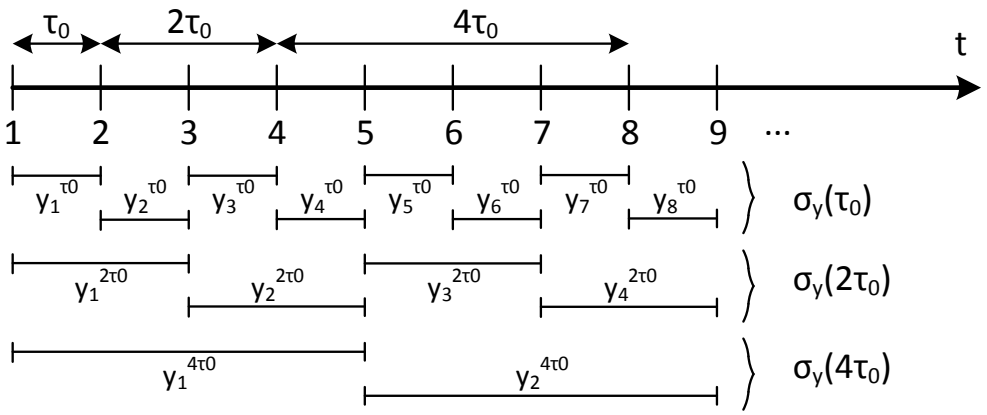

Figure 4: Time stability with different integration time [4]

The time slot τ_0 (defined by gate time of the frequency counter) defines the integration of the

phase noise of the oscillator. Within this gate time, the oscillations are averaged and calculated to a mean value $y_k^{x\cdot\tau}$. The larger the time slot the less the frequency jitter. The Allan Deviation can be calculated as [4]

$$\sigma_y^2(x\cdot\tau) = \frac{1}{2\cdot p}\sum_{k=1}^{p}[y_k^{x\cdot\tau} - y_{k+1}^{x\cdot\tau}] \quad \text{with} \quad p = \text{int}\left(\frac{t_{meas}}{x\cdot\tau}\right) - 1 \tag{2}$$

with t_{meas} as the absolute measurement time. The Allan Deviation compares two neighboured averaged values and results in a difference between the two values. The deviation between the values results in the stability of the system. With higher measurement time the Allan Deviation lowers until the random walk of a system is reached.

Within this thesis frequencies are synchronized / stabilized in different ways. Different types of oscillators are used with different phase noise characteristics, but the principle of stabilization stays constant. The main focus of this thesis is the transport of frequency and time which also implies additional instability. The target is to create a connection between two spots that adds as less instability to the oscillators performance as possible.

2.2 (Optical) Atomic Clocks

Clocks with highest performances are a combination between microwave frequency or optical light interfering with hyperfine structures of electrons of atoms or the nucleus of the atom itself. But the overall functionality of any atomic clock is similar if in the microwave or in the optical area.

An oscillator (described in the prior section) is defined by ultra low phase noise for high frequency stability. The random walk must be controlled, that the second continuously stays constant. As mentioned before, the oscillator would drift to a random frequency. Therefore a norm (mostly a hyperfine level of an electron transition) is used to stabilize the randomly running frequency. Under same environmental conditions the electron transition of the norm is not changing. Characteristic for a norm is that the bandwidth Δf of the transition is as narrow as possible compared to the transition frequency f_0. E.g. the $^2S_{1/2} - {}^2F_{7/2}$ (octupole) transition of an $^{171}Yb^+$Ion has a theoretical linewidth of $\Delta f < 1$ nHz at a transition frequency of $f_0 \approx 6.42 \cdot 10^{14}$Hz [8].

The norms changed during the last years. Starting from a Caesium atom for microwave standards, the development for microwave standards continued to current Rubidium or Hydrogen clocks.
In the early 1980s the first Optical Atomic Clocks (OAC) started with Hydrogen or Iodine. Also development changed the used atom norms to Strontium, Ytterbium, Aluminium or Mercury. An excerpt of the development of time standards is shown in Figure 5.

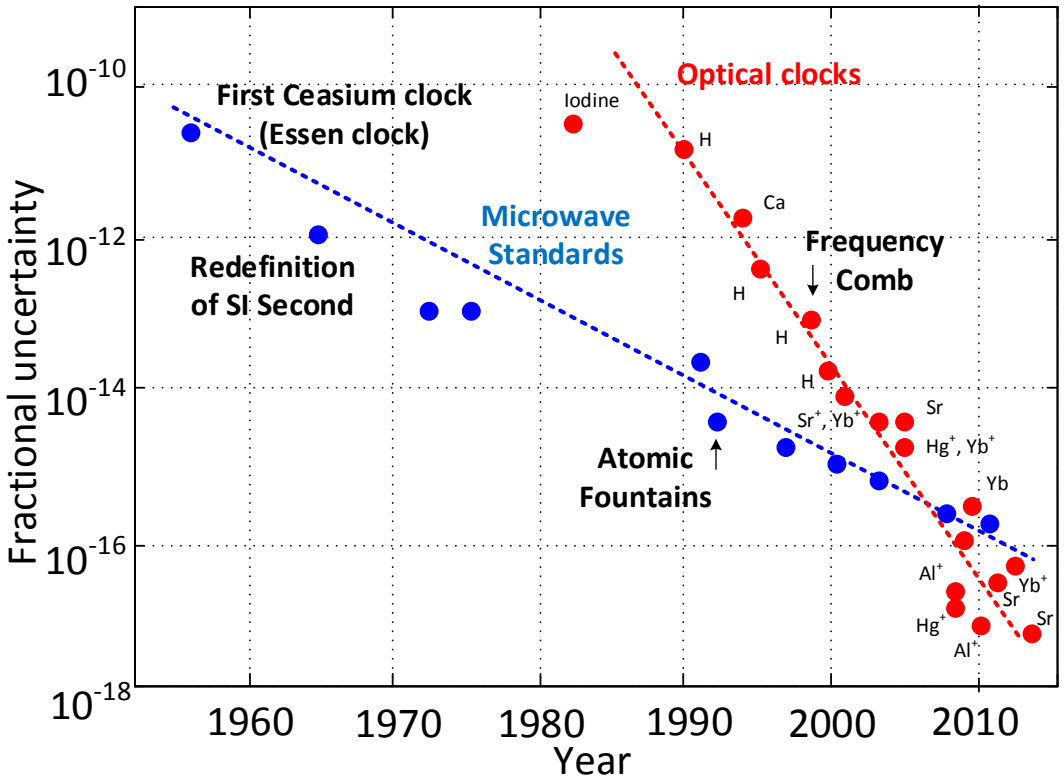

Figure 5: Development of clock accuracy [9]

The development of both clock types (microwave clocks and optical clocks) shows remarkable performance gains during the last 50 years and continues. Nevertheless as illustrated in Figure 5 the performance gain with optical standards overtook the microwave standards in less development time. But this contains only the performances of time standards.
Their development stages are quite different, since Microwave/High Frequency (HF) Standards are already available for space applications (e.g. Galileo) and for commercial purpose whereas optical standards are still in research stage.

The difference between HF and optical standards is the frequency of the electron transition. HF Standards are in the 10^9Hz area whereas optical clocks use frequencies about 10^{14}Hz (optical area). In Table 1 three HF Standards are listed.

Table 1: Examples of current HF standards and their performances

type	transition frequency	stability	accuracy
^{133}Caesium [10]	9 192 631 770 Hz	$2.0 \cdot 10^{-13}$	$2 \cdot 10^{-16}$
^{87}Rubidium [11]	6 834 682 611 Hz	$1.7 \cdot 10^{-13}$	$5 \cdot 10^{-15}$
^{1}Hydrogen [12]	1 420 405 752 Hz	$5.0 \cdot 10^{-14}$	$3 \cdot 10^{-16}$

The frequencies are manageable with HF electronics and are technologically advanced compared to optical clocks. The accuracy/uncertainty show the limit of the clock performances. Even with larger integration time (run time), this is the lowest achievable stability of a clock. As mentioned before the transition has same frequency transition at same environmental conditions. Dependent on technology limits like changing black body radiation (temperature) or particle collision, the transition is broadened or shifted in long term and creates a long time frequency drift. This drift occurs in all time standards.

The technological requirements of OACs exceed the requirements of HF Standards because their amount of laser systems is higher and their requirement on laser stability. Starting with the handling of the cooling system (exists also in HF Standards) which requires multiple laser systems, since Black Body Radiation or collisions within optical clocks have larger impacts on the instability (of function) of the clock. Unwanted decays in other energy levels occur statistically which implies system failure if not handled. Therefore additional repumper laser systems must be added to bring the electron back to its ground level. And finally the highly stable clock laser which serves as the new frequency standard must be locked on a highly stable cavity and must be controlled with the control atom(s).

For a better understanding Appendix A gives a general overview of complexity and performances of two basic types of OACs: Lattice Clocks and (Single) Ion Clocks. Also further references are given if more information is required.

Within Table 2 three different Lattice Clocks are summarized with their expected performances.

Table 2: Examples of different lattice clocks and their performances

Type	Transition Wavelength	Stability	Accuracy
^{199}Mercury	363 nm	$1.8 \cdot 10^{-16}$	$7 \cdot 10^{-18}$ [13]
^{87}Strontium	813 nm	$3.4 \cdot 10^{-15}$	$2 \cdot 10^{-18}$ [14]
^{171}Ytterbium	759 nm	$2.2 \cdot 10^{-15}$	$3 \cdot 10^{-18}$ [14]

Table 3 shows some examples of Single Ion Clocks.

Table 3: Examples of different ion clocks and their performances

Type	Transition Wavelength	Stability	Accuracy
^{199}Mercury^{+}	282 nm	$1.0 \cdot 10^{-16}$	$5 \cdot 10^{-18}$ [15]
^{88}Strontium^{+}	674 nm	$5.6 \cdot 10^{-16}$	$2 \cdot 10^{-17}$ [15]
^{172}Ytterbium^{+}	467 nm	$1.1 \cdot 10^{-16}$	$3 \cdot 10^{-18}$ [16]

As can be seen by the two tables, the performances of each OAC type exceeds the performance of a HF-Standard by two orders of magnitude. It must be mentioned, that these values are mostly theoretical since long time function ($>$ 1month) is not yet implemented. The development of OACs is in the laboratory phase and needs more time until it can be used for commercial applications. Nevertheless it is expected that future time standards are OACs dependent on their performance

gains. Especially Single Ion Clocks are in advantage for first space applications since their complexity is lower compared to Lattice Clocks. For now the only advantage of HF Standards is their technological status.

2.3 Frequency Combs for Time and Frequency Synchronization

The systems in this thesis for precise distance detection use short pulse lasers. Pulse lasers are sufficient if HF-Standards (H-Maser, Rb-Standards) should be synchronized. Their repetition rate is locked directly on the output frequency of the standard. However the measurement/synchronization of OACs require additional stabilization of the pulse laser.

This section is a rough overview of Optical Frequency Combs (OFC) and their application for future OACs including their interaction.

An OFC is an updated short pulse laser. Short pulses are generated within a mode locked oscillator. A mode locked oscillator contains multiple harmonics created by a cavity. To create a mode lock, multiple stabilization functions are available like active optical components (active mode locking [17]) or passive mode locking (e.g. SESAM or CNT [18] [19]).

Any technology is applicable for measurements done within this thesis. The requirement is the shortness of the pulses. Nevertheless concerning space applications the focus lies on compactness, robustness and long time function. Optical fibre technology fulfils all requirements and has performances which are necessary for any applications.

Anyhow the output of a short pulse laser are equidistant short pulses. The time between the pulses (repetition rate) is defined by the oscillators length and can be very different, dependent on the purpose of the pulse laser. The shortness of the pulses corresponds to the mode locking of the laser. Within this thesis 'short' means pulses with durations below 1 ps at repetition rates in the HF area (100 MHz).

That short pulses create a 'comb' in the frequency area due to Fourier Transformation is part of Section 2.5. They create multiple harmonics of the repetition rate in the frequency area:
The shorter the pulses, the broader the spectrum (see Equation 7, envelope term).

Additionally to the repetition rate, the Carrier Envelope Offset Frequency (CEO) occur.
The origin of the CEO and its handling is described in Appendix B. If more detail is required further references are mentioned.

Together (repetition rate and CEO) the output spectrum of an OFC in the frequency area is as shown in Figure 6.

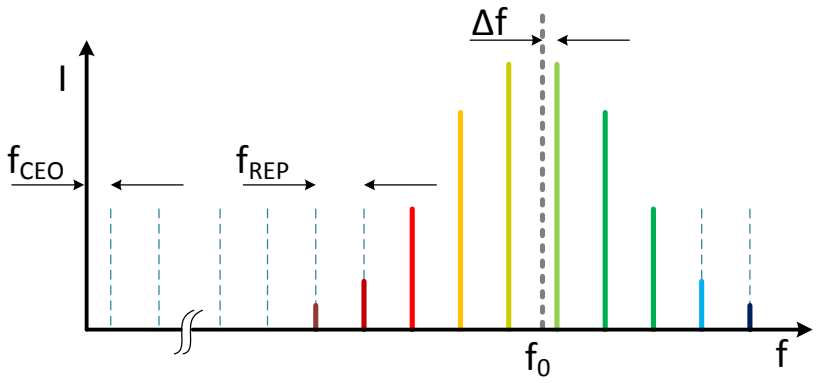

Figure 6: Illustration of an Optical Frequency Comb [20]

The optical spectrum contains multiple 'comb' lines with distances defined by the repetition rate and the CEO. The difference between a short pulse laser and an OFC is the stabilization of the CEO. When the CEO is stabilized a random optical frequency f_0 (10^{14}Hz), overlapped with the output spectrum of the OFC, can be defined by

$$f_0 = n \cdot f_{REP} + f_{CEO} + \Delta f$$

with Δf as the overlap frequency between neighboured comb tooth and laser which should be measured. Since f_0 is in the 10^{14}Hz area (optical area) and the repetition rate at $f_{REP} \approx 10^8$Hz, the integer 'n' is about 10^6. The exact value must be calculated by a two point measurement at different repetition rates.

The OFC is therefore a connection between the electronically measurable frequencies f_{REP}, f_{CEO} and Δf and the optical frequency f_0. Hence optical light is directly electronically measurable and transferable to the electronic area. If two optical clocks should be compared, which have a large distance between them, the optical light is transferred to the HF-area. The repetition rate contains the same stability as the output laser of the OAC. The repetition rate can then be transported from one spot to another and is then transferred back again into the optical area. If the repetition rate is synchronized between the two spots the control of f_{CEO} and Δf creates a possibility for comparison of both OACs.

When time or frequency of HF-Standards should be synchronized, the CEO stabilization is not required. This thesis shows a new system how HF-standards can be synchronized over long distances without loss of information using a short pulse oscillator. If the pulse laser is updated to an OFC the new system would also be capable of synchronize OACs.

2.4 System Requirements

Precise distance measurements are implied in space missions for multiple functions and purposes.

Within this thesis two mission types are considered. Their system requirements on distance measurement are the basis to elaborate the systems created in this thesis.
Since the methods should be able for time and frequency transfer, the main mission to define the system requirements is the Galileo mission. Nevertheless a comparison with other missions could yield into new applications for the methods presented in the present thesis.

2.4.1 GRACE / GFO

Gravity Recovery and Climate Experiment (GRACE [21] [22]) consists of two identical spacecrafts that circulate about 220 km apart in a polar orbit 500 km above Earth. GRACE maps earth's gravity field by making accurate measurements of the distance between the two satellites, using GPS and a microwave ranging system. It is providing an efficient and cost-effective way to map earth's gravity field with unprecedented accuracy. The results from this mission are yielding crucial information about the distribution and flow of mass within earth and its surroundings [23].

The GRACE mission started in 2002 and provides successfully gravitational field measurements of the earth over more than 14 years. The secondary mission is GRACE follow-on (GFO) which should be launched with a scheduled launch-date in 2017.

The GFO mission is equal to the prior GRACE mission except that an updated ranging system is installed. The prior mission used K-Band for ranging, similar to a time-of-flight method. GFO has a Michelson interferometer for measurements with two active sources. The GFO mission is the first implementation of an optical link between two satellites for interferometric detection.

2.4.2 GALILEO

The Galileo System serves as the reference system, since the system would benefit additionally using a time and frequency synchronization between the satellites.

The complete Galileo constellation consists of 24 satellites plus spares (two active spares per orbit). With the satellites taking about 14 hours to orbit Earth at altitudes of 23.222 km, there are at least four satellites visible at the same time anywhere in the world. The satellites are placed in three orbital planes at an angle of 56 degrees to the equator, which will provide coverage up to the polar regions [24].
Figure 7 shows an illustration of the Galileo system with some selected spots.

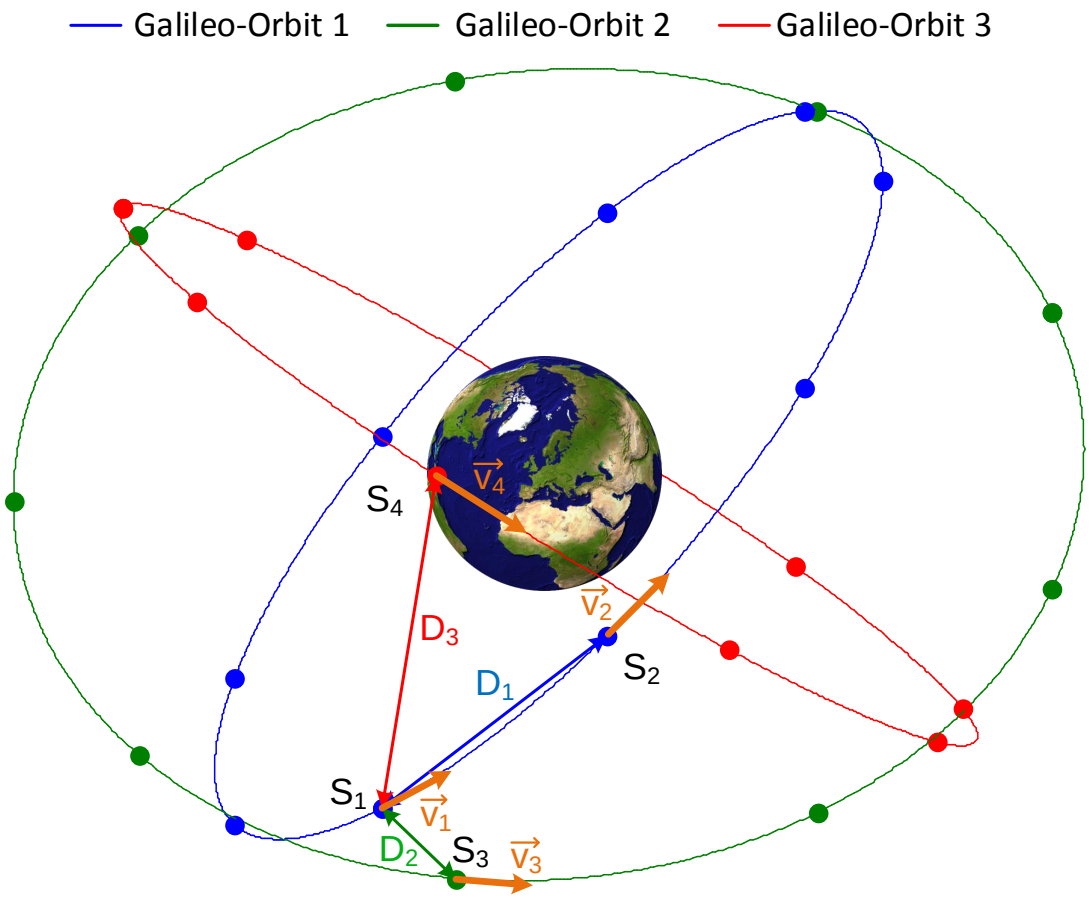

Figure 7: Galileo Constellation

Within the figure four satellites are chosen for further characterization. Their distances and velocities are defined as

- D_1 = Distance between satellites S_1 and S_2 (both Orbit 1)
- D_2 = Distance between satellites S_1 and S_3 (Orbit 1 and 2)
- D_3 = Distance between satellites S_1 and S_4 (Orbit 1 and 3)
- $\vec{v}_x$ = Velocity vector of satellite S_x

Between one orbit and another occurs the largest velocity and distance changes. An example is shown in Figure 8, between Satellite 1 and all other satellites in the second orbit.

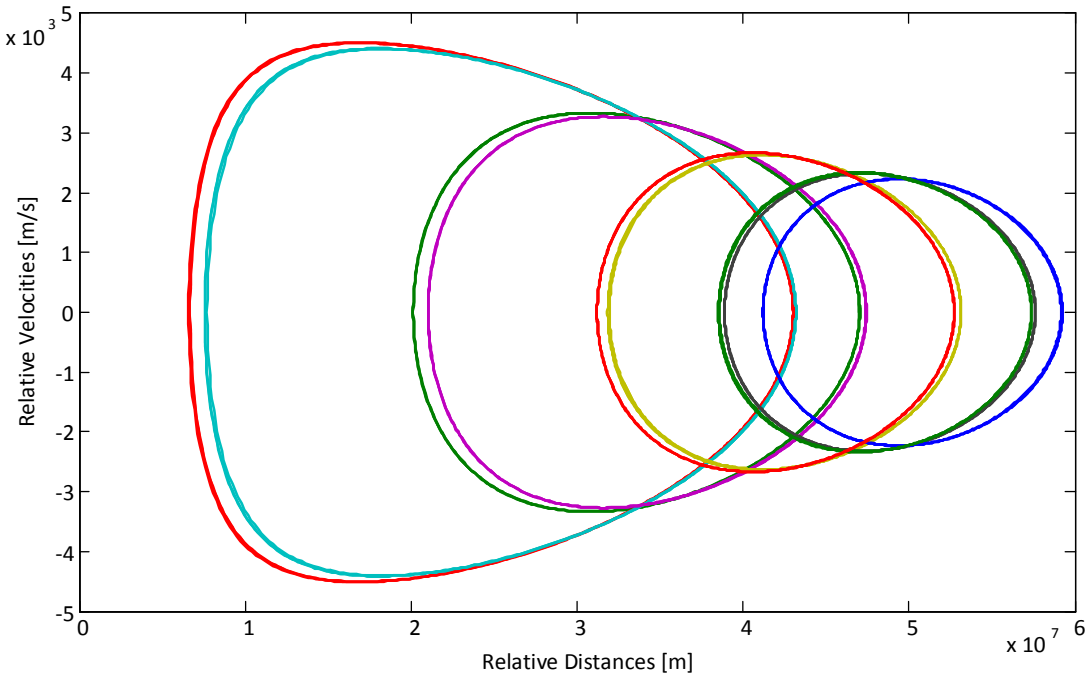

Figure 8: Correlation between distance and relative velocity of two satellites on two different Galileo orbits

Relative velocities with $v_{rel} = \langle \vec{v}_1, \vec{v}_{2,3} \rangle > 4\,\text{km/s}$ occur and the correlated distance changes. The most significant changes can be seen at the two largest rings in Figure 8, which would be the nearest satellites to Satellite 1 at the crossing points of the orbits. These satellites have at the nearest distance at $D \approx 6000\,\text{km}$ the highest velocity changes. To establish at these points an optical link would be most challenging since the targeting of the satellite would require fast moving optic setup. Nevertheless these satellites have the highest requirements on dynamics, therefore this scenario defines the requirements for the distance measurement systems. Also these satellites are closest to each other, which implies the highest probability to create an optical link.

All distances and velocities between satellites are oscillating continuously, even within the same orbits. The defined distances D_1, D_2 and D_3 have within their epoch of 1 day the deviations as illustrated in Figure 9.

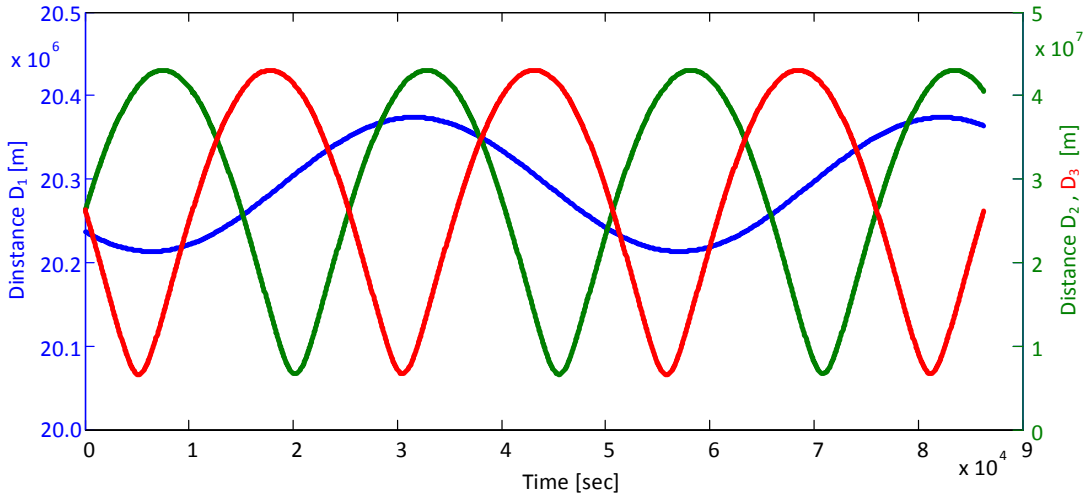

Figure 9: Excerpt of possible satellite links with correlated distances

Even within the same orbit the distances have oscillations between $D_{1,min} \approx 20.2 \cdot 10^6$m and $D_{1,max} \approx 20.4 \cdot 10^6$m. The distance change fits a sinusoidal function, as shown by the blue line in Figure 9.

The distances D_2 and D_3 oscillates between $D_{min} \approx 6 \cdot 10^6$m and $D_{max} \approx 45 \cdot 10^6$m.
Both distances have same the shape as well as similar amplitudes and differ only in the phase. Therefore in future investigations only one scenario is used.

D_1 is the scenario of neighboured satellites on the same orbit. It can be seen/defined as the 'simplest' way to create an optical link between two satellites. But as already shown, an distance oscillation occurs which implies relative velocity changes and relative accelerations. These values are shown in Figure 10 of one epoch (1day).

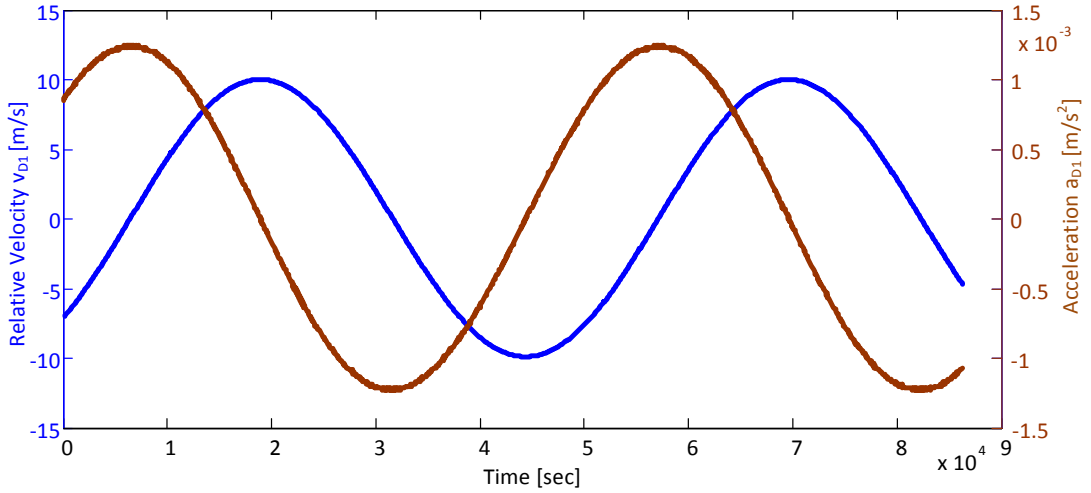

Figure 10: Velocity and acceleration deviation of D_1

In the same orbit velocities of $v_{rel} > 10\,m/s$ occur. The sinusoidal shape of the velocity results in an acceleration.
The relative acceleration between the satellites reaches $a_{rel} < 1.5\,m/s^2$.

Higher velocities and accelerations occur between two satellites in different orbits. An example is shown for the distance D_2 in Figure 11.

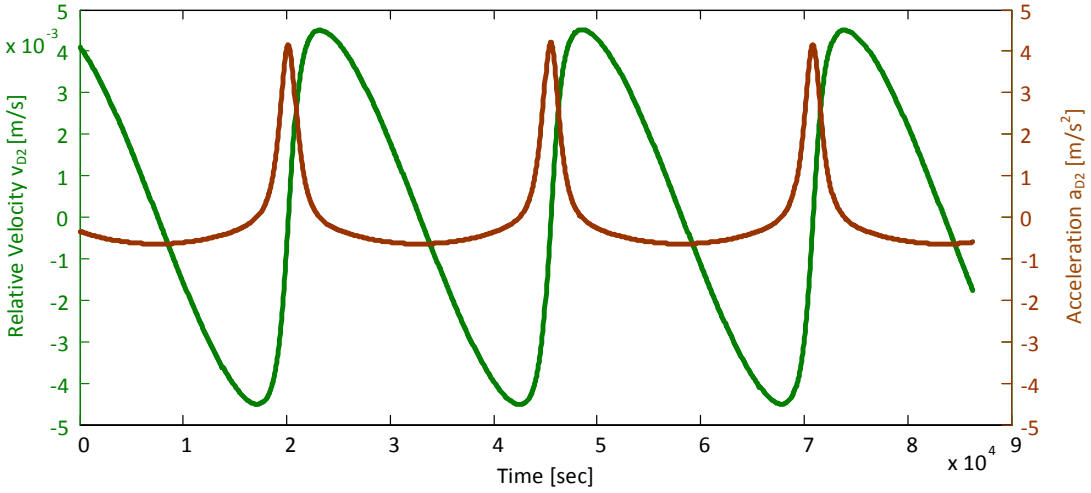

Figure 11: Velocity and acceleration deviation of D_2 and D_3

The relative velocities between satellites S_1 and S_3 reach values $v_{rel} > 4\,km/s$ and accelerations $a > 4\,m/s^2$. This implies higher requirements to the optical setup and to the time and frequency transfer as well compared to the scenario of D_1.

The example with satellite S_1 and S_3 is equal to the scenario S_1 to S_4. A phase difference between the deviations can be observed.

These values are taken into account for the characterization of the measurement systems. Even without the issues of the optical setup, any dynamic in the system challenging for time and frequency synchronization.

Why choosing the Galileo mission as a reference for time and frequency synchronization?
Prior studies OCTAGON [25] and OCTAGON2 [26] showed promising results on GNSS using optical atomic clocks. Galileo would profit in performance using only one optical clock which could be used as master clock for all other satellites. A inter-satellite time transfer would stabilize the whole system that less updates from ground stations would be necessary. Also the performance for localization on earth surface would improve. The performance would increase using one optical clock on each orbit since the time to update each satellite decrease. If more than one clock would be active in Galileo, the possibility of time and frequency comparison between two optical clocks would open new possibilities on science measurements, since the satellites change in velocity, hight and position. These could be used for gravitational measurements, fine structure constant or relativity measurements [27] [28] [29] [30].
If multiple OACs within a Galileo system are installed, the Galileo system could create a 'world clock', available for everybody and more stable as any clock construct on earth surface.

2.4.3 Requirement Summary of Mission Scenarios

The systems GFO and Galileo have different requirements on distance resolution. Since all missions have changing distances, the system itself must be able to handle dynamics.
The values are summarized in Table 4.

Table 4: Example of two missions using high precision distance measurements

Type	GFO [31] [32]	Galileo [24]
Target Distances [m]	$210 \cdot 10^3$	$6 \cdot 10^6$ to $60 \cdot 10^6$
Distance resolutions	$\Delta l < 240\,\text{nm}$	$\Delta l < 1\,\mu\text{m}$
Occurring Velocities	$v_{rel} < 3\,\text{m/s}$	$v_{rel} > 4\,\text{km/s}$

As Table 4 shows the Galileo reference has the highest dynamic. The GFO mission requires the highest distance resolution.

Any measurement or synchronization system uses time standards for distance calculations. Missions like GFO use Michelson Interferometry for relative distance changes. Their laser system is stabilized to an optical cavity and is stable within short time ($f > 1\,\text{Hz}$) whereas the system created during this thesis is based on frequency detection for distance detection. The longer the integration time the better the distance resolution.

The distance resolution using time standards is limited to

$$\Delta d = D \cdot \sigma_y(1\,s)$$

Using e.g. a Rb-Standard to measure the distance of D = 1 m would result in a distance resolution of $\Delta l \approx 10^{-12}$m (1 pm) at 1 s measurement time. The resolution would increase with further integration time. These are theoretical values since the optical setup is mostly the limiting factor of the measurement.
Therefore there are two limits of distance determination: the used time standard and the optical setup. The system with the lowest performance defines the limit.
With increasing distance the theoretical accuracy using time standards gets more inaccurate in distance resolution. An illustration between theoretical resolution and time standard is shown in Figure 12. The requirements for the described space missions are plotted as well.

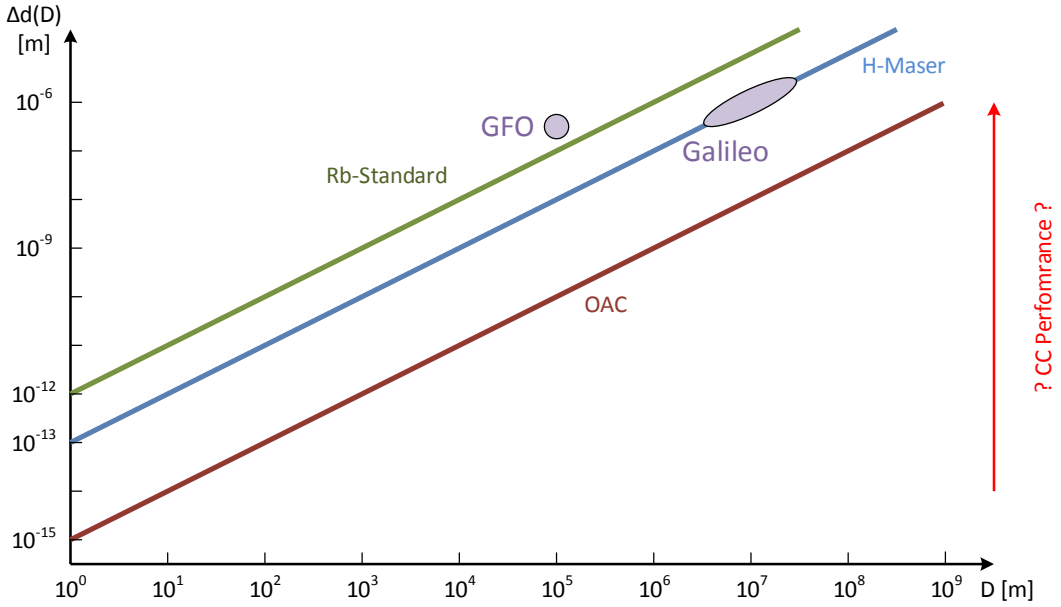

Figure 12: Correlation between absolute distance, distance resolution and available time standard

Figure 12 shows the theoretical limit using different time standards for absolute distance measurement. The measurement time to reach these performances is defined to 1 s. Increasing integration time would result in higher accuracy, with $\Delta d \propto \tau^{-1/2}$ [4].

The GFO mission which implies Michelson Interferometry would also be manageable with a Rb-Standard. The Galileo scenario would require the absolute distance resolution which is also defined by their inner time standard. The H-Maser defines the absolute distance resolution to $\Delta d < 1\mu$m at 1 s measurement time. Using optical atomic clocks would increase the time dependent distance resolution by two orders of magnitude.

For time and frequency synchronization the dynamic of the mission scenario correlates with a

frequency shift due to movement of the target, the Doppler Effect.
The Doppler Effect [33] is defined as

$$f_D = f_0 \cdot \frac{\sqrt{1 - \frac{v^2}{c}}}{1 - \frac{\vec{v} \cdot \vec{e}}{c}} \tag{3}$$

with

f_D =	shifted Doppler frequency	f_0 =	frequency at v = 0
$\vec{v}$ =	velocity vector of the moving object	$\vec{e}$ =	unit vector between measurement point and target
c =	speed of light		

The Doppler Effect is highest, when the target is moving in the same direction to the measurement point. It must then be calculated which impact the movement of the target has on the frequency shift.

Equation 2.4.3 can be modified to

$$v_{rel} = \frac{\left(\frac{f_D}{f_0}\right)^2 - 1}{\left(\frac{f_D}{f_0}\right)^2 + 1} c$$

To reach stabilities as required for any atomic clock the Doppler frequency is defined as $f_D = f_0(1 \pm \sigma_y)$. This results in a velocity resolution per clock

Table 5: Requirements on velocity measurement

Clock type	$\sigma_y(1\,s)$	$\Delta v_{rel}(1\,s)$
Rb-Standard	10^{-12}	332.8 μm/sec
H-Maser	10^{-13}	33.28 μm/sec
opt. Clock	10^{-15}	332.8 nm/sec

For frequency transmission within a GNSS it requires a precise velocity detection to calculate a Doppler shift. The information of the modification of the reference frequency must be transmitted to the target satellite or must be adapted within the prime satellite before synchronization.

These are in total the requirements which are necessary to detect absolutely an object (see Table 4). Also in dynamic systems, the measurement setup must be able to detect precisely the velocity to enable time and frequency synchronization (see Table 5).

2.5 FDDM Method

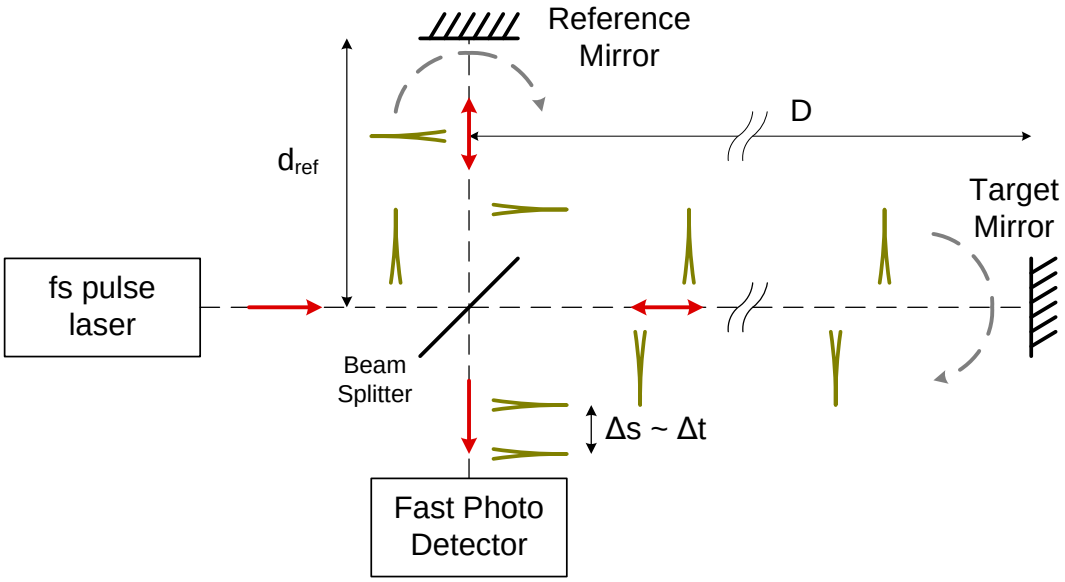

Figure 13: A general Michelson Setup using fs pulses to reference path and target

The measurement of the offset of different incoming pulses can be described as

$$\Delta s = n l_{osc} - 2 \cdot D - 2 \cdot d_{ref} \tag{4}$$

with

$\Delta s =$ the offset when the two pulses are overlapped, or a time offset with $\Delta s = c\Delta t$

$l_{osc} =$ the optical length of the fs oscillator $\left(l_{osc} = \frac{c}{f_{REP}}\right)$

$n =$ Integer value of the pulses within the target path

$D =$ the path to the target

$d_{ref} =$ a reference path (which can be zeroed with adequate setups)

$$D = \frac{c}{2}(nT + \Delta t) - d_{ref} \tag{5}$$

The values T and d_{ref} can be measured. The speed of light c stays constant. Hence there remain the two unknown values n and D. Therefor a two point measurement must be done. A way for a two point measurement is to vary the repetition rate of the oscillator. An example of the correlation between repetition rate and time offset is schematically shown in Figure 14 .

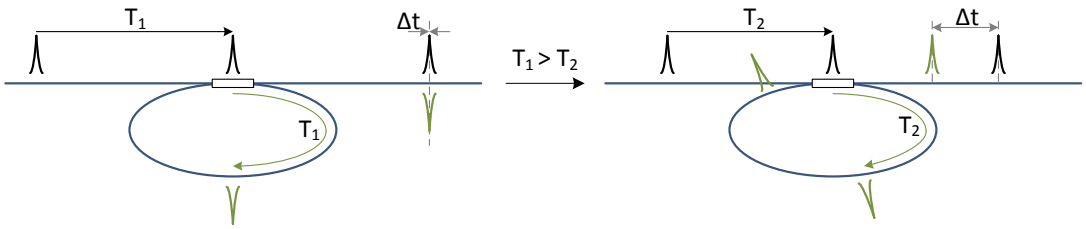

Figure 14: Example of correlation between repetition rate and Δt

Thus the control and read out of the repetition rate correlates with the distance resolution.
To evaluate the time offset the FDDM method is hereby used with an comparably simple setup and calculation effort.

To simplify the theoretical derivation the pulses are defined as Gaussian pulses. It's clear for the writer about the fact that short pulses of an optical oscillator are not defined by a normal distribution but by a sinc function. For the systems used in this thesis this assumption has no negative influence since the results of the measurements fit the theory (see Section 4).

Therefore multiple pulses with time distance t_0 and pulse width σ can be described as

$$f(t) = \frac{1}{\sqrt{2\pi}\sigma} \sum_{m=1}^{\infty} e^{-\frac{(t-mt_0)^2}{2\sigma^2}} \tag{6}$$

Using a Fourier Transformation of this signal results in

$$\mathcal{F}(\omega) = \frac{1}{\sqrt{2\pi}\sigma} \int_{-\infty}^{+\infty} dt\, e^{-i\omega t} f(t)$$

$$\mathcal{F}_m(\omega) = \frac{1}{2\pi\sigma} \int_{-\infty}^{+\infty} dt\, e^{-i\omega t} \sum_{m=1}^{\infty} e^{-\frac{(t-mt_0)^2}{2\sigma^2}}$$

$$\mathcal{F}_m(\omega) = \frac{1}{2\pi\sigma} \int_{-\infty}^{+\infty} dt\, e^{-i\omega t} \left(e^{-\frac{(t-t_0)^2}{2\sigma^2}} + \sum_{m=2}^{\infty} e^{-\frac{(t-mt_0)^2}{2\sigma^2}} \right)$$

To simplify the following calculations only the scenario for m=1 is considered

$$\mathcal{F}_1(\omega) = \frac{1}{2\pi\sigma}\int_{-\infty}^{+\infty} dt\, e^{-i\omega t} e^{-\frac{(t-t_0)^2}{2\sigma^2}} = \frac{1}{2\pi\sigma}\int_{-\infty}^{+\infty} dt\, e^{-i\omega t - \frac{(t-t_0)^2}{2\sigma^2}}$$

$$\mathcal{F}_1(\omega) = \frac{1}{2\pi\sigma}\int_{-\infty}^{+\infty} dt\, e^{\frac{-1}{2\sigma^2}((t-t_0)^2+2i\omega\sigma^2 t)} = \frac{1}{2\pi\sigma}\int_{-\infty}^{+\infty} dt\, e^{\frac{-1}{2\sigma^2}((t-t_0)^2+2i\omega\sigma^2 t)}$$

$$\mathcal{F}_1(\omega) = \frac{1}{2\pi\sigma}\int_{-\infty}^{+\infty} dt\, e^{\frac{-1}{2\sigma^2}(t^2-2tt_0+t_0^2+2i\omega\sigma^2 t)} = \frac{1}{2\pi\sigma}\int_{-\infty}^{+\infty} dt\, e^{\frac{-1}{2\sigma^2}(t^2-2(t_0-i\omega\sigma^2)t+t_0^2+(t_0-i\omega\sigma^2)^2-(t_0^2-i\omega\sigma^2)^2)}$$

$$\mathcal{F}_1(\omega) = \frac{1}{2\pi\sigma}\int_{-\infty}^{+\infty} dt\, e^{\frac{-1}{2\sigma^2}((t-(t_0-i\omega\sigma^2))^2+t_0^2-t_0^2+2i\omega\sigma^2 t_0+\omega^2\sigma^4)}$$

$$\mathcal{F}_1(\omega) = \frac{1}{2\pi\sigma}\int_{-\infty}^{+\infty} dt\, e^{\frac{-(t-(t_0-i\omega\sigma^2))^2}{2\sigma^2}} e^{-i\omega t_0} e^{\frac{-\omega^2\sigma^2}{2}}$$

$$\mathcal{F}_1(\omega) = \frac{1}{\sqrt{2\pi}} e^{\frac{-\omega^2\sigma^2}{2}} e^{-i\omega t_0} \underbrace{\int_{-\infty}^{+\infty} dt\, \frac{1}{\sqrt{2\pi}\sigma} e^{\frac{-(t-(t_0-i\omega\sigma^2))^2}{2\sigma^2}}}_{=1}$$

$$\mathcal{F}_1(\omega) = \frac{1}{\sqrt{2\pi}} e^{\frac{-\omega^2\sigma^2}{2}} e^{-i\omega t_0}$$

including m pulses ($\mathcal{F}_m(\omega)$) it seems that $\sum_{m=1}^{\infty} 1 = \infty$. Each pulse includes a defined value of energy, which is also connected to the complete output power which is constant for the system. This means that the optical power $P = \frac{\text{Energy}}{\text{time}}$ can be implemented in the formula.

$$\mathcal{F}_m(\omega) = P \underbrace{e^{\frac{-\omega^2\sigma^2}{2}}}_{\text{envelope}} \underbrace{\sum_{m=1}^{\infty} e^{-im2\pi f t_0}}_{\delta(f-mf_{REP})} \tag{7}$$

The result of Equation 7 shows a common definition of a frequency spectrum of a short pulse laser. The constant P is defined as the power output. The envelope part defines, dependent on the length of the pulses, the broadness of the spectrum. The smaller 'σ' the broader the expected spectrum. The sum of the complex part creates multiple harmonics at $f_{REP} = 1/t_0$.

The overlap of two pulse trains with equal f_{REP} but different time offsets can be described using two times Equation 6. Their time offset Δt between the pulse trains can be modified. It can be defined that one pulse train has a time offset $\frac{-\Delta t}{2}$ and the second a time offset with $\frac{+\Delta t}{2}$, visualized in Figure 15.

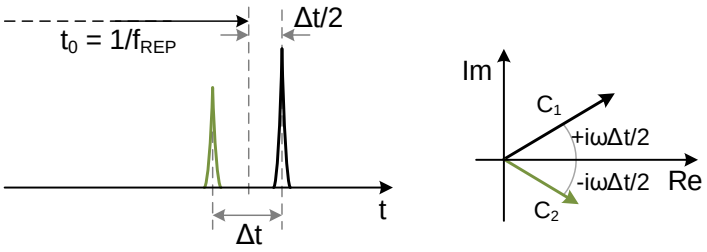

Figure 15: Overlap of two pulse trains with f_{REP} and time offset Δt and its correlation in the complex area

Because m pulses propagate the reference path equal to the target path, the variable m is equal to both pulse trains.
This results in

$$\mathcal{F}(\omega) = e^{\frac{-\omega^2\sigma^2}{2}} \sum_{m=1}^{\infty} (P_1 e^{-im\omega(t_0-\Delta t/2)} + P_2 e^{-im\omega(t_0+\Delta t/2)})$$

$$\mathcal{F}(\omega) = e^{\frac{-\omega^2\sigma^2}{2}} \left(P_1 e^{+i\omega\Delta t/2} + P_2 e^{-i\omega\Delta t/2}\right) \sum_{m=1}^{\infty} e^{-imft_0}$$

$$\mathcal{F}(\omega) = e^{\frac{-\omega^2\sigma^2}{2}} \left(P_1 e^{+i\omega\Delta t/2} + P_2 e^{-i\omega\Delta t/2}\right) \delta(f - mf_{REP}) \tag{8}$$

Equation 8 shows therefore a spectrum in the frequency area with multiple harmonics of the repetition rate of the oscillator and their amplitude correspondent to the time offset Δt. As described here, the constants P_1 and P_2 are mean power values of each pulse train. They correlate quadratic with the electric field of each pulse which in turn is linear to measurable voltage. This is an absolute value of the complex vectors shown in Figure 15. Estimating $\sigma \ll \omega$ results in $e^{-\omega^2\sigma^2} \to 1$. Also that an optical power correlates with an electronically measurable voltage ($P_x \propto U_x^2$), the voltage can be described as

$$U^2 = |\mathcal{F}(\omega)|$$

$$U = \sqrt{(U_1 + U_2)^2 \cos^2(\omega\Delta t/2) + (U_1 - U_2)^2 \sin^2(\omega\Delta t/2)}$$

$$\xrightarrow{\delta(f-mf_{REP})} U_m(\Delta t, U_1, U_2) = \sqrt{(U_{1,m} + U_{2,m})^2 \cos^2(2\pi mf_{REP}\Delta t/2) + (U_{1,m} - U_{2,m})^2 \sin^2(2\pi mf_{REP}\Delta t/2)}$$

where U_m is the measurable value of the m-th harmonic of the repetition rate and $U_{x,m}$ the measurable value of the harmonic of the reference path or the target path, respectively. A simplification can be done using a relative time offset $dt = f_{REP} \cdot \Delta t \in [0, 1]$ and arithmetic calculations to

$$U_m(dt, U_{1,m}, U_{2,m}) = \sqrt{U_{1,m}^2 + U_{2,m}^2 + 2U_{1,m}U_{2,m}\cos(m2\pi dt)} \tag{9}$$

To simplify the correlation between the time offset and the characteristic of the amplitude of the harmonics of the repetition rate, multiple scenarios are visualized: A first simplification is the usage of relative voltage like

$$dU_m = \frac{U_m}{U_{1,m} + U_{2,m}} \quad \text{with} \quad dU \in [0, 1] \subset \mathbb{R}$$

The additional assumption that all $U_{x,m}$ have equal amplitudes simplifies further visualizations. Within Figure 16 a scenario with overlapping pulses is shown.

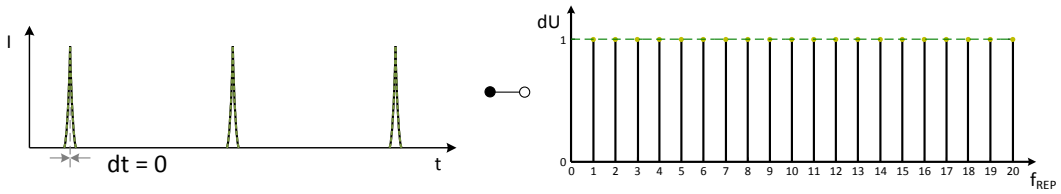

Figure 16: Correlation between time and frequency domain with dt = 0

The frequency domain looks like a ”comb” of multiple harmonics of the repetition rate. The overall envelope is defined by the pulse duration (see Equation 8 ’σ’). In Figure 16 the first 20 harmonics are illustrated. The comb would continue to infinity (with given assumptions) but for visualisation of the effect, the first 20 harmonics are considered to be sufficient. To characterize the behaviour at different dt values Figure 17 illustrates a shift from dt = 0 to dt = 0.05.

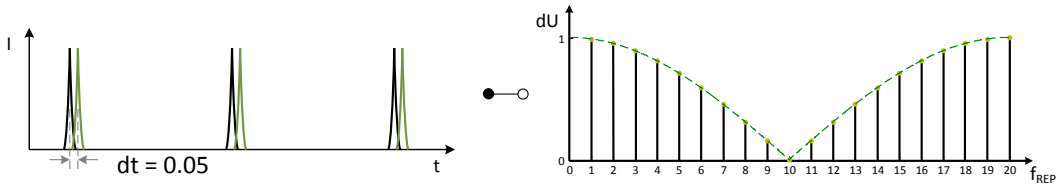

Figure 17: Correlation between time and frequency domain with dt = 0.05

The envelope part in Equation 9 lowers the amplitude of the 10^{th} harmonic to 0 due to the dt shift. The 20^{th} harmonic already reaches its maximum again. The first and second harmonic are still near their maximum. If the dt shift would be done continuously from dt = 0 to dt = 0.05 the 20^{th} harmonic would have shown an amplitude trend as indicated with the green dotted line, a norm cosine function ($|\cos(x)|_{x=0}^{x=\pi}$).

The next step to dt = 0.1 can be seen in Figure 18.

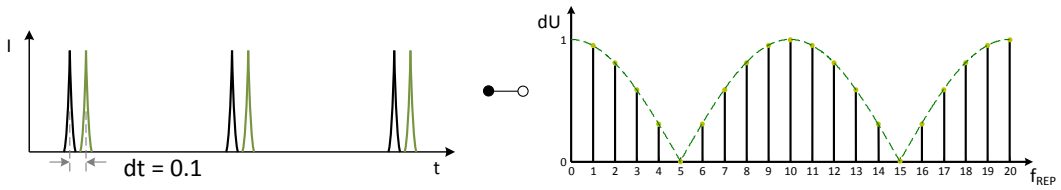

Figure 18: Correlation between time and frequency domain with dt = 0.1

The 5th harmonic decreases to its minimum 0 whereas the 10th and 20th harmonics reach the maximum again. During a shift from dt = 0 to dt = 0.1 the 20th harmonic already oscillated two times. The trend of the 20th harmonic from a shift between dt = 0 to dt = 0.1 could be seen in the green dotted line with $|\cos(x)|_{x=0}^{x=2\pi}$

For illustrating a larger step dt is switched to 0.25 as can be seen in Figure 19.

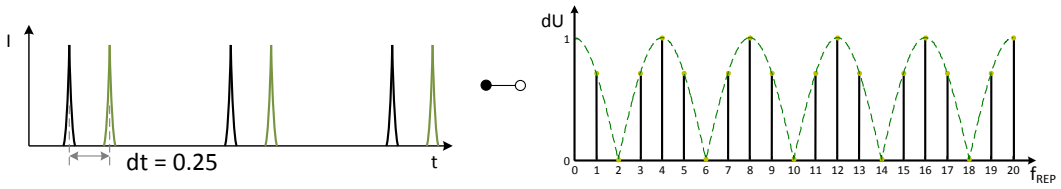

Figure 19: Correlation between time and frequency domain with dt = 0.25

At this state, all harmonics show a clear oscillation since the second harmonic vanishes and the first harmonic also shows notable decrease. If the shift from dt = 0 to dt = 0.25 of the 20th harmonic would have been recorded, the trend would fit the green dotted line with $|\cos(x)|_{x=0}^{x=10\pi}$.
The maximum of oscillations can be seen when dt = 0.5 which is illustrated in Figure 20.

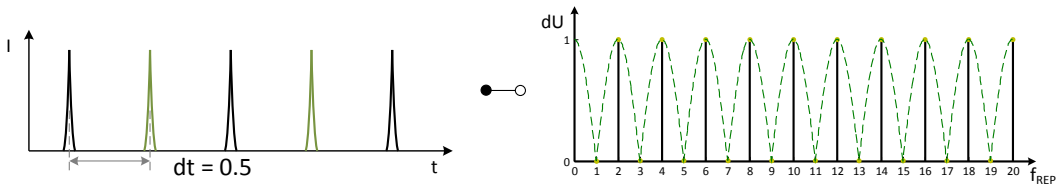

Figure 20: Correlation between time and frequency domain with dt = 0.5

In this case the spectrum equals to doubled repetition rate. Important to know that this is the symmetric case for dt. The 20th harmonic oscillated 20 times between dt = 0 and dt = 0.5 with the norm function $|\cos(x)|_{x=0}^{x=20\pi}$ (see green dotted line in figure 20).

To clarify the amplitude trend of a harmonic, Figure 21 shows the trend for the first four harmonics with a dt shift from dt = 0 to dt = 1.
In this example the pulses from reference path ($P_{1,m}$) and target path ($P_{2,m}$) have still equal amplitudes. With this input, the oscillation can be described by

$$\xrightarrow{U_{1,m}=U_{2,m}} U_m = \sqrt{2}U_{1,m}\sqrt{\cos(1+(m2\pi dt))} = \sqrt{2}U_{1,m}\sqrt{2\cos^2(m\pi dt)}$$

$$\text{with} \quad dU_m = \frac{U_m}{U_{1,m}+U_{2,m}}$$

$$\Rightarrow dU_m = |\cos(m\pi dt)| \tag{10}$$

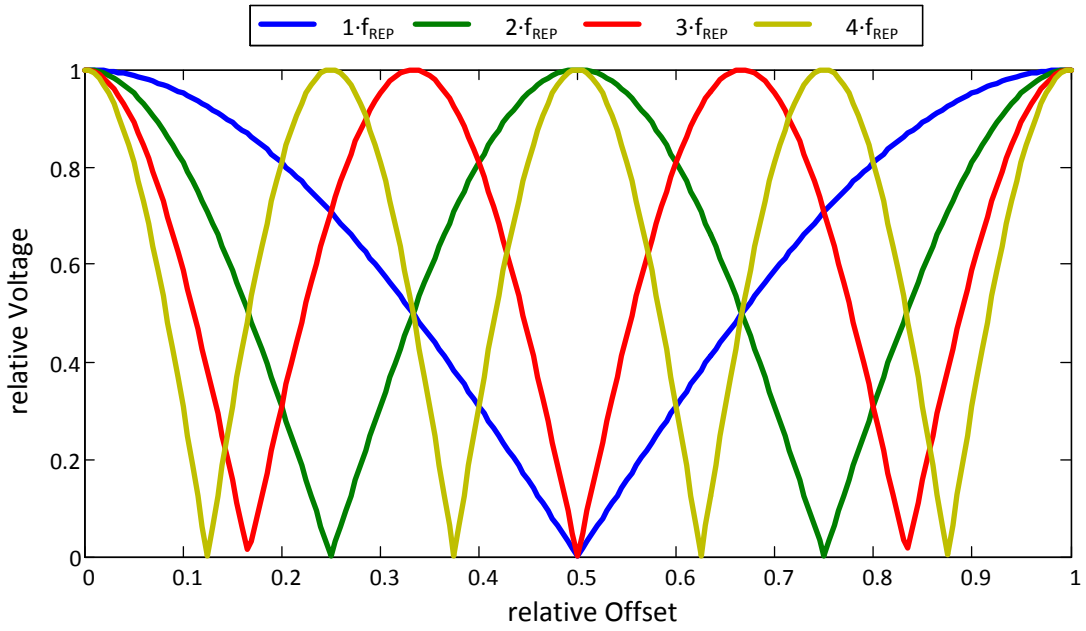

Figure 21: Amplitude characteristic of the first four harmonics

In Figure 21 it can be seen, that an increasing number of harmonic correlates linear with an oscillation from dt = 0 to dt = 1

Taking into consideration the amplitude variation of target and reference path $U_{1,m}$ and $U_{2,m}$ the signal shown in Figure 21 must be adapted. The variation of the signal with different amplitudes is shown for the first harmonic of the repetition rate. The same behaviour would be seen at higher harmonics as well.

$$\xrightarrow{m=1} U = \sqrt{U_1^2 + U_2^2 + 2U_1U_2\cos(2\pi \cdot dt)}$$
$$\xrightarrow{dt=0.5} U = \sqrt{(U_1 - U_2)^2} = |U_1 - U_2|$$
$$\Rightarrow dU(dt = 0.5) = \frac{|U_1 - U_2|}{U_1 + U_2}$$

for the relation $U_1/U_2 = x$ this results in

$$dU(dt = 0.5) = \frac{x - 1}{x + 1} \quad \text{with} \quad x \in [0, 1] \subset \mathbb{R} \tag{11}$$

Some examples for the variation of the harmonic signals are shown in Figure 22.

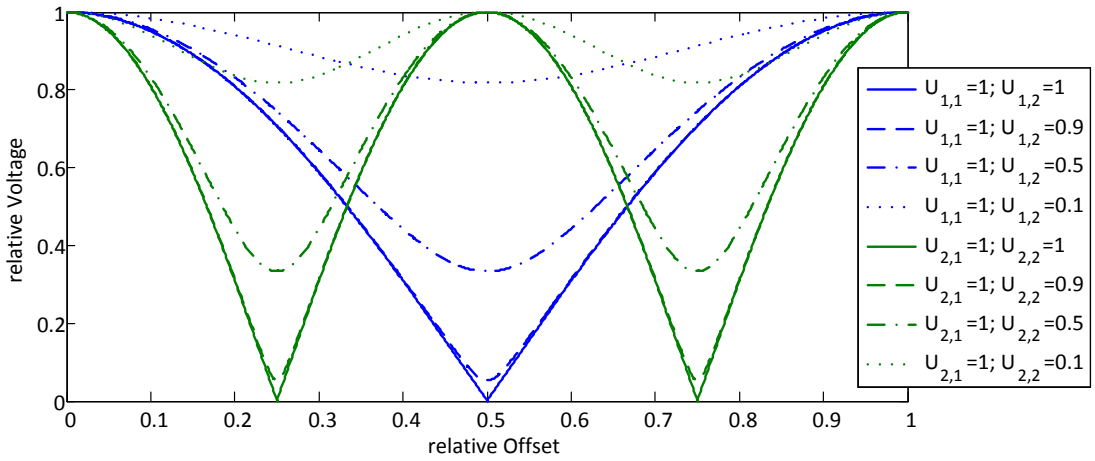

Figure 22: Amplitude characteristic dependent on non equal incoming pulse intensities

The higher the difference between both intensities the lower the amplitude of the oscillation.
It can be seen that characterization of the intensity of reference and target paths must be done precisely. The FDDM signal reacts directly from any attenuation of one signal (see Section 2.6.3). Nevertheless an additional calculation/modification of the signal results in a signal which is independent of signal variation in its function. This update is described in Section 2.6.1.

2.6 Cross Correlations

Within this chapter two types of cross correlations (CC) are described. A CC is a correlation between two signals which depend on each other due to the measurement principle. The created error signal can than be used for stabilization, characterization or measurements. A CC is mostly a amplification of measurement resolutions of a system.

2.6.1 FDDM CC

The signal shown in Figure 21 in section 2.5 gives the possibility not only to measure the amplitudes of each harmonic, but also to use their amplitude (voltage) within a CC. This is then called the FDDM CC.
The error signal for the CC is created using neighboured harmonics. As an example the 12^{th} and 13^{th} harmonics are shown in Figure 23 based on Equation 10.

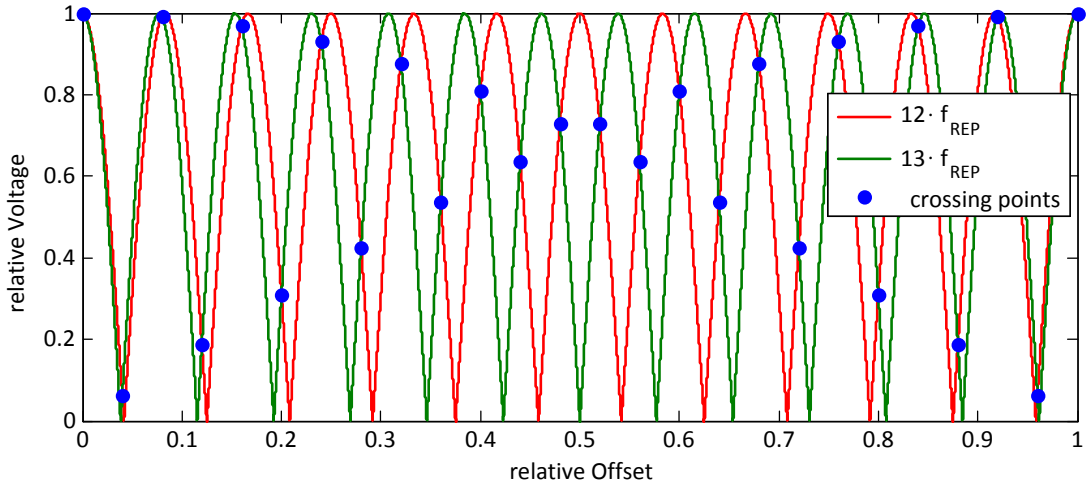

Figure 23: Illustration of the 12^{th} and 13^{th} harmonics and their crossing points

The harmonics mentioned here are only representative, because they are used later in the measurements (Section 3: Measurement Setups, Section 4: Measurements). It could be any higher harmonic. Most important, that two neighboured harmonics are used.

In Figure 23 the 12^{th} and 13^{th} harmonics are oscillating within the 'dt' shift from dt = 0 until dt = 1 with the trend defined in Equation 10.

1) The crossing points indicate '2m+1' equidistant dt values.
2) The slopes of the neighboured harmonics are opposed at crossing points.
3) The voltage value of each crossing point is singular in dt $\in [0, 0.5]$.

to 1): The FDDM method uses one harmonic for distance resolution. The number of the harmonic defines the resolution of the system. With an increasing number 'm' the dt resolution increases.

to 2): The higher the slopes of the measurement system the better its resolution. Since the slopes of neighboured harmonics at the crossing points are contrary the subtraction of the harmonics increase the slope at the crossing point.

to 3): If 'dt' is chosen that one of the crossing points occur, only the measurement of the current voltage results in the required dt definition. If a system is stabilized only on the crossing points, the voltage value of the points results in the required 'dt' value.

To use all the characteristics of the crossing points, the neighboured harmonics must be subtracted from each other. This includes a previous separation of each harmonic and the subtraction afterwards. A common setup for this is illustrated in Figure 24. Other possibilities like lock-in amplifiers are also applicable, but the here described setup has its advantage of its simplicity (see Section 3.2.4)

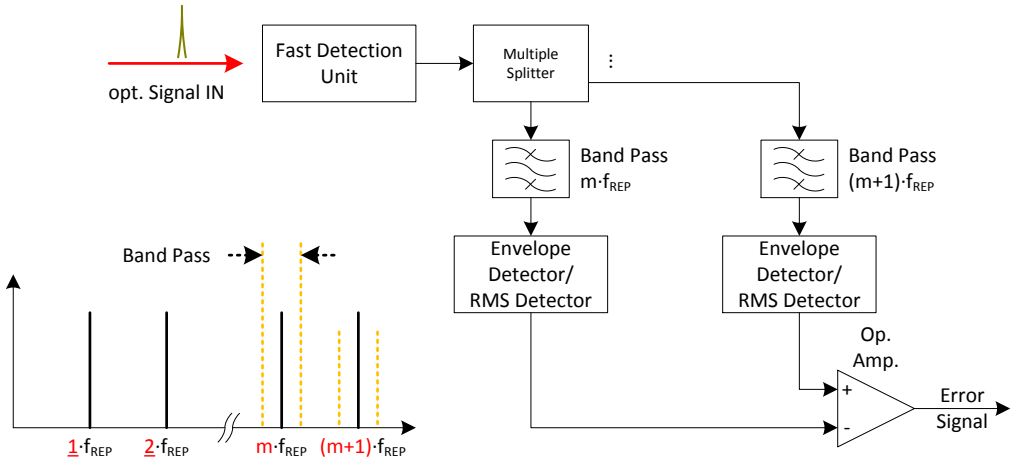

Figure 24: Simplified overview of a possible setup to create the FDDM CC signal

The setup is created as follows:

- Fast optical detector
- Band pass
- Subtracting circuit (operation amplifier)
- Multiple splitter
- Envelope Detector

The optical pulses are detected by a fast detection unit. The faster the detection unit, the higher the harmonic that can be detected. The importance of the frequency range is described afterwards.

A multiple splitter is used, for separating the large frequency spectrum in multiple channels. The number of channels depends on how many other channels are required for further measurements. Each additional channel lowers the amplitude of the signal. Splitters have variations of their behaviour dependent on the frequency. This is also important for later signal characterizations.

The band pass is used to separate one harmonic from the other. Special filter types (e.g. SAW filter) are capable of filter even highest frequencies ($> 5\,\text{GHz}$) with small bandwidths. The attenuation dependent on each harmonic is mostly different.

The envelope detector is capable of measure the absolute amplitude of a carrier frequency. The device is also available for even highest frequencies ($> 5\,\text{GHz}$) and fast modulations ($> 1\,\text{MHz}$). The amplitude characteristic depends on the frequency.

The subtracting circuit subtracts one harmonic from the other. By modifying the circuit, the signal can be balanced to create a norm function to calculate with Equation 10.

Using the input as seen in Figure 23 and the setup shown in Figure 24 results in an output presented in Figure 25.

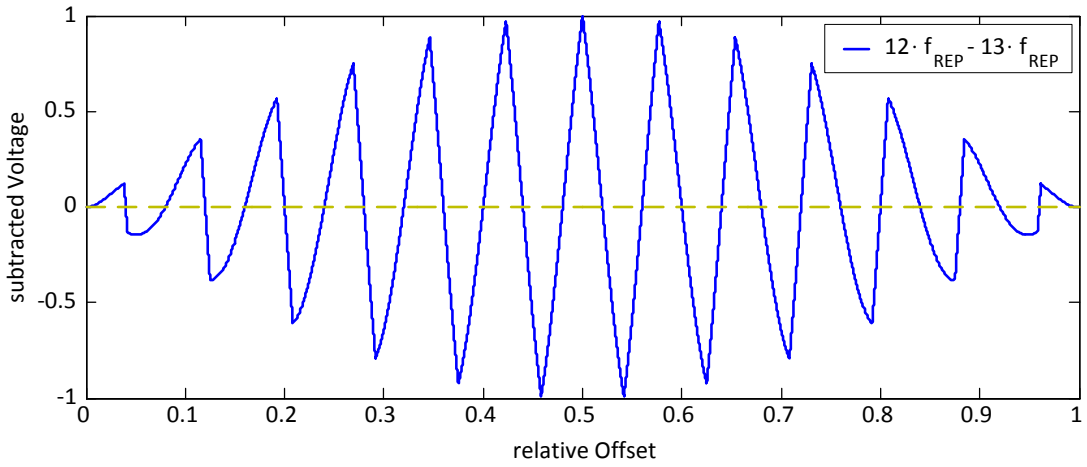

Figure 25: FDDM CC signal with 13$^{\text{th}}$ harmonic subtracted from 12$^{\text{th}}$ harmonic

As can be seen in Figure 25 the output has larger slopes as the original signal itself. The higher the slope of the signal, the higher the resolution of the system.
Generally a system can be locked with this signal to an object by implementing the error signal into the complete setup, that the oscillator locks its repetition rate to the distance of the object. By reading out the frequency the distance can be accurately measured.

The FDDM CC signal varies with different amplitudes of the harmonics. Additional calculation must be done, to ensure the performance of the FDDM CC method. As calculated for the FDDM signal Equation 9 is used with

$$U_m(dt, U_{1,m}, U_{2,m}) = \sqrt{U_{1,m}^2 + U_{2,m}^2 + 2U_{1,m}U_{2,m}\cos(m2\pi dt)}$$
$$U_{m+1}(dt, U_{1,m+1}, U_{2,m+1}) = \sqrt{U_{1,m+1}^2 + U_{2,m+1}^2 + 2U_{1,m+1}U_{2,m+1}\cos((m+1)2\pi dt)}$$

for neighboured harmonics m and m+1.

For $U_{CC} = U_m - U_{m+1}$ it results in following equation:

$$U_{CC} = \sqrt{U_{1,m}^2 + U_{2,m}^2 + 2U_{1,m}U_{2,m}\cos(m2\pi dt)} - \sqrt{U_{1,m+1}^2 + U_{2,m+1}^2 + 2U_{1,m+1}U_{2,m+1}\cos((m+1)2\pi dt)}$$

Is the CC signal used for a stabilization loop, the loop tries to zero the CC signal. This means, the stabilization points of the FDDM CC method depend on voltages of the separate harmonic voltages. Further calculations must be done to define exactly the position of the zero crossing points.

With the expression $U_{CC} \stackrel{!}{=} 0$ the mentioned equation can be written as

$$\sqrt{U_{1,m}^2 + U_{2,m}^2 + 2U_{1,m}U_{2,m}\cos(m2\pi dt)} = \sqrt{U_{1,m+1}^2 + U_{2,m+1}^2 + 2U_{1,m+1}U_{2,m+1}\cos((m+1)2\pi dt)} \tag{12}$$

To define the zero crossing points of the CC signal by a basic scenario, all amplitudes are equal ($U_{1,m} = U_{2,m} = U_{1,m+1} = U_{2,m+1}$). This basic scenario is defined in Equation 10 with

$$|\cos(m\pi dt)| = |\cos((m+1)\pi dt)|$$
$$0 = \cos((m+1)\pi dt) \pm \cos(m\pi dt)$$

$$0 = \underbrace{\sin\left(\frac{\pi}{2}dt\right)}_{\Rightarrow dt_1} \underbrace{\sin\left((2m+1)\frac{\pi}{2}dt\right)}_{\Rightarrow dt_2}$$
$$dt_1 = 0$$
$$dt_2 = \frac{2n}{2m+1} \quad n \in [0, m] \subset \mathbb{N}$$

$$0 = \underbrace{\cos\left(\frac{\pi}{2}dt\right)}_{\Rightarrow dt_3} \underbrace{\cos\left((2m+1)\frac{\pi}{2}dt\right)}_{\Rightarrow dt_4}$$
$$dt_3 = 1$$
$$dt_4 = \frac{2n+1}{2m+1} \quad n \in [0, m] \subset \mathbb{N}$$

The zero crossing points can be summarized to

$$\bigcup dt_x = dt_{zc} = \frac{n}{2m+1} \quad \text{with} \quad n \in [0, 2m+1] \subset \mathbb{N} \tag{13}$$

The zero crossing points are equidistant with a separation of $\frac{1}{2m+1}$. If a stabilization is used that zeros the U_{CC}, higher harmonics also result in a more practical application since more points can

be used for stabilization.

The slope at each zero crossing point results in the resolution of the system. For calculation of the derivation the square root of the square cosines is used

$$\forall m \in \mathbb{N} \xrightarrow[U_{1,m}=U_{1,m+1}]{U_{1,m}=U_{2,m}} U_{CC} = \frac{U}{\sqrt{2}}\left(\sqrt{(1+\cos(m2\pi dt)} - \sqrt{(1+\cos((m+1)2\pi dt)}\right)$$
$$\xrightarrow{U=dU} U_{CC} = dU\left(\sqrt{\cos^2(m\pi dt)} - \sqrt{\cos^2((m+1)\pi dt))}\right)$$

This results in

$$\partial_{dt}U_{CC} = dU\left(\frac{\cos((m+1)\pi dt)}{\sqrt{\cos^2((m+1)\pi dt)}}(m+1)\pi\sin((m+1)\pi dt) - \frac{\cos(m\pi dt)}{\sqrt{\cos^2(m\pi dt)}}m\pi\sin(m\pi dt)\right) \quad (14)$$

Equation 14 is calculated numerically for each crossing point.
The repetition rate and the m-factor of the harmonic defines the slope at each crossing point. Since the repetition rate can be modified by oscillator design, the question is, if the oscillator frequency has an influence on the slope.

Therefore an example for visualization can be used:

Two oscillators have different repetition rates, but the FDDM CC method uses the same centre frequency between their m^{th} and $(m+1)^{th}$ harmonic. Figure 26 shows the estimated situation.

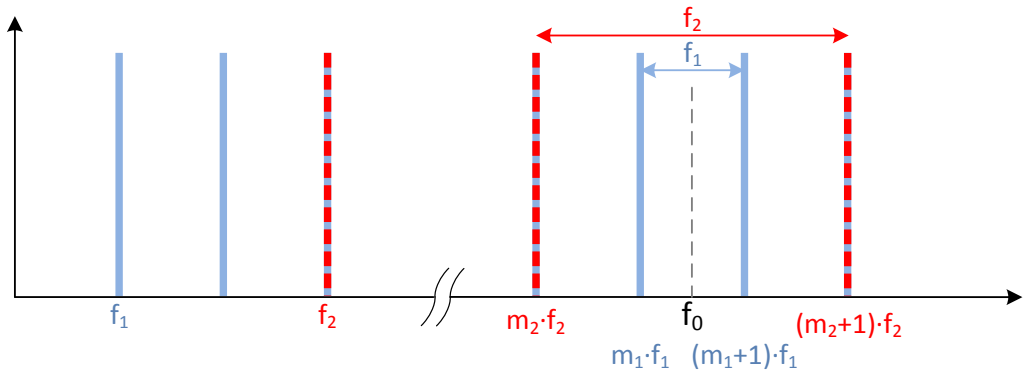

Figure 26: Two oscillators with same centre frequency but different repetition rates

In this example $f_2 = 3 \cdot f_1$. The case that f_0 is equal for both repetition rates, is when $m_1 = 3 \cdot m_2 + 1$. With Equation 14 the slope can also be defined by the time offset Δt by

$$dt = f_{REP} \cdot \Delta t \quad \Rightarrow \quad \partial_{dt} U_{CC} = \partial_{\Delta t} U_{CC} \cdot f_{REP} = a_t$$

Each repetition rate creates its own zero crossing points at $dt_{zc,x}$ of the FDDM CC signal. Solving Equation 26 at the zero crossing points creates multiple slopes $a_{t,x}$.
Using the upper example results therein in $a_{t,2} \subset a_{t,1}$.

This means that the repetition rate of an oscillator does not affect the slope/resolution of the system. The active element of the resolution of the system is the center frequency f_0 between the m^{th} and $(m+1)^{th}$ harmonic.

Table 6 gives an example taking into account the upper mentioned circumstances.

Table 6: Multiple CC slopes with different repetition rates
center frequency f_0 = 13.5

f_{REP} = 9 , m = 1		
dt_{zc}	$\frac{dU}{dt}$	$\frac{dU}{\Delta t} f_{REP}$
0.00	0.00	0.00
0.33	8.16	73.46
0.67	-8.16	-73.46
1.00	0.00	0.00

Note:
cells with same color
have same a_t at same dt_{zc}

f_{REP} = 3 , m = 3		
dt_{zc}	$\frac{dU}{dt}$	$\frac{dU}{\Delta t} f_{REP}$
0.00	0.00	0.00
0.11	-27.84	-83.53
0.22	9.67	29.01
0.33	-24.49	-73.64
0.44	18.17	54.52
0.56	-18.17	-54.52
0.67	24.49	73.46
0.78	-9.67	-29.01
0.89	27.84	83.53
1.00	0.00	0.00

f_{REP} = 1 , m = 13		
dt_{zc}	$\frac{dU}{dt}$	$\frac{dU}{\Delta t} f_{REP}$
0.00	0.00	0.00
0.04	84.68	84.68
0.07	-9.85	-9.85
0.11	83.53	83.53
0.15	-19.56	-19.56
0.19	81.26	81.26
0.22	-29.01	-29.01
0.26	77.89	77.89
0.30	-38.07	-38.07
0.33	73.46	73.46
0.37	-46.61	-46.61
0.41	68.04	68.04
0.44	-54.52	-54.52
0.48	61.70	61.70
0.52	-61.70	-61.70
0.56	54.52	54.52
0.59	-68.04	-68.04
0.63	46.61	46.61
0.67	-73.46	-73.46
0.70	38.07	38.07
0.74	-77.89	-77.89
0.78	29.01	29.01
0.81	-81.26	-81.26
0.85	19.56	19.56
0.89	-83.53	-83.53
0.93	9.85	9.85
0.96	-84.68	-84.68
1.00	0.00	0.00

The slope at zero crossing point is independent of the repetition rate of the used oscillator. The important factor of the slope is the centre frequency f_0 of the neighboured harmonics of the FDDM CC signal. The higher the centre frequency the higher the slope.
The oscillator frequency makes no difference in the FDDM CC signal, when it's used for a stabilization or distance resolution.

Higher frequencies can be of advantage, because they increase the multiple factor 'n' of Equation 5. Smaller changes in the repetition rate create larger changes in dt, which makes is more manageable to calculate the 'n' factor. Nevertheless at higher frequencies the choice of the band pass filter is limited, since less harmonics can be used. Also especially at higher frequencies, the choice of adequate filters for neighboured harmonics could be challenging.

The zero crossing points and their related slopes are calculated by Equation 13 and Equation 14 respectively. Until now an estimation is done that the amplitudes of the used harmonics are equal. This helps to defined a basic function of the FDDM CC signal. Nevertheless the harmonics signal can vary by different electronic imperfection or the measurement environment. A change in the CC signal can then be observed.

To simplify the estimations, Equation 12 can be divided into two different cases.

Case 1: - the harmonics of a single path (reference or target) have the same amplitude
- the amplitudes of one path are lower than the other
$\Rightarrow U_{1,m} = U_{1,m+1} \quad \cup \quad U_{2,m} = U_{2,m+1}$

Case 2: - the amplitudes of both paths are the same
- the harmonics of a single path (reference of target) have different amplitudes
$\Rightarrow U_{1,m} = U_{2,m} \quad \cup \quad U_{1,m+1} = U_{2,m+1}$

Case 1 can appear, if the path to the target object receives an attenuation due to the long distance.

Case 2 can appear, if the electronic response differently on frequencies.

For case 1 Figure 27 shows an illustration in the frequency domain and the resulting harmonics signal.

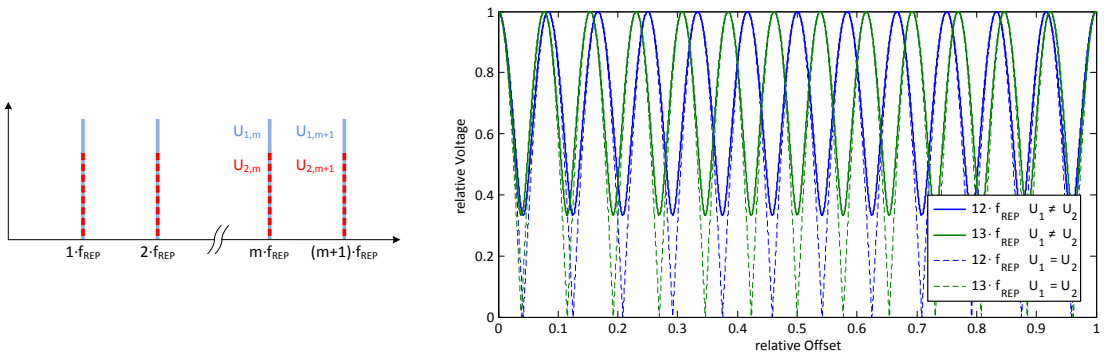

Figure 27: Case1: one path has lower intensity than the other

In Section 2.5 it is already mentioned what happens to the FDDM signal if one path is different from the other (see Figure 22). In case for the zero crossing points Equation 12 can be simplified by using $U_{1,m} = U_{1,m+1}$ and $U_{2,m} = U_{2,m+1}$ which results in

$$U_{1,m}^2 + U_{2,m}^2 + 2U_{1,m}U_{2,m}|\cos(m2\pi dt)| = U_{1,m}^2 + U_{2,m}^2 + 2U_{1,m}U_{2,m}|\cos((m+1)2\pi dt)|$$
$$|\cos(m2\pi dt)| = |\cos((m+1)2\pi dt)|$$

This is the same correlation as in Equation 13 and therefore the dt_{zc} values for the zero crossing points can be calculated. Despite a difference between the intensities the two paths do not change the zero crossing points of the FDDM CC signal.

For case 2 Figure 28 shows an illustration in the frequency domain and the resulting harmonics signal.

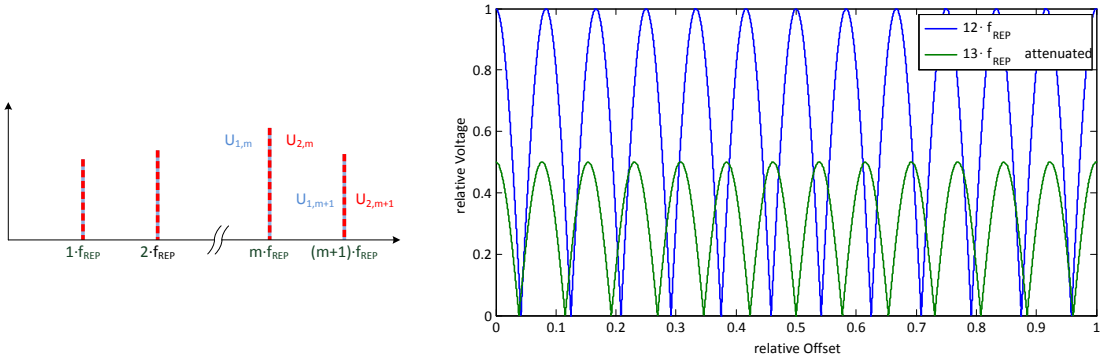

Figure 28: Case 2: amplitudes of m^{th} and $(m+1)^{th}$ harmonics are different

In case 2 ($U_{1,m} = U_{2,m}$ and $U_{1,m+1} = U_{2,m+1}$) Equation 12 can be simplified by

$$2U_{1,m}^2 + 2U_{1,m}^2\cos(m2\pi dt) = 2U_{1,m+1}^2 + 2U_{1,m+1}^2\cos((m+1)2\pi dt)$$
$$\xrightarrow[U_{1,m+1}=U_{m+1}]{U_{1,m}=U_m} U_m^2(1+\cos(m2\pi dt)) = U_{m+1}^2(1+\cos((m+1)2\pi dt))$$
$$\rightarrow \frac{U_m^2}{U_{m+1}^2} = \frac{(1+\cos((m+1)2\pi dt))}{(1+\cos(m2\pi dt))}$$

This results in

$$f_{zc} = \frac{U_m^2}{U_{m+1}^2} = \frac{\cos^2((m+1)\pi dt)}{\cos^2(m\pi dt)} \tag{15}$$

Equation 15 shows, that the zero crossing points depend on the correlation between the m^{th} and $(m+1)^{th}$ amplitude. An illustration of the zero crossing points and the amplitude correlation can be seen in Figure 29.

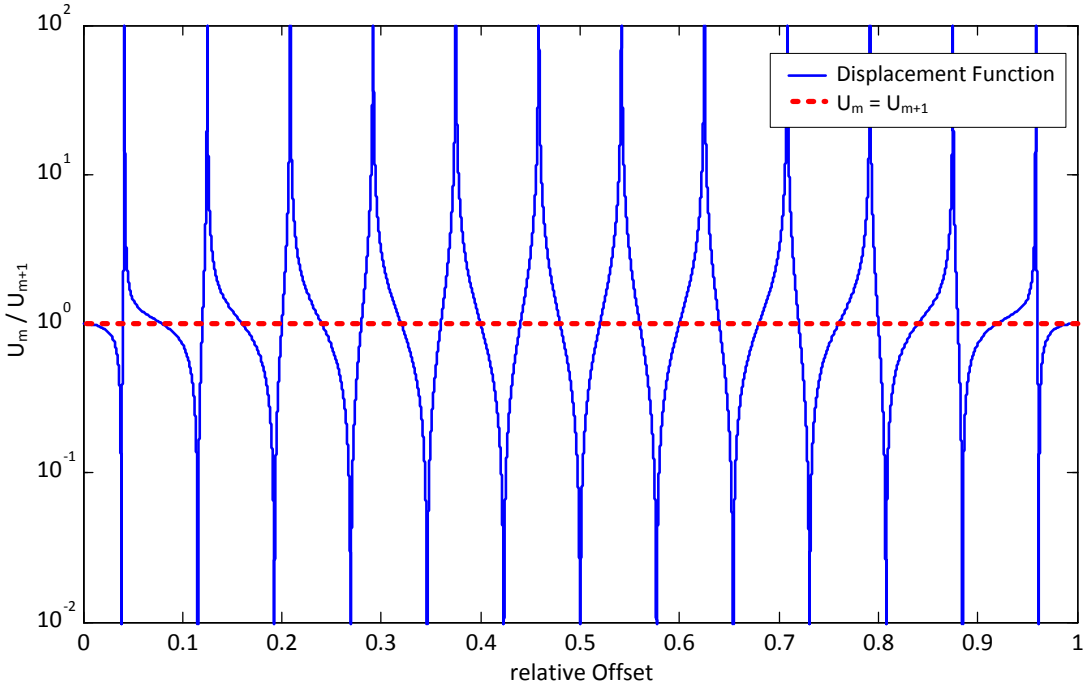

Figure 29: Example for displacement function for the 12^{th} and 13^{th} harmonic

The zero crossing points receive a change dependent on the absolute amplitude of the m^{th} and $(m+1)^{th}$ harmonic.
It also matches the limits of the function to

$$\lim_{U_m \to 0} f_{zc} \to \cos((m+1)\pi dt) = 0$$
$$\Rightarrow dt = \frac{n + 1/2}{m+1} \quad \text{with} \quad n \in [0, m+1] \subset \mathbb{N}$$

$$\lim_{U_{m+1} \to 0} f_{zc} \to \cos(m\pi dt) = 0$$
$$\Rightarrow dt = \frac{n + 1/2}{m} \quad \text{with} \quad n \in [0, m] \subset \mathbb{N}$$

These results fit the origin signal of unperturbed m^{th} or $(m+1)^{th}$ harmonic. For this extremes the points are touching points and no crossing points. To illustrate the influence of each case, some examples are shown in Figure 30.

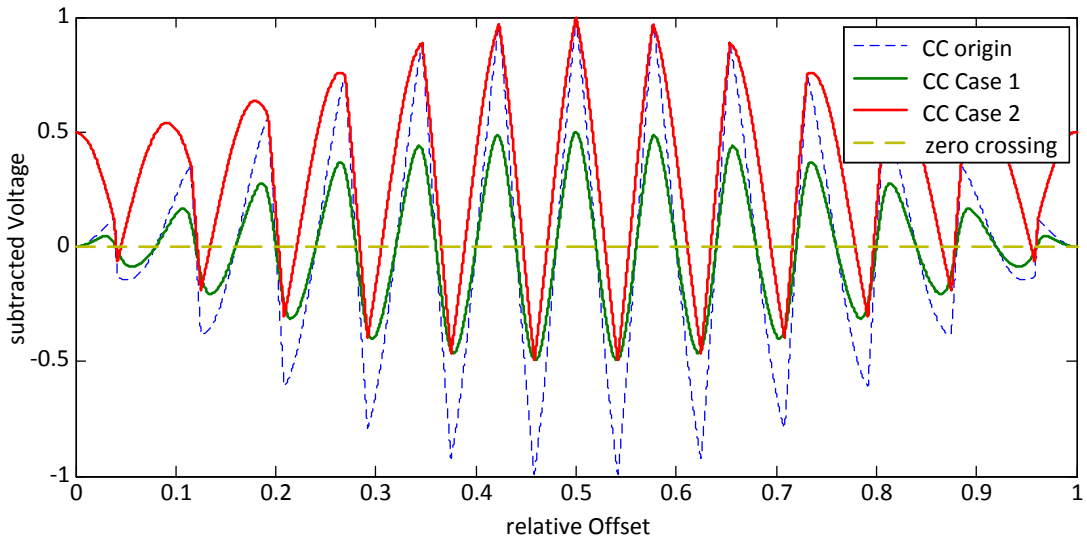

Figure 30: Illustration of different cases influencing the FDDM CC signal

If the incoming pulses receive an attenuation (case 1) the slope of the CC signal is lower. But the lock-in range, as well as the zero crossing points are the same. Whereas the influence of different absolute amplitudes between the neighboured harmonics result in a shift of the zero crossing points dependent on the function f_{zc} defined in Equation 15. Also the distances between the zero crossing points are not equal.
This shift has no influence on any frequency transmission but a non negligible effect to the time synchronization, since every dt-shift is connected with a distance offset.
Since this offset is dependent on the detection setup, it is a constant failure which must be characterized.

2.6.2 BOCC Method

To reach highest resolutions the measurement system must be updated with a Balanced Optical Cross Correlator (BOCC). BOCC systems are already used for frequency distribution and for lengths stabilization ([34] [35]). Since space applications are in the focus of this thesis, the BOCC is characterized for space relevant properties.

To enable the method of BOCC the pulses of the reference and the target path must overlap. Therefore the time offset is zeroed as illustrated in Figure 31.

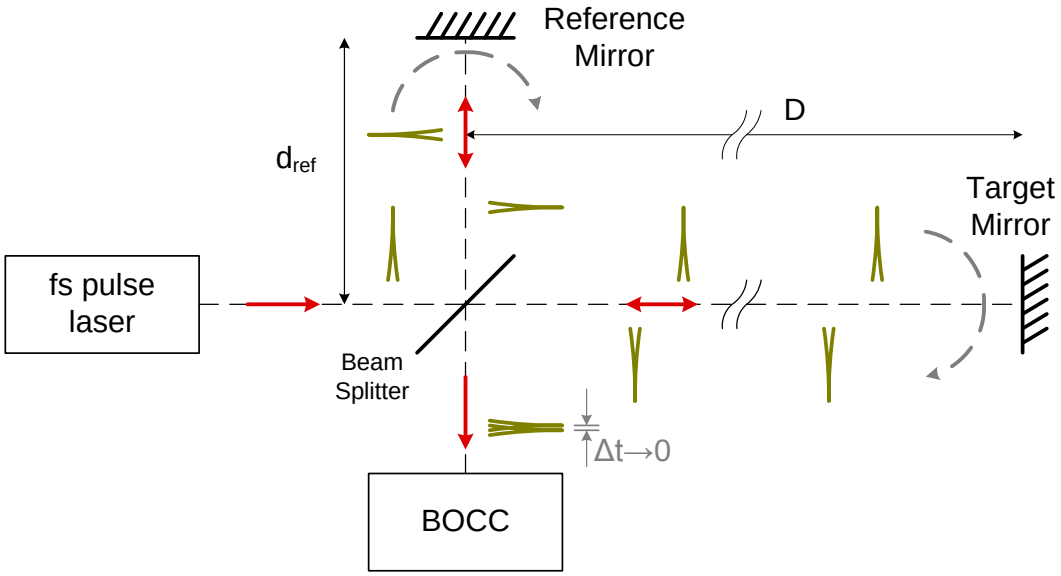

Figure 31: Additional BOCC setup included in the general setup

Frequency shift or changing the reference results in the modification of 'dt'. The FDDM method simplifies the adjustment since all harmonics are at their maximum when $\Delta t = 0$. Pulse durations of $t_{pulse} < 500$fs require special effort for overlap, because the pulse length correlates to $l_{pulse} = 1.5\mu$m. The BOCC function is only available at this region, whereas the FDDM CC method is applicable at any 'dt' value.

Within the BOCC setup the pulses are overlapped in a non-linear crystal.
For the propagation of an optical wave in optical materials the total polarization $\vec{P}$ is necessary. For higher intensities of the propagating laser pulse the energy level exceeds the linear region and the polarization must be defined by Taylor expansion [36].

$$\vec{P} = \varepsilon_0 \left(\chi^{(1)} \cdot \vec{E} + \chi^{(2)} : \vec{E}^2 + \chi^{(3)} : \vec{E}^3 + \mathcal{O}(4) \right) \tag{16}$$

with ε_0 = vacuum permittivity $\chi^j, j \in \mathbb{N}$ the j^{th} order tensor of susceptibility:
$\chi^{(1)}$ defines the linear refraction index of a material.

$\chi^{(2)}$ is responsible for second harmonic generation and sum-frequency generation.
$\chi^{(3)}$ as third order of nonlinearity influences the pulse. This order is responsible for the third harmonic generation, the four-wave mixing and the nonlinear refraction. Also the self phase modulation is included.

The second order of nonlinearity is essential for BOCC function. By using special materials or modified fibers $\chi^{(2)}$ can be amplified so that the second order effect exceeds the first and third order effect. The second order of polarization within a material provoked by an electric field $E(t) = Ee^{-i\omega t} + c.c.$ is defined as ([37])

$$P^{(2)}(t) = 2\varepsilon_0\chi^{(2)}EE^* + \left(\varepsilon_0\chi^{(2)}E^2e^{-i2\omega t} + c.c.\right) \tag{17}$$

The Second Harmonic Generation (SHG) term can be recognized by the 2ω exponent in Equation 17. The usage of material with a birefringent characteristics requires Phase Matching. Materials with ferroelectricity characteristics, e.g. perovskite-type crystals, can be used by applying Quasi-Phase-Matching.

These types of crystal posses in two directions different refractive indices: n_o in ordinary and n_e in extraordinary axis [37]. This birefringence $\Delta n = n_o - n_e$ is also a characteristic for the behaviour of the pulses propagating through the crystal. Because the refractive indices are different, the optical paths are different dependent on the optical axis. This dependency on polarization implies an additional requirement to the optical setup.

Rectangular pulses in n_o and/or n_e direction with time offset $dt = 0$ create SHG when phase of the SHG light matches the refractive index of one direction $n_{2\omega} = n_o$ or $n_{2\omega} = n_e$.
Two types of crystals for phase matching are defined [37]

Type I	The light is converted only from one axis to another with $n_{2\omega}^{o,e} = n_{\omega}^{e,o}$
Type II	The light of both axis are interacting with $n_{2\omega}^{o,e} = 1/2(n_{\omega}^{o} + n_{\omega}^{e})$

Type I crystals do not suit the BOCC purpose. Time shifts between pulses 'dt' result in change of SHG but the propagation direction is unclear. Both pulses propagate through the crystal with the same refractive index. There is no further information about the shift between the two pulses.

Type II is the proper choice because the rectangular axis has different optical path lengths. Therefore the pulses propagating through the crystal result in an additional time shift which is defined by the crystal length and its birefringence by $\Delta t_{add} = \frac{l_{crystal}}{\Delta n \cdot c}$.
Passing two times the crystal (forward and backward) the additional time shift is doubled.

Equation 17 shows that the conversion of the SHG light is oscillating since the phase does not match perfectly the SHG light. Since perovskite-type crystals, e.g. Potassium Titanyl Phosphate, have ferroelectric character the crystals can be periodically poled (PPKTP). The period of counter-direction polling is defined by original wavelength and birefringence of the crystal with $\Lambda = \frac{\lambda}{\Delta n}$.

This is called quasi phase matching and is limited to a narrow bandwidth of wavelength.

Important to know that values like periodicity of the crystal or dimension of the converting area are in the micro-meter area. This implies challenging handling of the used optic setup. Also the robustness of the setup depends on the simplicity of the conversion.

As mentioned before, an additional time offset occurs during propagating forward and backward through the crystal. This additional time offset can be seen, since one pulse is faster than the other. Within the crystal the faster pulse pass partly by the slower one. This results in a fractional autocorrelation of the pulses.
Forward and backward are then resulting in a fractional autocorrelation in both directions.

To have similar intensities of the SHG light forward and backward, the additional time shift must be between the incoming rectangular pulses. An illustration of the time shift between the pulses can be seen in Figure 32.

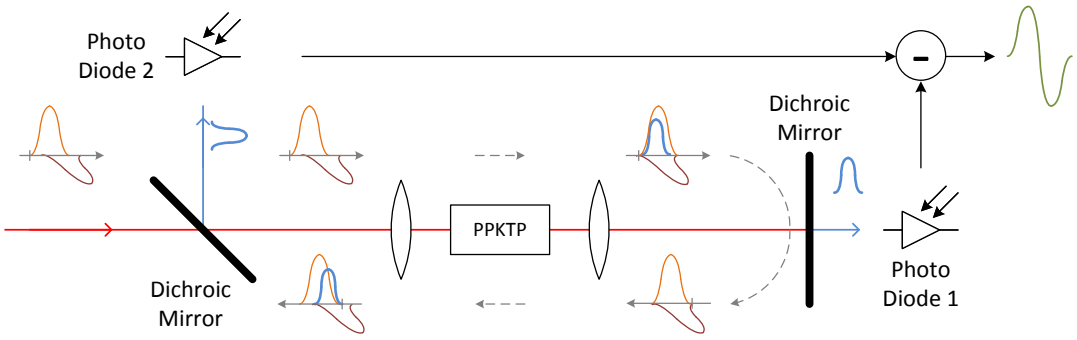

Figure 32: General functionality of a BOCC setup

The incoming rectangular pulses pass a dichroic mirror which is transparent for the origin light and reflective for the SHG light. The light beam must be focused within the crystal. A precise adjustment of the focusing lens maximises the SHG intensity ([38]) and results in a higher performance of the BOCC setup. After forward propagating the crystal, the light must be collimated again to reach a second dichroic mirror. The second mirror is transparent for SHG light and reflective for the origin light. The pulses pass backwards the crystal and create SHG light again and an additional time shift between the pulses.

The SHG light is 'filtered' by the dichroic mirrors. Optical detection units measure their intensities. Subtracting the measured SHG intensities of the detection units of each other results in the BOCC specific s-shaped form.
With modification of the time shift the complete BOCC signal can be fully characterized. As can be seen in Figure 33 the BOCC signal has its zero crossing point when the pulses have the Δt_{add} before propagating.

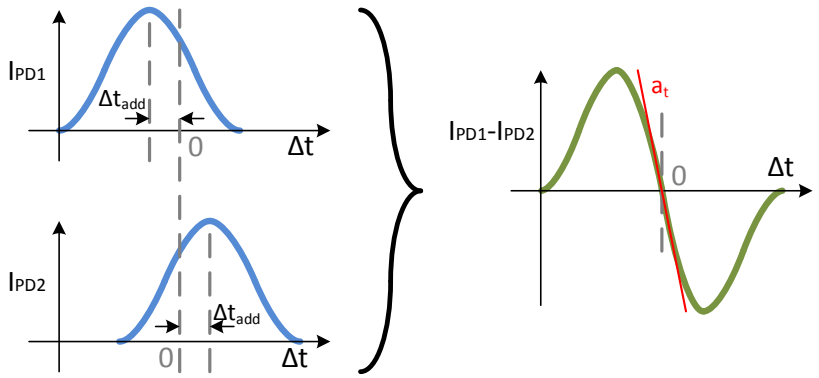

Figure 33: Creating the BOCC differential signal

The grade of SHG conversion defines the BOCC signal and its sensitivity (a_t) at its zero crossing point (dt_{zc}). This is important for the performance of a BOCC system used for time and frequency transfer.

This section is a summary of the BOCC system with general information about its functionality. The main focus is the complexity of SHG generation and detection. Polarization, precise optical setup and SHG generation of pulses with $t_{pulse} < 500\,fs$ is resulting in a complex system.

2.6.3 CC Resolution

The signal output of any CC setup results in a distance resolution, since any shift of the repetition rate can be recorded/stabilized. The slope "a_x" generated by any system (FDDM CC or BOCC) the intensities defines the resolution of the system with

$$\Delta s = \frac{\Delta U}{a_s} \Rightarrow \Delta t = \frac{\Delta U}{c \cdot a_s} = \frac{\Delta U}{a_t} \tag{18}$$

Two different types of slopes can be implemented:
The slope dependent on lengths variations a_s in $\frac{Volt}{meter}$
or the slope dependent on time variations a_t in $\frac{Volt}{second}$.

Dependent on the required value, a_s (for distance resolutions) or a_t (for time/frequency resolution/distribution) can be used. Typical values in this thesis for a_s are in the range of $\frac{mV}{mm}$ and for a_t is within the range of $\frac{mV}{ps}$.
Also an important fact is that every Δs and equivalent Δt is correlated with the time resolution of the system between two points. Assuming that the the path between to points is known within Δs the transport of a signal with optical pulses refer to a uncertainty of the time in $\Delta t/c$. Therefor it can be defined that

$$t = \frac{1}{f} \Rightarrow \Delta t = \frac{-\Delta f}{f^2} \xrightarrow{|t| \to \tau} \frac{\Delta t}{\tau} = \frac{\Delta f}{f}$$

The value τ is hereby the integration time of the measurement. This equals to the Allan Deviation

$$\sigma_y(\tau) = \partial_t \Delta t = \frac{\Delta s}{c\tau} \tag{19}$$

In conclusion any measurement system with a time / length resolution better than a local oscillator is usable for time and frequency transmittance.

It must be mentioned that a time/frequency transfer can only be as good as the frequency source on which the system is stabilized. The here mentioned methods for time and frequency transfer are therefore ”only” links between two points. Aim of the setup is to create a connection between two points for time and frequency transfer without any loss of information or stabilization.

Since frequency transmittance depends on the deviation of the lengths resolution, the time transmittance results directly from the absolute distance.

The information of length jittering / frequency jittering can also be used to characterize the optical oscillators.
Each CC system creates a slope a_s or a_t where the signal depends on voltage.The higher the jitter of the voltage, the higher is the inaccuracy of the system. When a stabilization loop is installed, the measurement of the failure signal results in the possible stabilization limit of the oscillator with [6]

$$\sigma_y = \frac{\Delta l}{c} = \frac{\Delta s}{c} = \frac{\Delta U}{a_s c} \quad \text{and} \quad \sigma_y = \sqrt{\int_{f_{min}}^{f_{max}} df\, S_y(f)} \tag{20}$$

The power spectral density ($S_y(f)$) can hereby measured using the recorded failure voltage of the stabilization system.

In summary the slope of the error signal of FDDM CC or BOCC (a_x) result in time and frequency resolution for the pulse dependent measurement system. This is the main characteristic of any system. The value of a_x defines the whole applicability either distance resolution or time and frequency transfer. Main target is to create highest slopes for most precise systems and handling with these slopes for measurements and stabilizations.

3 Setups and Characterizations

In this section a detailed overview of the different measurement setup is given.
In Section 3.1 the optical oscillators used in this thesis are described and characterized. These two used oscillators use two different types of technologies as well as different stabilization units.

Afterwards in Section 3.2 the used electronic setups especially designed for this thesis are shown. General electronic devices (frequency counter, electronic spectrum analyzer, analogue devices) are not further described.

In Section 3.3 the interaction between the electronic and the used optical oscillators are explained, to get an overview how modification and stabilization of repetition rate is done.

Since some free beam setups are necessary for measurement and characterization Section 3.4 describes those setups and their modifications.

All setups are especially designed to fulfil the requirements defined in Section 2.4. This implies not only the measurement performances. Since the systems are predefined for space applications also compactness, robustness, automation and handling are in the focus of their design.

3.1 Optical Oscillator Characteristics

Within this thesis two different types of optical oscillators are used. Both oscillator have short pulses with pulse durations about 300 fs. For amplification of the pulses the element Erbium is used with its maximum amplification at 1560 nm. The oscillators use Polarization Maintaining (PM) fibres. Handling with polarization dependent effects is easier using PM fibres compared to standard single mode fibres.

3.1.1 SESAM Oscillator

The function of the first oscillator used in this thesis is based on Semiconductor Saturable Absorber Mirror (SESAM).

This oscillator is already used in a further study described in more detail in [20].
Some excerpts are shown here to have an overview of the system, and how to use it for measurements.

The simplified setup of the SESAM oscillator is illustrated in Figure 34.

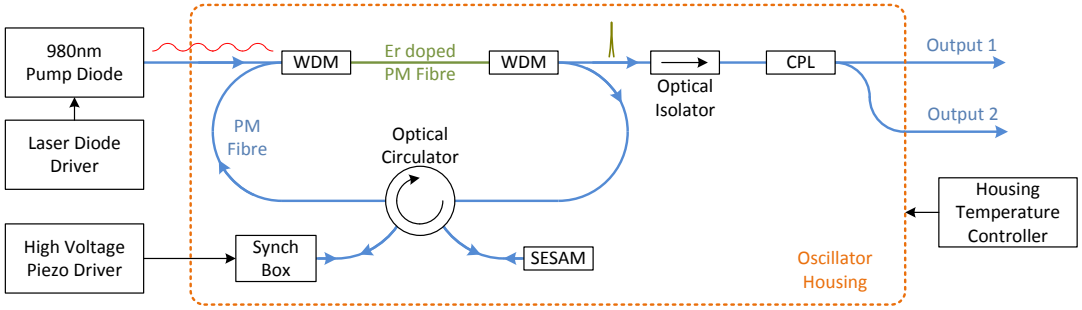

Figure 34: simplified setup of the used SESAM oscillator

The oscillator itself consists of an input fibre for a pump laser. Wave Division Multiplexers (WDM) connects the pump laser with the inner circle or to separate partly the created pulses to the output fibre. The ring contains PM fibre, Er doped PM fibre for amplification, a SESAM mirror for mode locking, a Synchronization Box (SynchBox) for modification of the repetition rate and an optical circulator. Since reflections back into the oscillator creates disturbances in function, an optical isolator prevent from backward propagating photons. This oscillator has also two optical outputs created by an optical Coupler (CPL).

The ring oscillator is pumped by a 980 nm pump diode which is controlled by a laser diode driver. The oscillator contains the SESAM to create short pulses. To start mode locking, the pump diode is modified. Once mode locking is achieved, the pump power can be shifted to modulate the output power. A detailed description can be found in [20].

Within this thesis, the pump power is not modulated in short time ($f_{mod} < 1$ Hz). This would be necessary when the oscillator is updated to use as an optical frequency comb. The Carrier Offset Frequency can then be modulated and stabilized.
Within this thesis 'only' the optical output power is important for further applications. Thus the pump power is set at the beginning of each measurement setup and then kept constant. Important to know that this oscillator is sensitive to pump power jitter. Pumping jitter results in jitter of optical output power of the oscillator. This has an influence on the FDDM method, since the amplitudes of the multiple harmonics are influenced by the jitter. The less jitter the optical oscillator generates, the better the resolution of the FDDM method (see Section 2.5). Therefore the pump diode is set to a point where less jitter occurs.

The created pulses propagate also to the SynchBox which is used for frequency modulation. Figure 3.1.1 shows the setup of the SynchBox and lists the frequency modulation.

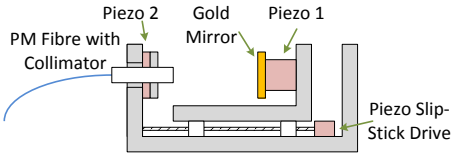

Property	Slip-Stick	Piezo 1	Piezo 2
Freq. shift	185 kHz	350 Hz	60 Hz
Stroke	200 nm/Step	6 μm	1 μm
Bandwidth	$<$ 1Hz	$<$ 20 kHz	$<$ 20 kHz

Figure 35: Synchronization Box for repetition rate adjustment

As can be seen in Figure 3.1.1, the SynchBox is the only part within the oscillator which is not in fibre. The pulses propagate a collimator and are reflected back into the collimator by a gold mirror. The collimator itself is mounted on a piezo crystal. The gold mirror is mounted on a piezo crystal as well. A piezo slip stick drive can be used, which moves the whole gold mirror setup.

The piezo slip stick drive has the largest frequency shift of all three piezo elements. The repetition rate can be changed up to 185 kHz. Since the drive moves the mechanical setup, the modulation frequency is slow. Therefore it is used generally only for rough frequency adjustment and then kept constant. This is important, since the frequencies of both optical oscillators must have equal frequencies if frequency stabilization is need.

The piezo element connected with the gold mirror is then used for stabilization of the repetition rate. The modulation frequency is limited by the used high voltage piezo driver to $f_{mod} < 1$ kHz which is sufficient for stabilization since the frequency stability is less than 1 Hz. And the frequency range of 350 Hz is also sufficient to be stabilized without time limit.

The complete oscillator is within an aluminium housing. Since temperature fluctuations cause frequency shifts, the housing is temperature stabilized using a temperature controller. The housing temperature can be kept constant within $\Delta T < 0.01$ K. The temperature control can also be used, to manipulate the repetition rate of the oscillator.

3.1.2 CNT Oscillator

The second oscillator used in this thesis is based on the Carbon Nano Tube (CNT) technology for mode locking [39] [40].

This technology promises a simple handling compared to other mode locking systems (SESAM). A fibre connector can be covered by a CNT solution which is covered again with a protection solution. By closing the ring of the fibre connector the oscillator is ready. Of course dispersion management and exact frequency determination are challenging. Within a further master thesis the oscillator is created and characterized [41]. Here only its mayor characteristics are shown.

The setup is shown in Figure 36.

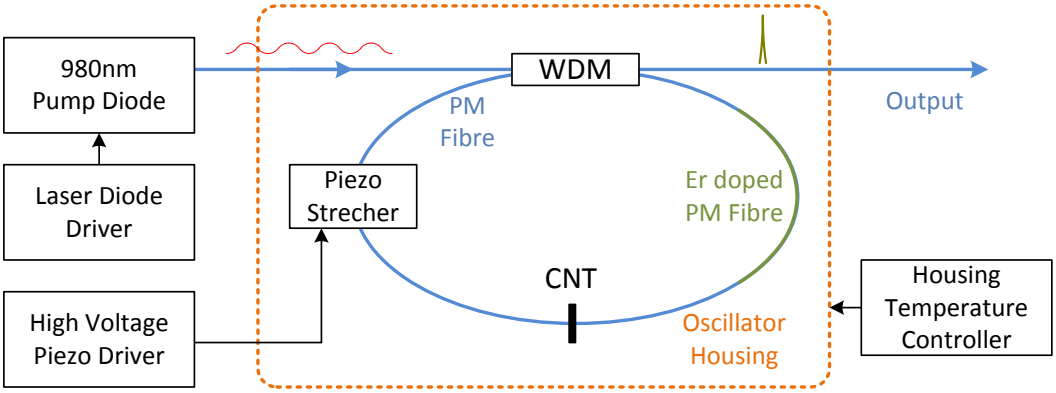

Figure 36: simplified setup of the used CNT oscillator

The CNT oscillator is designed as a ring oscillator (same as SESAM oscillator).
As can be seen in Figure 36 the oscillator design is simpler compared to the SESAM oscillator, since less passive components (circulator, WDMs) are used. The pump laser is connected with a Wave Division Multiplexer. This WDM is also capable of act as a in fiber coupler. A part of the generated pulses are separated from the ring as an optical output.

The pump laser reaches a Erbium doped fiber for amplification. The CNT covered fiber connector is then responisble for mode locking. With the pump power the mode lock can be activated. Once activated, the output power of the oscillator can be modulated by changing the pump power.

The ring length correlates with the repetition rate of the oscillator. The SESAM oscillator with its frequency about 79 106 000 MHz ([20]) is the target for the frequency of the CNT oscillator. The fibre ring is installed within an aluminium housing. Its temperature is kept constant using a temperature controller to $\Delta T < 0.01$ K.

For stabilization of the repetition rate in short time a piezo stack is connected to the ring as can be seen in Figure 3.1.2.

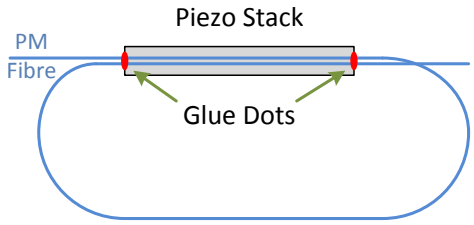

max. Frequ. Shift	Stroke	Bandwidth
800 Hz	32 μm	40 kHz

Figure 37: Piezo Strecher for repetition rate adjustment

The fibre of the ring is pretensioned and glued to a piezo stack. If voltage is applied to the piezo stack, the repetition rate lowers. By using a fiber loop the frequency shift can be doubled. The piezo stack has a frequency shift of 800 Hz using voltages up to 150 V. The control bandwidth is limited by the high voltage piezo driver to $f_{mod} < 1\,kHz$. This is sufficient since the frequency stability of the oscillator is less than 1 Hz.

The repetition rate of the CNT oscillator can totally be modified with housing temperature in long time within several kHz and in short time by the piezo strecher. Nevertheless the CNT oscillator is not as flexible in frequency as the SESAM oscillator with its SynchBox. Therefore if both oscillators are used, the repetition rate of the SESAM oscillator is modified (piezo slip stick driver) to reach the CNT repetition rate.

CNT oscillators are still in development phase. The handling of the CNT layer with protection cover is challenging. A mode lock state is comparatively easy installed, but imperfection at production or long time usage result in a degradation of the CNT layer. After long time usage, the CNT layer looses its mode locking property.

But the CNT technology has its advantages in simplicity, handling and performance. To create a passive mode locked laser manageable hardware requirements have to be observed (CNT liquid, cover emulsion, dispersion control and length control [41]). Also the usage of PM fibres creates the possibility of polarization dependent applications. In contrary to the SESAM oscillator this oscillator is completely in-fibre (no SynchBox) and therefore robust against mechanical influences. During the tests, the oscillator shows less correlation to pump jitter, which is an additional advantage for the FDDM method.

By further development of this technology the disadvantages can be improved or solved, thus the technology promises a money saving opportunity with highest performances for any applications on ground or space.

3.2 Electronic Devices

For control of the oscillator and for different measurements, electronic devices are specially created. The overall performances are described in this section. Some interesting facts are explained in more detail in the Appendix. If the reader is interested in the completely detailed hardware setup, further references are mentioned in this section as well.

In Section 3.2.1 a synthesizer board is described which is designed for low noise applications. The board is additionally implemented for multiple other boards as well.
Since frequency measurement is an important factor for frequency transportation a frequency comparator is designed, which is described in Section 3.2.2.
For the FDDM method a FDDM Board is created. Its setup is described in Section 3.2.3.
To create the FDDM CC signal a Subtracter Board is created, which is shown in Section 3.2.4.

3.2.1 Low Noise Synthesizer Board

The used oscillators are not specificly designed for a 'common' frequency like a multiple of 10 MHz. The frequency of the oscillators is about 79 106 500 Hz. Since the frequency is absolute necessary for precise measurement, the generation of the frequency must be done equally. Therefore a synthesizer specially created for this purpose fulfils the required stabilities and accuracies with the combination of compactness and possibility of variability.

The requirements for the synthesizer board are:

- best frequency stability
- automated function
- frequency flexibility
- applicable for space

A simplified overview is shown in Figure 38

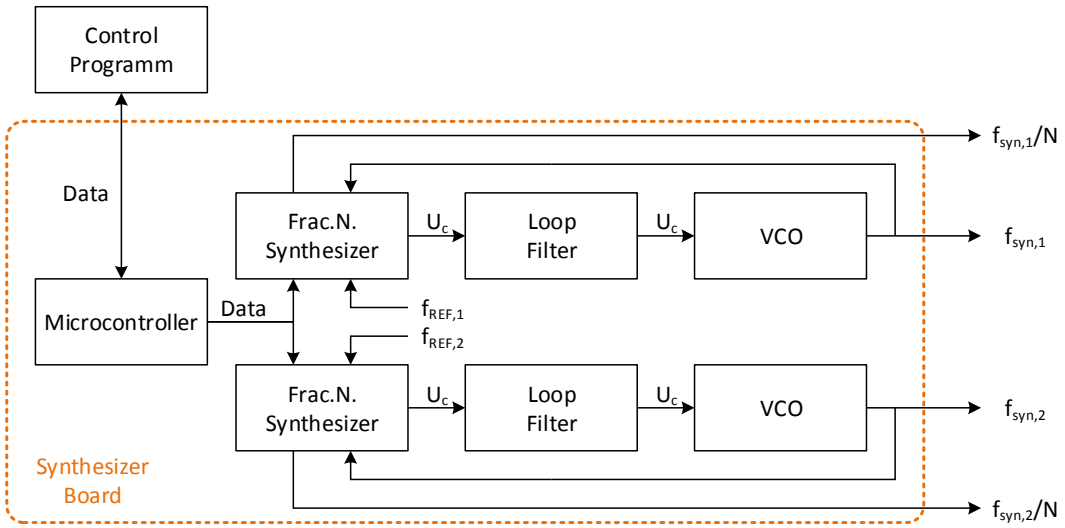

Figure 38: Schematic setup of the designed synthesizer board

Frequency sources are ultra low noise Voltage Controlled Oscillators (VCO). They are controlled by a fractional N synthesizer which is a digital device with multiple functions ([42]). The control loop of synthesizer and VCO is closed by a loop filter which is essential for the overall performance.
The frequency input can be any frequency source: Frequency Standards (Rb-Standard, H-Maser) or the repetition rate of the optical oscillators itself.
Since the synthesizer requires digital input for controlling, a micro controller is used for primary programming of the synthesizer. It also is used as interface between synthesizer and control program. For simple usage, the control software is programmed with LabView.

For best frequency stabilities, ultra low noise VCOs are used. Generally the frequency of a high stable oscillator stays constant over longer time ($t > 1\,s$). Thus VCOs are in use with low

modulation frequency $f_{mod} < 100\,Hz$ which results in low phase noise performances. Standard noise characteristics of VCO used in this thesis are $S_\Phi(10\,Hz) < -80\,dBc/Hz$ and $S_\Phi(1\,MHz) < -150\,dBc/Hz$.

The control of the VCOs is done by Fractional N Synthesizers. Their advantage is the frequency resolution of 38 bit ($\approx 2.7 \cdot 10^{11}$). This enables any fine adjustment of frequency. The N-Synthesizer is also capable for frequency division by 2^n with $n \in \{0, 1, 2, 3, 4, 5\}$ ([42]). The fractional part is then a short pulse output as can be seen in Figure 38 by $f_{syn,x}/N$.

The frequency flexibility is in conflict with the stability of a VCO. The higher the frequency range of a VCO the higher the phase noise. Therefore one synthesizer board contains two VCOs which create a multiple frequency output. Following frequencies are available.

f_0 of VCO [MHz]	f_0 / 2 [MHz]	f_0 / 4 [MHz]	f_0 / 8 [MHz]
$400 \approx 5 \cdot f_{REP}$	200	100	50
$640 \approx 8 \cdot f_{REP}$	$320 \approx 4 \cdot f_{REP}$	$160 \approx 2 \cdot f_{REP}$	$80 \approx 1 \cdot f_{REP}$
$960 \approx 12 \cdot f_{REP}$	$480 \approx 6 \cdot f_{REP}$	$240 \approx 3 \cdot f_{REP}$	120

With this combination of VCOs every necessary multiple of repetition rate can be generated. All VCOs have sufficient frequency shift, to reach the specific frequency of $f = x \cdot 79\,600\,500\,Hz$ [20]. Also if a comparison with a frequency standard (H-Maser) is required, 100 MHz can be generated.

An important part of the Synthesizer Board is the Loop Filter and its correlation to the connected oscillator type (VCO or optical oscillator). The issues and its management is described in more detail in Appendix C.

In summary a Synthesizer Board is created for highly stable frequency generation. The measured frequency stability of $\sigma_y(1\,s) = 2 \cdot 10^{-13}$ is sufficient for the applications within this thesis. The frequency adjustment is done automatically with a software controlled micro controller and the digital synthesizer. To create variable frequencies with high stability, the board is set up with various VCOs. The synthesizer internal divider allows to create all necessary frequencies. It can be also adapted to be connected directly to an optical oscillator. All used electronic devices are available for space applications with space qualified devices.

3.2.2 Frequency Comparator

For verification of the Synthesizer Board a phase comparator is used (see Appendix C, [43]). This phase comparator has only the possibility of a 100 MHz input as reference and measurable frequency. This is not applicable for further measurements since the optical oscillators have frequencies at about 79 MHz which can vary up to 185 kHz. Therefore a low noise frequency comparator is created to measure every occurring frequency with the same resolution that the stability of the synthesizer board.

The frequency comparator is designed and created within a Bachelor Thesis [44] which was initiated and supervised by the author of this thesis. The excerpts here are an overview describing the specific functions.

The name 'frequency comparator' is different from the high precise phase comparator, since with this setup frequencies are compared. The phase comparator defines its input with 100 MHz and the phase difference between the reference and the input is monitored.

With this setup, the frequency itself is monitored with high precision. The general principle can be seen in Figure 39.

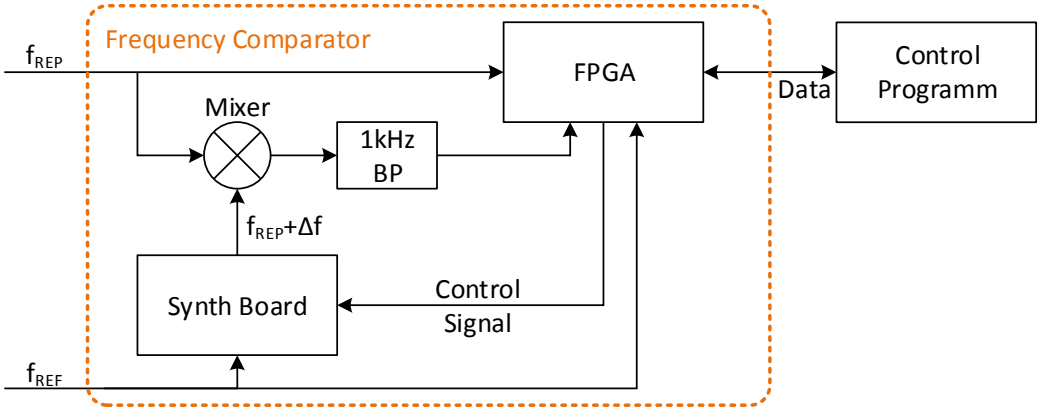

Figure 39: Schematic setup of the high resolution frequency counter

For autonomic functions, a Field Programmable Gate Array (FPGA) is used. Its advantage lies within its speed of data administration, data control and the communication with other software and hardware. The FPGA as a simplified processor has the possibility to create a complete autonomous device which can be adapted to any electronic function. Since space qualified FPGAs exist this board is also adaptable for space applications.

The frequency comparator board has two inputs. One is the reference signal (e.g. 10 MHz of Rb-Standard) and the second is the frequency which is to be measured (e.g. repetition rate of the optical oscillator). The reference input serves for the synthesizer and for the FPGA whereas the FPGA has itself an additional 200 MHz reference quartz oscillator.

For a rough frequency measurement the repetition rate is measured directly by the FPGA using the method of a reciprocal frequency counter [45]. Within 10 ms the frequency can be measured with an accuracy of $\Delta f < 60$ Hz. This rough frequency count is necessary to adapt the Synthesizer Board. In parallel the frequency measurement of the FPGA continuous.

When the frequency is roughly known the synthesizer board is adapted to the repetition rate, with an offset of about 1 kHz. As mentioned in Section 3.2.1 the synthesizer board creates frequen-

cies with stabilities until $\sigma_y(1\,s) = 2 \cdot 10^{-13}$. This frequency is then mixed with the repetition rate. The created interference frequency f_{IF} is filtered with a bandpass with its centre frequency at $f_{BP} = 1\,kHz$.

The repetition rate can be described as

$$f_{REP} = f_{IF} + f_{syn} \quad \text{with} \quad f_{IF} = \frac{N_{IF}}{N_{FPGA}} f_{FPGA}$$

where

N_{IF}	is the counter value of the interference signal (1 kHz, $N_{IF}(1\,s) = 10^3$)
N_{FPGA}	is the counter value of the FPGA reference signal (200 MHz, $N_{ref}(1\,s) = 2 \cdot 10^8$)
f_{FPGA}	is the FPGA internal reference signal (200 MHz)

The duration of the GATE time is coupled to the frequency which is to be measured. The start time of the GATE timer is connected to the input frequency f_{IF} and starts counting until the predefined integer N_{IF} is reached (reciprocal frequency counter). In parallel the counter of the reference frequency f_{PPGA} starts as well. When N_{IF} is complete the FPGA calculates with the prior defined equation the frequency f_{IF}, and continuous the next measurement.
Since N_{IF} stays constant, the error of this measurement method is defined by the counter value N_{FPGA}. The integer failure can be maximum 1 counter value. This results in a failure of

$$\partial_{N_{FPGA}} f_{IF} = \partial_{N_{FPGA}} \frac{N_{IF}}{N_{FPGA}} f_{FPGA} = N_{IF} f_{FPGA} \frac{-\Delta N_{FPGA}}{N_{FPGA}^2}$$

$$\Rightarrow \Delta f_{IF} = f_{IF} \frac{\Delta N_{FPGA}}{N_{FPGA}}$$

$$\text{with} \quad f_{IF} = 10^3 Hz \quad N_{FPGA}(1\,s) = 2 \cdot 10^8 \quad \Delta N_{FPGA}(1\,s) = 1$$

$$\Delta f_{IF}(1\,s) = 5 \cdot 10^{-6} Hz$$

The accuracy of a 1 s measurement time can be calculated with

$$\sigma_y(1\,s) = \Delta f / f_0 = \frac{\Delta f_{IF} + \Delta f_{syn}}{f_0}$$

$$\frac{\Delta f_{IF}(1\,s)}{f_0} = \frac{5 \cdot 10^{-6} Hz}{8 \cdot 10^8 Hz} = 6 \cdot 10^{-14} \qquad \frac{\Delta f_{syn}(1\,s)}{f_0} = 2 \cdot 10^{-13}$$

$$\Rightarrow \sigma_y(1\,s) < 3 \cdot 10^{-13}$$

The noise of the synthesizer board is about three times higher than the error signal of the reciprocal frequency counter system. The system of the frequency counter could also be used to

measure H-Maser frequency without loss of information.

In summary the frequency comparator is specially designed for the application of repetition rate detection. Its measurement speed and its automatic function are the two highest advantages of this device. All occurring frequencies within this thesis can be detected using the internal synthesizer board for creating an interference frequency which is then precisely detected by a FPGA. The frequency is continuously measured and the data is communicated to a software program (LabView) which calculates the frequency. The measurement rate of this frequency comparator is limited to the interference frequency f_{IF}.

3.2.3 FDDM Board

The FDDM Board is an essential part of all electronic devices since every further development (FDDM CC) is done after having the possibility to measure several harmonics independently of each other. The description how to measure the FDDM signal is already given in Section 2.6.1. This section describes the setup and characteristic of the FDDM Board in detail.

This board is designed and created within a Master Thesis [46] which was initiated and supervised by the author of this thesis.

The task of this device is to separate several harmonics from each other and create an output who is related to the amplitudes of the harmonics. The created setup is shown in Figure 40.

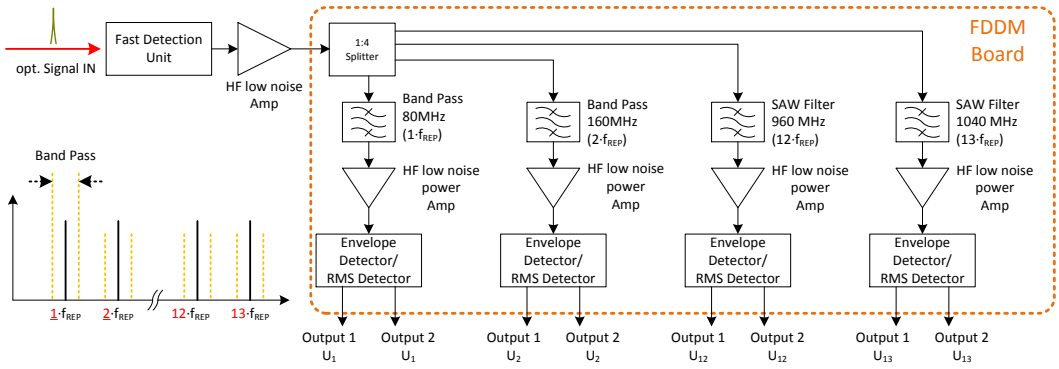

Figure 40: Schematic setup of the FDDM board for harmonic separation and detection

The input for the FDDM Board is the broad spectrum of the fast detection unit. The signal is divided in four different paths by a broadband frequency splitter. After the splitter there are bandpass filters which select one specific harmonic for each path: $1^{st}, 2^{nd}, 12^{th}, 13^{th}$. Afterwards the separated harmonics are amplified. The amplitude detection is done by a envelope detector which has multiple outputs for measurements.

A main focus lies in the balance of the amplitudes of the 12th and 13th harmonic since with them the FDDM CC signal is created. Nevertheless the amplitude management of the first and second harmonic is also important to receive clear voltage measurements.

The general hardware setup and its issues dependent on amplitude variations are explained in Appendix D. Target is to reach high Signal to Noise Ratio (SNR) from each harmonic including a similar/equal amplitude.

In summary a device is created which separates the 1st, 2nd, 12th and 13th harmonics. The amplitudes are controlled that after the envelope detector voltages of $U_{out} \approx 2\,V$ are reached. Two outputs are available: one for precise measurements or stabilizations (U_{ENV}) and one for additional monitoring (U_{RMS}). The modulation bandwidth of the harmonics is with $f_{mod} > 1\,MHz$ sufficient for any application in this thesis. The amplitudes of the harmonics are not completely equalized which must be done afterwards with the Subtracter Board, described in Section 3.2.4. Since all electronic devices are available with space qualification the board can be adapted for space applications.

3.2.4 Subtracter Board

The Subtracter Board is compared to the other electronic devices a simple setup. It contains an operational amplifier, a Proportiaonal Integral and Differential (PID) controller, an offset and gain controller and a low pass filter.
Nevertheless the modification of the amplitudes of the harmonics is an essential part of the functionality of any CC method (FDDM CC or BOCC). Therefore this board must be designed properly for each application.
The setup is illustrated in Figure 41.

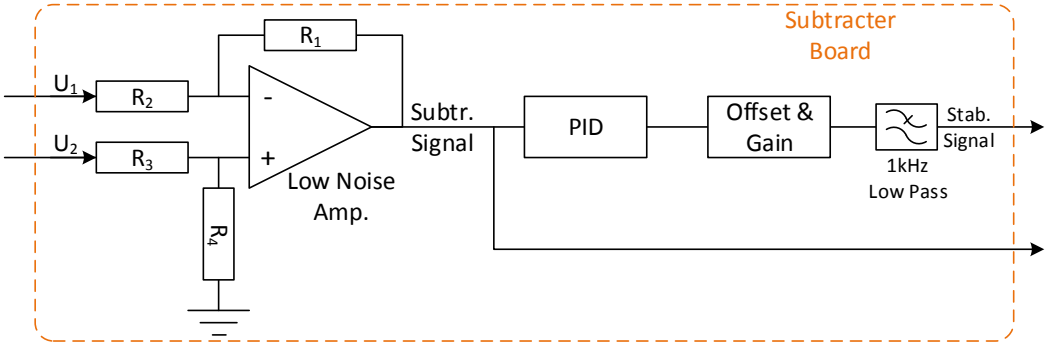

Figure 41: Overview of the subtractor board to create a stabilization signal

The operational amplifier is designed as a subtracter of the inputs U_1 and U_2. The subtracted signal can be modified by changing the resistors values with

$$U_{\text{substr.}} = \frac{(R_1 + R_2)R_4}{(R_3 + R_4)R_1} U_2 - \frac{R_2}{R_1} U_1$$

The adjustment of the subtracted signal is especially important for the FDDM CC signal as described in Section 2.6.1. Since the voltage outputs of the FDDM Board have no equal amplitudes, the adjustment has to be done with the resistors. Target is to modify the subtracted signal to a norm FDDM CC signal. Also amplification of the CC signal to receive higher slopes is done with this setup. A Subtracter Board is then adjusted to one specific FDDM Board.

For the BOCC setup, the Subtracter Board is less crucial since the electronic outputs of each photo diode (forward and backward) can be amplified directly at the measurement device. Even when amplitude inequality influences the absolute distance resolution, the failure is minimized by the pulse duration itself.

The subtracted signal is divided into an output for monitoring and to PID controller. The monitoring output is used to measure the origin CC signal. CC slope and zero crossing points are defined by this output. Dependent on the resistor values, the CC signal gets its characteristic.

The PID controller values depend on the slope of the CC signal and must be adjusted to each oscillator. Since the overall modulation frequency is limited by the piezo stacks to 'only' 1 kHz the D-part of the controller is not in use.

Since $U_{\text{subtr.}}$ varies between $\pm 5\,\text{V}$ and the high voltage amplifier for the oscillators can only handle positive voltages, the PID output is modified by an offset and gain unit. The output signal should be $U_{\text{out}} > 0\,\text{V}$.

Finally the output signal is filtered by a 1 kHz low pass filter. The high voltage amplifier of the oscillators limited to this modulation frequencies. To avoid additional noise for stabilization also the voltage is filtered.

In Summary the Subtracter Board contains simple electronic devices compared to the other created devices. Its input are two voltages from the measured harmonics of the FDDM Board or the BOCC setup. One of its output is a stabilization signal for high voltage amplifiers with $U_{\text{out}} \in [0\,\text{V}, 5\,\text{V}]$. The second output is a monitor signal to control the stabilization performance.
Even if it is a comparatively simple setup, it has a very strong impact of further stabilizations, since the CC signal is modulated within this device. Also necessary is the usage of low noise electronics that the electronic is not the limit factor of any stabilization.

3.3 Interaction Oscillator and Electronic Devices

The two different oscillators are installed within a setup which is then defined as 'Oscillator Setup'. Each setup has then similar controlling, stabilization inputs and outputs:

Controls	Inputs	Outputs
Pump Power	Stabilization Signal [0 V, 5 V]	500 fs Pulses, $P_{RMS} < 10$ mW
Temperature	Piezo Driver Input (for SESAM Oscillator)	$x \cdot f_{REP}$, $P_{out} \approx +5$ dBm

The two Oscillator Setups are similar in performance and handling. This enables fast transposition between two systems since interfaces are equal. Some measurements need high frequency variability (SESAM oscillator), others need low jitter performance (CNT oscillator). Or a measurement can be verified with both systems.
The setup can be seen in Figure 42.

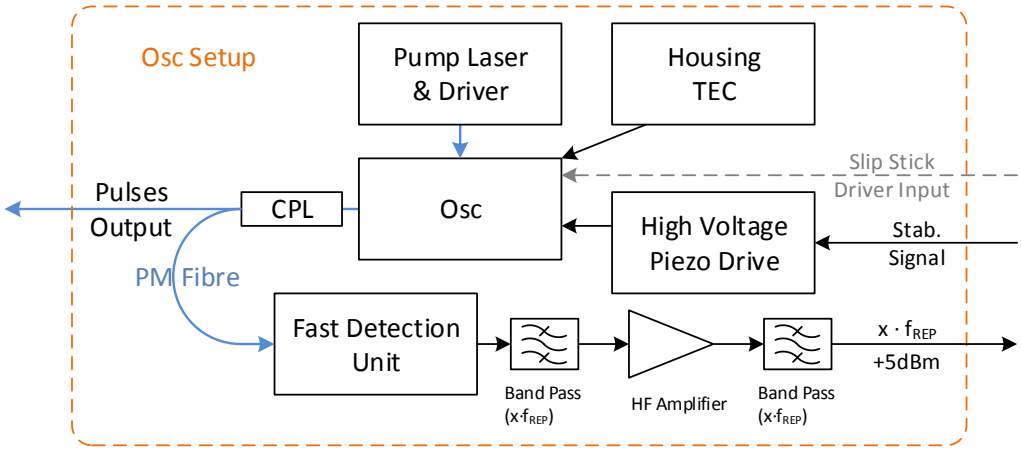

Figure 42: Setup to stabilize the oscillator with a stabilization signal

For repetition rate stabilization a Rb-Standard is used. Its performance is limited to $\sigma_y(1\,s) = 10^{-12}$ (see Section 2.2). The frequency generation is done by the synthesizer board or a frequency generator. The frequency generator has even more variability but with less performance. Both systems generate a frequency which is a reference for the repetition rate. A PID controller is necessary to stabilize the repetition rate to the created frequency.
By modification of the synthesizer board, the control of the repetition rate is also possible without additional PID controller and VCO.
Both possibilities to lock the repetition rate to the Rb-Standard are illustrated in Figure 43.

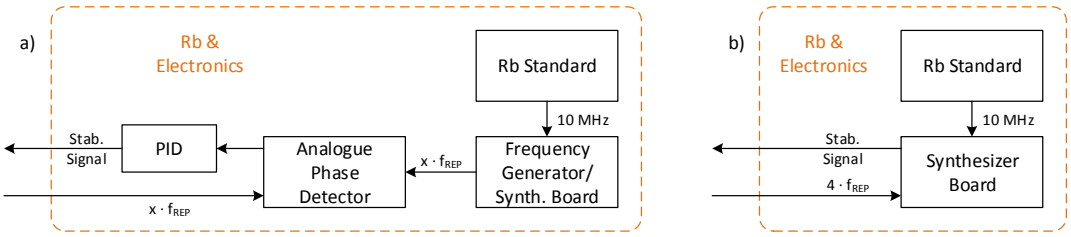

Figure 43: Two possibilities for a stabilization unit for the oscillator setup

In Figure 43 a) a standard system for stabilization can be seen. A frequency generator or the synthesizer board can be used to create the required frequency. A PID controller receives the input of the generated frequency and the repetition rate. The controller output is then adapted to the controlled oscillator.

In Figure 43 b) the voltage output of the synthesizer is connected to the oscillator system after the loop filter: using the optical oscillator instead of the VCO (see Figure 38). Since the optical oscillator has very low phase jitter ($S_y < 1\,\text{fs}$) the adaption of the loop filter is simpler compared to a VCO because a lower noise figure must be handled. The PLL to control the repetition rate is then designed especially for one optical oscillator.
Because the synthesizer has a voltage output of $U_{out} \in [0\,\text{V}, 5\,\text{V}]$ it is ready to use.

The disadvantage of the direct use of the synthesizer is that the synthesizer is not designed to handle low frequencies ($f_{REP} < 300\,\text{MHz}$). Therefore the 4^{th} harmonic is selected ($f_0 \approx 316\,\text{MHz}$) and stabilized with the synthesizer system. Creating adequate frequency filters is still manageable at this frequency without special HF hardware.

3.4 Free Beam Setups

Within the complete setup some free beam parts are used. These are necessary to verify the FDDM method, the BOCC and the stabilization of a defined lengths. Also different measurement methods need different optical setups.

3.4.1 Michelson Setup

At the beginning of Section 2.5 in Figure 13 it is already mentioned that a Michelson Setup is required for any measurement method. Figure 44 shows the Michelson setup used in this thesis.

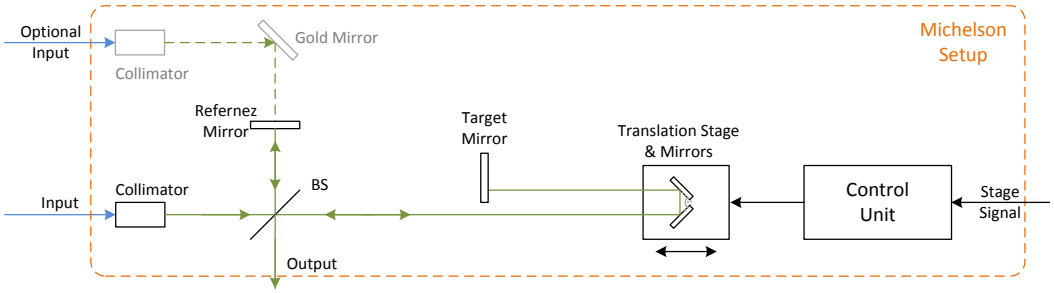

Figure 44: Michelson Setup to modify different path lengths and for measurement of FDDM signal

The setup is as typical as any Michelson Setup. The incoming pulses transmit through a beam splitter (BS) and are separated on the reference path and the target path. The reference mirror is coated with gold to ensure reflectivities $>$ 95% at 1560 nm .
The way to the target passes a rectangular mirror construction to another gold mirror.
The target and reference mirror are adjusted, that after passing the beam splitter again, the pulses ways are overlapping.
The translation stage is used, that the target path can be modified in lengths. The lengths modulation is required, to verify the signal change of the FDDM signal or the CC signals. Two different translation stages are used. One can be moved over 2 cm with step sizes about 1μm. The other has a slide length over 30 cm with a resolution at about 100 nm. The stages are not used in parallel. The last one is used only, when highest resolutions are required (BOCC). Otherwise the first stage is in use.
As can be seen in Figure 44 the pulses have to propagate two times the mirror construction which results in a doubled movement of the translation stage.
The movement of the translation stage is controlled by a control unit which can be operated manually or by a software program like LabView.

It is also possible to add another optical input. Hereby the reference mirror is used as an adjustment mirror for the second incoming pulses. The additional optical input can be a second optical oscillator or the input from a fibre extended path. This is necessary if a stabilization of a fibre or another oscillator is required.

The next Michelson Setup is nearly the same with the exception, that polarization is important. The additional optics are illustrated in Figure 45 .

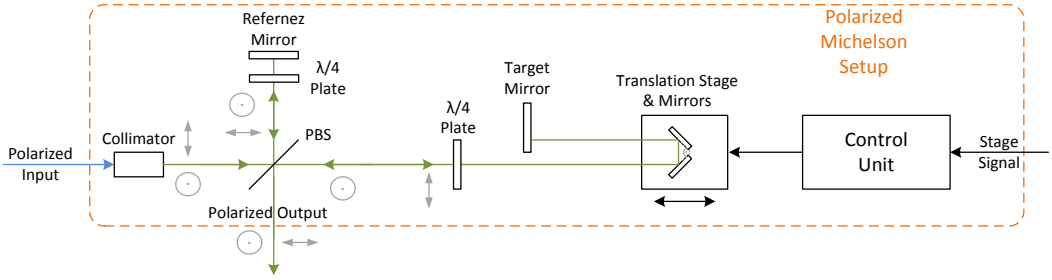

Figure 45: Michelson Setup with polarization dependencies for BOCC measurements

The additional optic components are the polarized beam splitter and the lambda/4 plates. Since a pm fibre is used for pulse propagation, the collimator for the incoming pulses can be rotated, that the polarized beam splitter divides the pulses in the two directions. After the polarized beam splitter, the two time passing of the pulses through a lambda/4 plate rotates the pulses by 90 that after the polarized beam splitter, the way of the pulses overlap again.
It is necessary that the pulses of the different paths have a perpendicular polarization.

This setup can also be used if the polarization status is not required. With the lambda plates, the intensities can be controlled precisely, to ensure, that from each path the intensity of the pulses are the same.

3.4.2 BOCC Setup

The BOCC setup is also a free beam setup.
An overview can be seen in Figure 46.

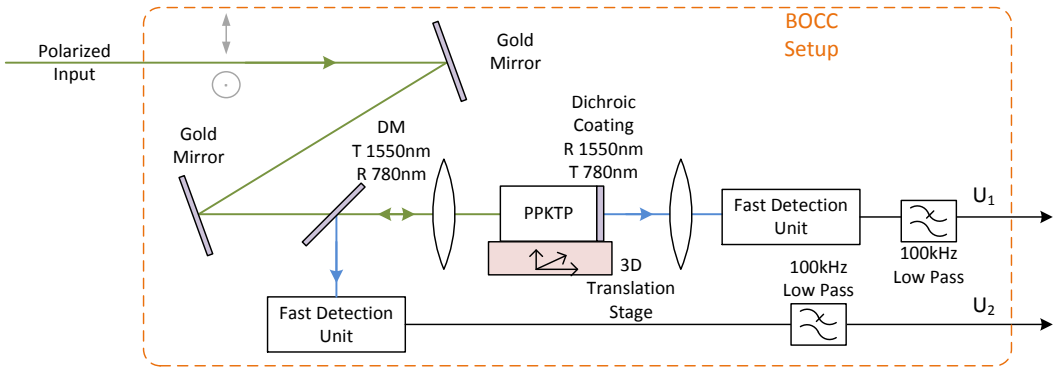

Figure 46: BOCC setup

The incoming perpendicular pulses propagate through an adjustment setup of different gold mir-

rors, to have multiple degrees of freedom for adjustments. After the mirrors, the pulses pass a dichroic mirror with transparency at 1560 nm and a reflection at 780 nm.

Since the pulses have an optical diameter of multiple mm, they must be focused for the PPKTP. Also the information of the waist results in the efficiency of the frequency doubling effect. The PPKTP crystal has a lengths of 4 mm. With Equation [38] (see Section 2.6.2) the waist can be calculated to ω_0 = 18.6 μm. As can be seen by this value, the optical adjustment for the focal point into the centre of the crystal may be time consuming, even when the crystal is installed on a 3D translation stage. Also the sensitivity to mechanical disturbances makes it challenging to maintain a long time function. This is one of the biggest disadvantage of the BOCC system that the optical handling is much more complex compared to the FDDM setup.

The crystal is coated on the other side with a dichroic coating, that reflects 1560 nm light and transmits 780 nm light. The 1560 nm pulses are then reflected back and pass a second time the PPKTP crystal. The 780 nm generated pulses pass the coating to a second focusing lens. This lens is not as crucial as the first focusing lens since the frequency doubled pulses must be detected by the fast detection unit, which has a larger detection area as the crystal.
Back reflected pulses at 1560 nm create the 780 nm pulses which are then separated from the 1560 nm pulses by the second dichroic mirror. A fast detection unit measures the incoming 780 nm pulses. Since only the absolute power of the frequency doubled light is necessary, the signal is low passed at 100 kHz.
Any frequency modifying element of the oscillators (piezo elements) have modulation frequencies $f_{mod} < 10$ kHz. Higher frequencies often disrupt electronic devices, that faster frequencies are terminated with the low pass filter. The low pass filter also creates a mean value of the pulse powers.

With this setup, two voltages are created which are used to stabilize the time between the perpendicular pulses. The voltages U_1 and U_2 depend on the time shift between them.

4 Measurements and Interpretations

The FDDM method and the FDDM CC method are two new approaches of distance measurements and time and frequency distributions. Their characterization and applications are shown here. For comparison a BOCC setup is created. Since highest performances are expected of the BOCC it serves as reference for major aspects like performance, handling, robustness ... .

First the proof of concept is shown in Section 4.1 including verification, characterization and application, not only within static systems but in dynamic scenarios as well.
In Section 4.2 the BOCC system is created, verified and characterized also for space applications.
The FDDM CC signal is then described in detail in Section 4.3. Measurements and first stabilization applications are also shown in that section.
Since the main focus of all systems is within space applications (Galileo, GFO) the performances of the systems are summarized and compared with the two space missions (Section 4.4).

4.1 FDDM Method

The first measurements are done to prove the FDDM method. Therefore the basic signal is characterized and afterwards the first application for distance measurement is shown.

4.1.1 FDDM Verification

To prove the FDDM principle, a basic setup is created with a stabilized oscillator combined with a Michelson setup and a fast detection unit.

The proof of concept is done within a Bachelor Thesis [47] which was initiated and supervised by the author of this thesis.

The target mirror is moved manually since the translation stage covers only two time 30 cm but the values dt $\in [0, 1]$ correlate with a length between [0 m, 3.79 m] at a repetition rate of 79.106 MHz. An overview can be seen in Figure 47.

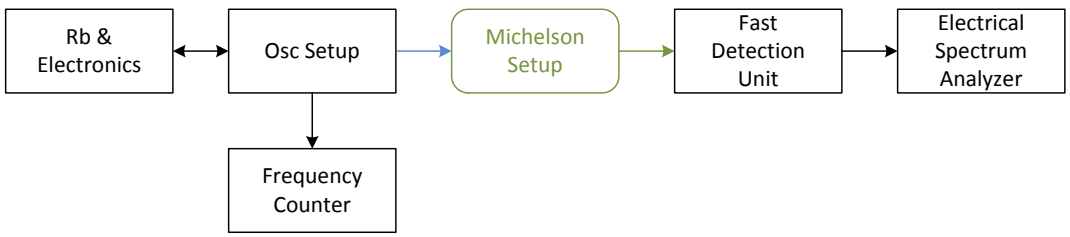

Figure 47: Schematic setup for verification of the FDDM method

By moving the target mirror the FDDM signal can be clearly defined, since distances are measured with measuring tapes and can easily be changed. The read-out of the harmonics is done

by a electrical spectrum analyzer, to receive the behaviour of multiple harmonics.

This is the verification of the FDDM principle. The measurements can be done between the distance of [0 m, 3.79/2 m] because the FDDM signal is symmetric to dt=0.5 (see Section 2.5). The results can be seen in Figure 48.

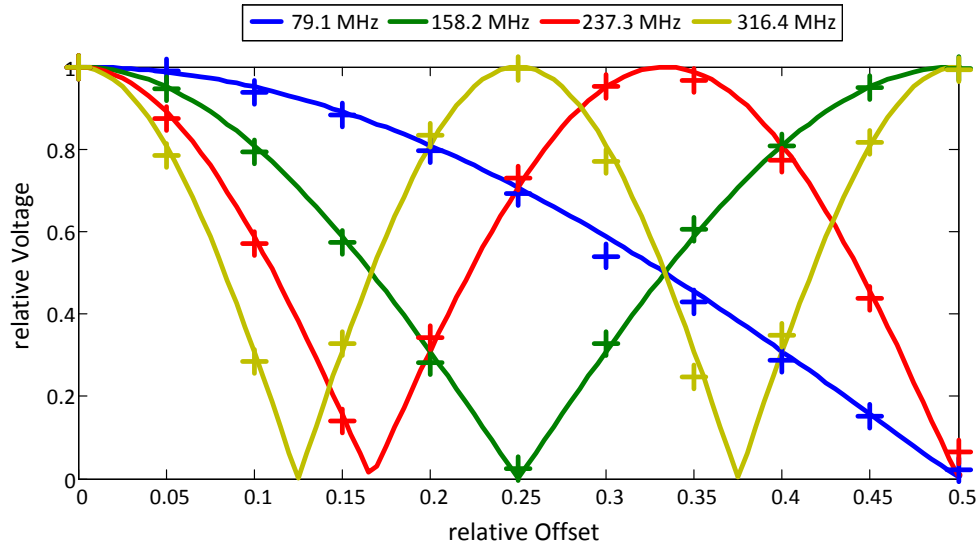

Figure 48: First measurements for verification of the FDDM principle

The measured points fit the predicted signal trend. The spots have a large uncertainty since the method using a measurement tape in the setup has a larger inaccuracy.
Figure 49 shows some examples of the measurement using the electronic spectrum analyzer.

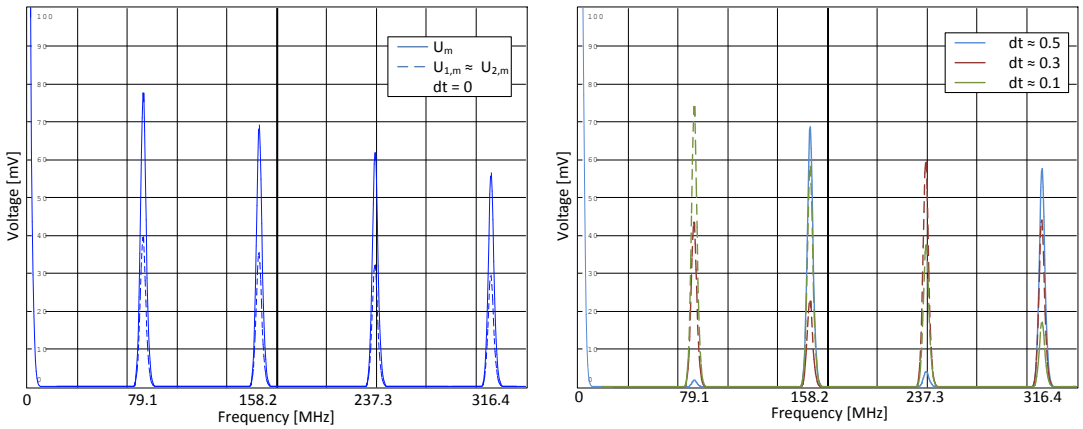

Figure 49: Electronic spectrum of the recorded first harmonics

At the left side of Figure 49 the voltage of the overlapped pulses (U_m) is shown and the single paths ($U_{1,m}$ and $U_{2,m}$) in dotted lines. The overlap (U_m) is here the reference at dt = 0.
At the right side of Figure 49 the relative offset is shifted to dt $\approx$ 0.1, dt $\approx$ 0.3, dt $\approx$ 0.5.

The behaviour of the amplitudes show, that the FDDM principle fits the theory shown in Section 2.5 and can be used for further measurements.

4.1.2 First Fibre Measurement

The FDDM method is working and should be shown at larger distances. The Michelson Setup is replaced by an optical fibre in combination with an in-fibre mirror and two fibre coupler. The setup is shown in Figure 50

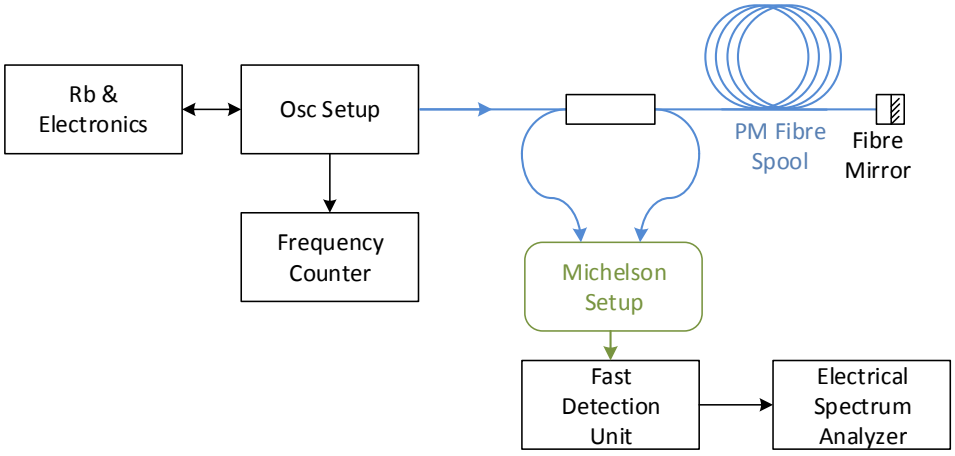

Figure 50: Setup for length measurement of an unknown fibre

To make use of the advantage of PM fibre oscillators, the whole setup is created with PM components. To split up the pulses in two directions a PM coupler is used. It facilitates the handling and increases the robustness of the setup, but since the reference path is the difference between two fibre lengths of the coupler, it can not be measured clearly. Measurements with the measuring tape have shown path differences below 1 cm between the arms. This is then the uncertainty used in this and the following setups.

The Michelson setup has been modified, for two fibre inputs.
The SESAM oscillator is placed in a thermal stabilized housing. To increase the effect of the amplitude variation, the repetition rate of the oscillator is varied by changing the housing temperature. The correlation between temperature and repetition rate is defined as $\Delta f/\Delta T \approx 2300$Hz/K [20]. The temperature is changed once by about 4 K. Before and afterwards, the harmonics are measured.
The measured values are listed in Table 7.

Table 7: Fibre lengths calculation with two point measurement

	m =	16	17		16	17
f_1 = 79 094 056 Hz	$U_{1,m}$ [mV]	35.2	22.4	f_2 = 79 084 822 Hz	37.0	23.5
	$U_{2,m}$ [mV]	35.0	22.0		37.3	23.7
	U_m [mV]	58.0	23.7		42.1	7.9

Here the 16th and 17th harmonics are used. It is a compromise between several requirements:

1) Using the highest available harmonic
2) Having sufficient SNR
3) Using harmonics which their amplitude is not at maximum

to 1): The higher the harmonic the higher the sensitivity dependent on lengths changes.

to 2): The electronic, especially the fast detection unit has its limits, because the created electronic board is designed for frequencies $<$ 1 GHz. Ultra high frequency electronic requires special electronic design, which was not implemented in this thesis. The fast detection unit attenuates higher harmonics which decreases the SNR. The lower the SNR, the higher the noise of other electronic components, that measurements result in a high inaccuracy.

to 3): The highest harmonic measured in this setup with sufficient SNR was the 18th. Because this harmonic is close to its maximum, the sensitivity due to frequency changes is not adequate for dt calculation

and by using Equation 9 dt can be calculated as

$$dt = \frac{\cos^{-1}\left(\frac{U_m^2 - U_{1,m}^2 - U_{2,m}^2}{2U_{1,m}U_{2,m}}\right)}{2m\pi} \tag{21}$$

to calculate the absolute distance with Equation 5 the multiple factor 'n' must be computed by

$$D = \left(\frac{n}{f_{REP}} + \Delta t\right)\frac{c}{2} + d_{ref} \quad \text{with} \quad \Delta t = \frac{dt}{f_{REP}}$$

$$\xrightarrow[d_{ref}=\text{const.}]{D=\text{const.}} \frac{n}{f_1} + \frac{dt_1}{f_1} = \frac{n}{f_2} + \frac{dt_2}{f_2}$$

$$\Rightarrow n = \frac{f_2 dt_1 - f_1 dt_2}{f_1 - f_2}$$

With the values of Table 7 the multiple factor 'n' can be calculated to n = 65. Using again Equation 5

$$D_x = \frac{(n + dt_x)c}{f_x 2n_{ref}} + d_{ref}$$
$$\Rightarrow D_1 = 85.55\,\text{m}$$
$$D_2 = 85.56\,\text{m}$$

with

dt_1 =	0.30	dt_2 =	0.31
f_1 =	79 094 056 Hz	f_2 =	79 094 056 Hz
d_{ref} =	0.43 m	n_{ref} =	1.4475 (Refractive index of fibre [48])
c =	speed of light		

The manual measurement with the measurement tape shows a length of the fibre of about D_{manual} = 85.68 m whereas the manual measurement caused a higher inaccuracy since the fiber is winded on a spool. Estimation of the diameter of the spool and the windings results in a total inaccuracy of about $\pm$20 cm.

The FDDM measurement shows that distances can be measured absolutely. With this setup, the distance is measured with an accuracy of about 1 cm.
Dependent to the distance, the frequency shift for 'n' estimation is correlated reciprocal. The higher the distance, the lower the frequency shift to calculate 'n'. At this measurement the housing temperature has to be changed, which is time consuming. If the target distance is large enough, the frequency hub of the SynchBox internal piezo stack would be sufficient for distance calculation, and faster respectively. And a faster measurement results in a measurement with a better distance resolution. Therefore it is expected, that for higher distances, the absolute distance resolution using FDDM can be improved.

For even higher precision in resolution, a different system is required: BOCC or FDDM CC.

4.1.3 FDDM Velocity Determination

After validation of the FDDM method the FDDM Board is created. Its application for amplitude separation is an advantage since the recording of the voltages can be done automatically e.g. with an Analogue Digital Converter (ADC).

The function test of the FDDM Board is also a first proof of the FDDM method to measure relative velocities between two objects.
To create an optical setup within the laboratory to simulate relative velocities which occur between navigation satellites is not executable and must be simulated.

One possibility to simulate any relative velocities is to use two electronically created short pulses with a phase offset or a frequency offset, since a relative movement of the target to the measure-

ment setup correlates with an oscillation of the harmonics.
The relative velocity between two objects using the FDDM method has same characteristic as for static systems. Figure 51 shows an example if the velocity is half of the oscillator lengths within 1 s.

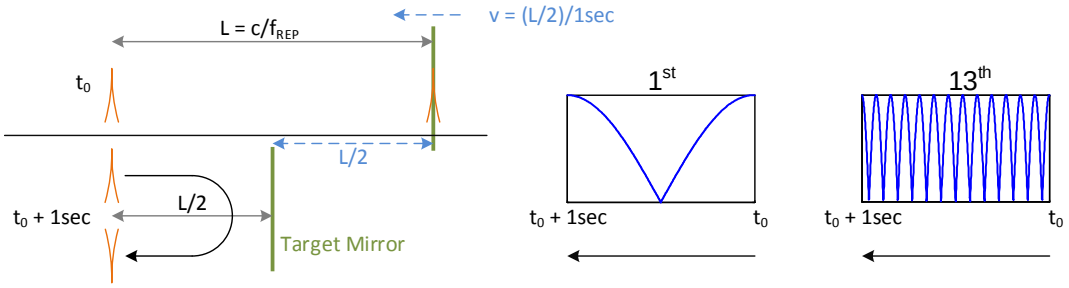

Figure 51: Example of correlation between velocity and FDDM deviation

The distance between two pulses is the oscillator length. If an object moves within 1 s the half oscillator lengths, the FDDM signal is passed from e.g. dt=0 to dt=1 within 1 s (see Figure 51). Therefore the velocity of the target is then calculated to $v_{obj} = \frac{L_{osc}/2}{1\,s}$. With the used oscillators the velocity would depend to $v_{obj} = \frac{c/79\,106\,500\,Hz}{2 \cdot 1\,s} \approx 1.896\,m/s$. Measuring the voltage of the harmonics and their change in time correlates with the target velocity.
If pulses from two different oscillators are overlapped and their repetition rate has a frequency difference of $\Delta f = 0.5\,Hz$ this simulates a target velocity of $v_{obj} = 1.896\,m/s$.

Since the fractional output of the synthesizer board creates short pulses, these can be used as a simulation of an optical oscillator with short pulses output. The signal output of the synthesizer board is illustrated in 52.

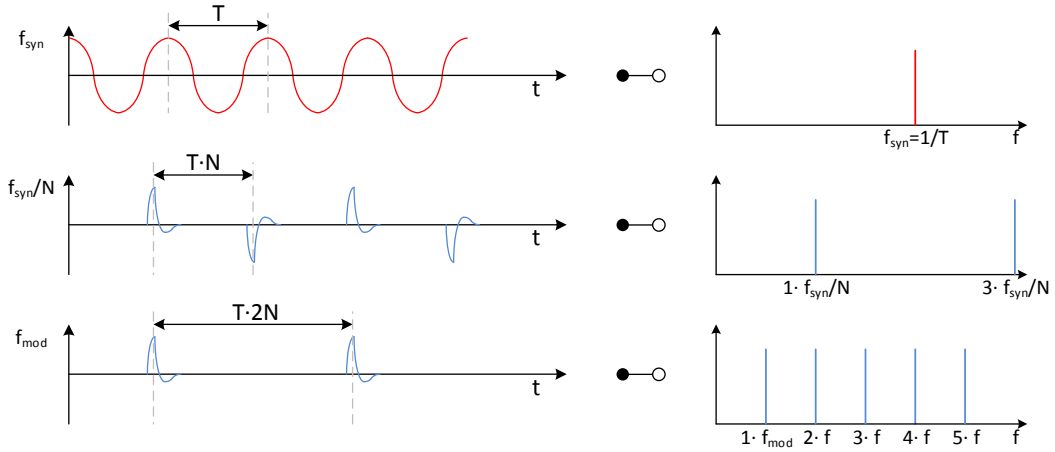

Figure 52: The synthesizer output and its Fourier transformed signals

The upper sine wave is the created frequency of the VCO output, stabilized by the synthesizer. Its Fourier transformation results in a single frequency peak at its specific frequency.
As described in Section 3.2.1 the synthesizer has a fractional output which is used to create multiple frequencies. The signal is pulsed with changing algebraic sign. This results in the frequency domain that only odd harmonics of the synthesized frequency are available. With an additional electronic setup using diodes, the negative voltage pulses are eliminated so a frequency spectrum is generated equal to the optical oscillators.

It is to mention, that creating short pulses electronically requires quite an effort. Since with this setup frequencies less than 1.5 GHz are used, this is possible with the fractional synthesizer installed on the synthesizer board. With this setup the higher harmonics are already strongly attenuated, but still detectable with the FDDM Board. If higher frequencies are used, the electronic becomes more complicate. This leads back to the comparably simple handling of optical short pulses. The measurement of the harmonics is then only limited by the electronic itself.

The example in Figure 52 shows a fractional value of N = 2. To receive equivalent frequencies as the optical oscillators the VCO is tuned to $f_{syn} = 4 \cdot f_{REP}$.

For validation of the system an electronic setup is created shown in Figure 53.

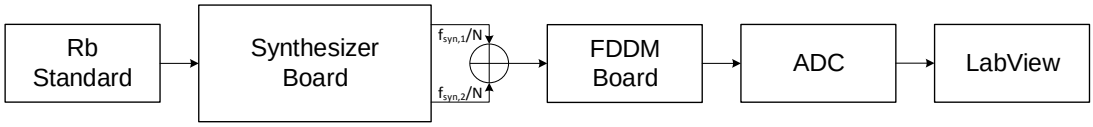

Figure 53: Schematic setup of electronically simulation of a FDDM measurement setup

The synthesizer board is stabilized on the Rb-Standard. Since two oscillators are installed on one board both fractional outputs are used and overlapped with a frequency mixer. Also important that with this setup phase shifting between the synthesizers is prevented. This signal is then connected to the FDDM Board. The signal equals the input of a reference path and a target path.
To simulate different velocity scenarios the frequency of the oscillators is modified. Since the frequencies of each synthesizer can be varied with a frequency resolution of $\Delta f < 1$ mHz precise velocity characterizations are possible.

The output of the FDDM Board (4 channels) is measured/digitalized with an ADC (with 10 kS/s/channel) and recorded by a software program (LabView).
The software varies the original FDDM signal for further calculations (see Figure 54).

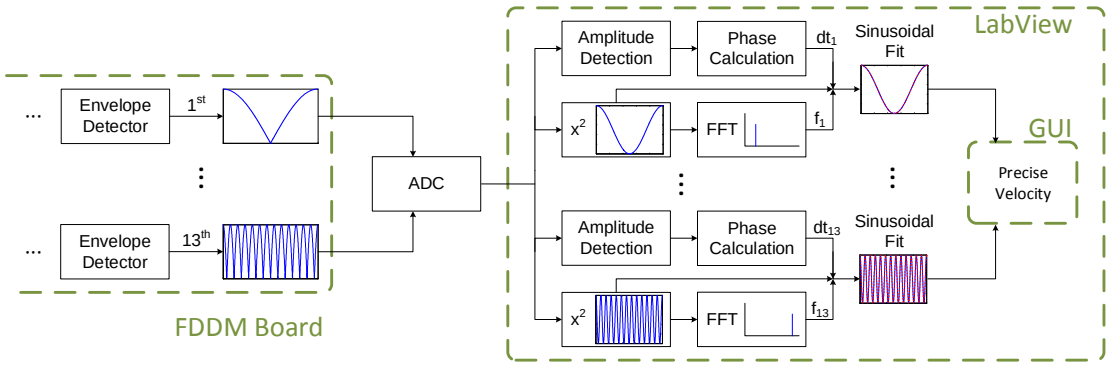

Figure 54: Schematic overview of the signal evaluation with LabView

Each harmonic is recorded by the software separately with 10 kS/s/channel. First the harmonics of each synthesizer board is detected (one synthesizer is disconnected) to simulate a theoretical FDDM signal. When both synthesizers are active, the amplitude of each harmonic can be used to calculate the phase (dt) of the current state.
The FDDM signal is defined by $U_m = |\cos(m \cdot \pi \cdot dt)|$. Using the intensity instead of voltages, the signal equals to $I_m = U_m^2 = \frac{1}{2}(1 + \cos(m \cdot \pi \cdot dt))$.
LabView enables a sinusoidal fit. The fit requires presetting with the rough inputs: amplitude, phase and frequency. The amplitude is already known from the first measurement and the phase can be calculated.
If there is a relative velocity between two objects, the FDDM signal starts to oscillate. The I_m oscillates equal to a cosine function. A Fast Fourier Transformation (FFT) results in the required rough frequency determination.

With all three inputs the velocity can be calculated. Since the dt-value is known for any sinusoidal fit also the absolute distance to the object can be calculated. The first and second harmonics are used for a rough dt determination whereas the 12^{th} and 13^{th} are used for precise velocity and position determination.

Several velocities are simulated. Their calculations are shown in Figure 55.

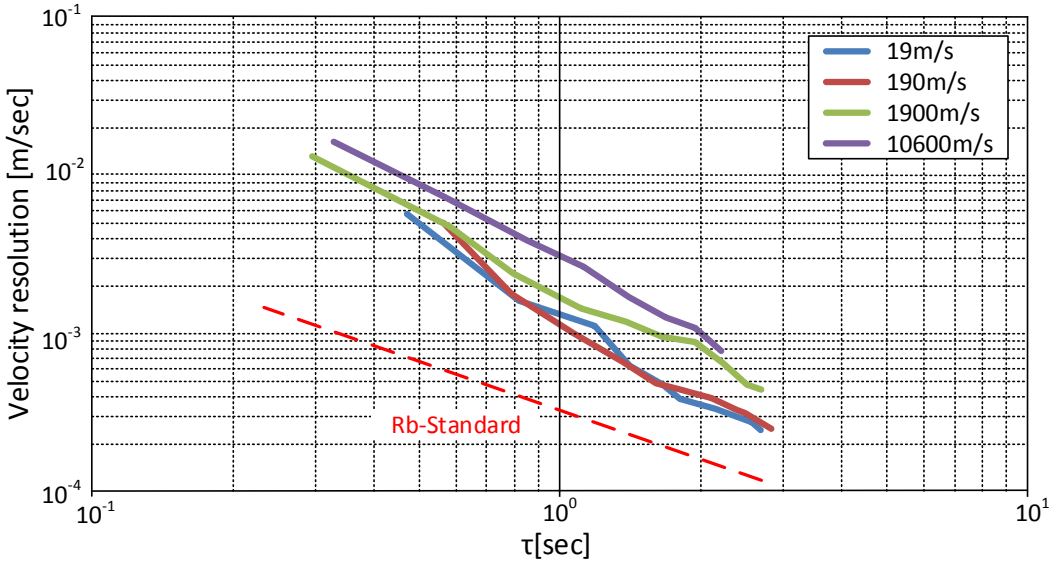

Figure 55: Velocity measurement using the FDDM Board for absolute distance measurement

The simulated velocities start from v_{rel} = 19 m/s and end at v_{rel} = 10.6 km/s.
Two properties are shown:

1) Velocities up to $v_{rel} > 10$ km/s can be measured
2) Using the FDDM Board in combination with an ADC increases the distance resolution

to 1) The system works properly. The simulation of velocities is successful using the synthesizers as pulse source. The FDDM Board in combination with the software enables a simple measurement method of velocity determination. Within Galileo scenarios velocities $v_{rel} > 4$ km/s occur (see Section 2.4.2) which can be measured.

to 2) At lower velocity values, the resolution for dt increases. At Section 4.1.1 the accuracy is limited to 1 cm. The combination of FDDM Board and ADC increases the performance by one order of magnitude. The limit factor of increasing the resolution is the speed of the ADC read out. Also the LabView software is computationally intensive since at every calculation a FFT and a fitting tool must be used.

The precise velocity determination is important for red shift of light between two systems (see Section 2.4.3). The measurement with FDDM method does not yet reach the requirement for any frequency standard. The Rb-Standard would require a velocity precision of $\Delta v_{rel}(1\,s) \approx 330\,\mu$m/s, highlighted by the red doted line in Figure 55.

FDDM Summary

The FDDM Board works properly. Simulated velocities $v_{rel} > 10$ km/s can be measured with accuracies $\Delta v_{rel} < 1$ cm/s. The absolute distance resolution increased to $\Delta s = 1$ mm and is measured automatically by a LabView software. The velocity determination is close to the limit defined by the used frequency standard itself.

This is the proof of concept and it is expected that there is more potential in measurement speed and accuracy using faster electronics with implemented functions using FPGAs. An improvement to reach the requirement of a Rb-Standard should be possible with further development effort. The used frequency standard is also the limit of the velocity determination.

4.2 BOCC System

The BOCC system is already in use for several distance characterizations [49]. The application specific for time and frequency distribution is a new focus. Also important to know is the characteristic of a BOCC setup relating to space application. Which effort is necessary and how complex is the overall setup compared to FDDM or FDDM CC?

The BOCC setup is characterized within a Master Thesis [50] which was initiated and supervised by the author of this thesis.
The excerpt here is an overview of the important factors of the BOCC performance.

In Section 4.2.1 the BOCC system is set up and characterized.
Afterwards in Section 4.2.2 first measurements using an optical fibre for relative distance measurement are done. Finally in Section 4.2.3 the BOCC is used for stabilization which results in its performance for frequency stabilization over long distances.

4.2.1 BOCC Characterization

For the BOCC setup, the Michelson Setup is changed to a polarized setup and the fine resolution translation stage is used. The overall setup is illustrated in Figure 56.

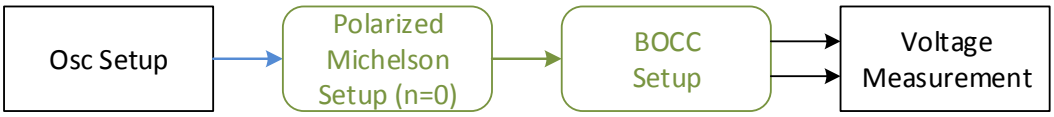

Figure 56: Setup to characterize the BOCC

The BOCC setup requires polarization control since within the PPKTP crystal the two pulses must be rectangular to each other. For characterization the reference path and target path have equal distances. A frequency stabilization of the oscillator is not necessary.

During the setup of the optics quite an effort is needed to manage the beam alignment to ensure that the beam stays focused within the crystal, including during the movement of the target mirror on the translation stage.

The length of the reference path stays constant whereas the length of the target path is varied by a translation stage. The used fine resolution translation stage has step sizes of 100 nm with a resolution of 50 nm. The pulses can than be measured by a time resolution of $\Delta t = 1/3 \cdot 10^{-15}$s. During the movement of the translation stage, two signals are recorded (SHG signals). One photo diode records the forward direction within the crystal. The second photo diode records the backward direction within the crystal.
The measurement can be seen in Figure 57

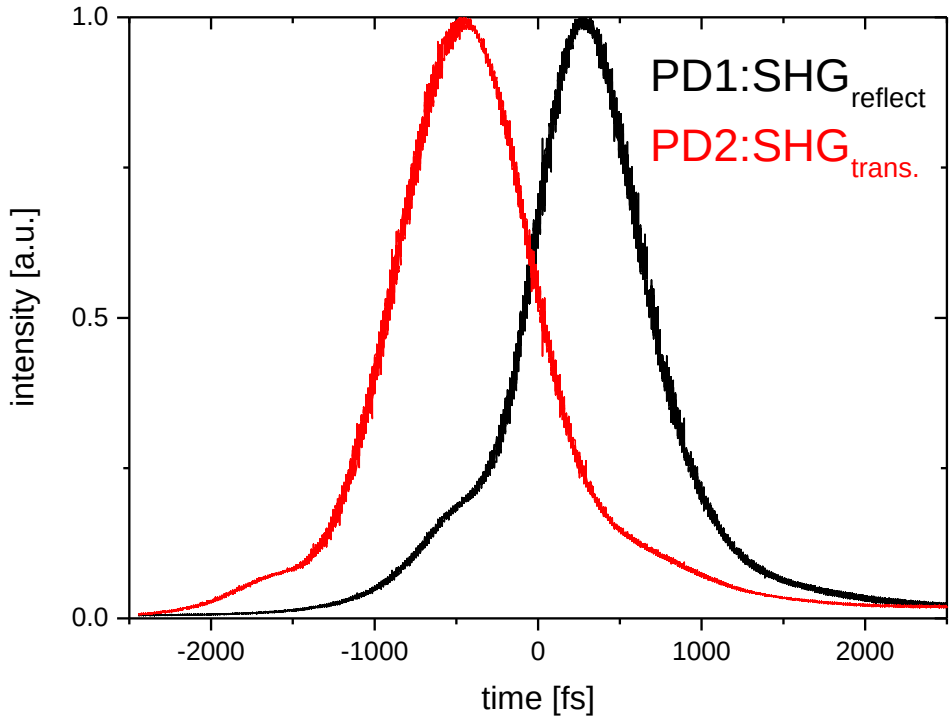

Figure 57: Characterization of the SHG signals [50]

The pulses propagate in air within a length of about 20 cm in both directions. It is assumed that the dispersion of the pulses is negligible compared to their pulse length. With this assumption the recorded signals are a autocorrelation of the pulses [51]. The pulse length is calculated to about 500 fs (black line in Figure 57).

The measurement setup is changed by increasing the target distance to 1/2 of the oscillator length to D $\approx$ 1.90 m. The multiple factor of the pulses within this target path is then n = 1.
The translation stage is shifted so that the intensities of the SHG pulses in forward and backward directions are equal.
Since frequency variations of the oscillator change the time offset, the repetition rate is stabilized on the Rb-Standard. The updated setup is illustrated in Figure 58.

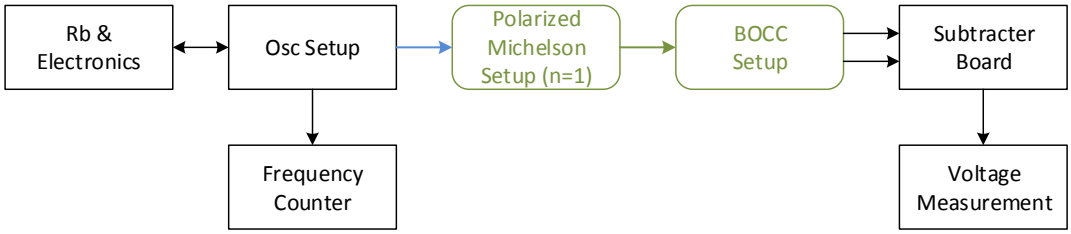

Figure 58: Setup to characterize the BOCC with n=1

To measure the cross correlation between the forward and backward signal the Subtracter Board is installed. The output of each photo diode is modified, that their amplitudes have equal amplitudes as shown before in Figure 57.
The multiple factor 'n' is set to '1' that a frequency shift results in a time offset of the incoming pulses. This can be calculated to

$$D_{1,2} = \frac{1}{c}(n \cdot T_{1,2} + \Delta t_{1,2}) + d_{ref,1,2}$$

$$\text{with} \quad D_1 = D_2 \quad \Delta t_1 = 0 \quad d_{ref,1} = d_{ref,2}$$

$$\Delta t_2 = n \cdot T_1 - n \cdot T_2 \overset{n=1}{=} \frac{f_2 - f_1}{f_1 f_2} \approx \frac{\Delta f}{f_0^2}$$

$$\Rightarrow \Delta s = \frac{\Delta f}{f_0^2} c$$

A frequency shift can also be used to measure the SHG signal. A shift of $\Delta f = 1\,\text{Hz}$ results in a length shift of $\Delta s \approx 50\,\text{nm}$. Therefore the characterization of the SHG signal is repeated by frequency shift but has same results.
It has to be mentioned, that the lock of the repetition rate onto a highly stable frequency standard (Rb-Standard) allows stabilizations of frequencies $\Delta f < 10^{-3}\text{Hz}$. This would result theoretically in time resolutions of $\Delta t < 2 \cdot 10^{-18}\text{s}$ or distance resolutions $\Delta s < 50\,\text{pm}$. This is however not possible due to imperfection of the optical setup, environmental loads or resolution of optical fringes of the pulse.

The SHG signal is the input of the Subtracter Board. The output of the Subtracter Board is measured with an ADC. The BOCC signal is shown in Figure 59.

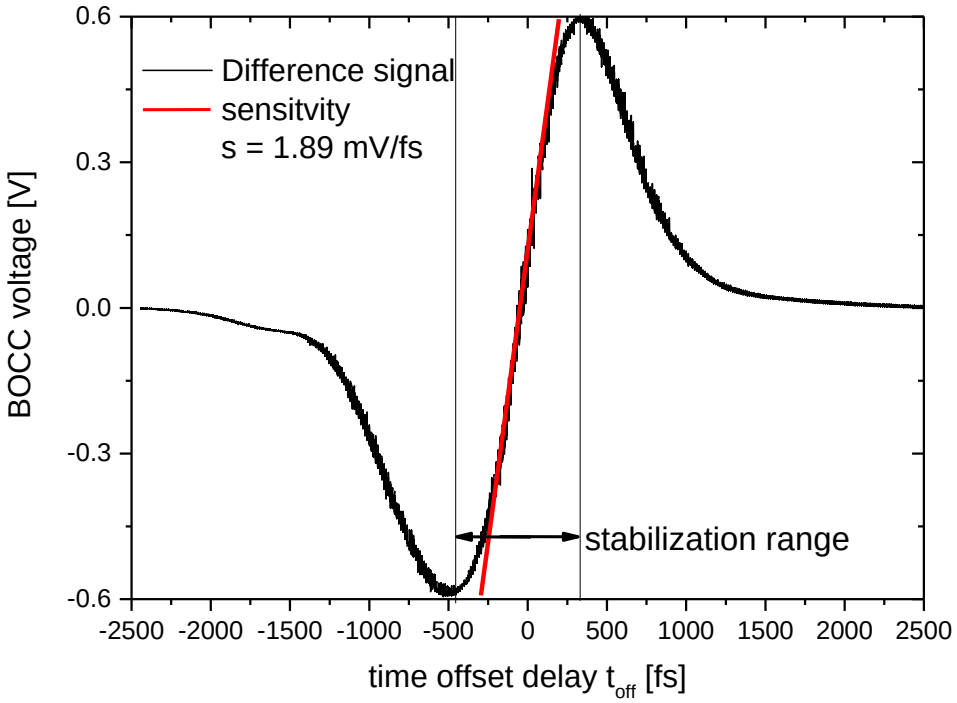

Figure 59: BOCC signal with slope and stabilization range [50]

The BOCC signal fits a s-shaped form as expected. The slope is calculated to a_t = 1.89 mV/fs (a_s = 6.4 mV/μm) at the zero crossing point.
Also illustrated a stabilization range. Within this range, the BOCC system can stabilize itself to the zero crossing point. If the stabilization is out of range, the BOCC signal drops out of the loop and must be adjusted again from the beginning.
To start a BOCC loop, the signal must be adjusted in advance within the stabilization range, which is an area of about 2.4 μm.

In summary the BOCC system is set up, verified and characterized. The used SESAM oscillator has pulses with FWHM with about 500 fs which can be measured by the BOCC by autocorrelation. A s-shaped BOCC signal is created with slopes of a_t = 1.89 mV/fs or a_s = 6.4 mV/μm.

4.2.2 BOCC Measurements

With the characterized slope distances can be measured. To increase the measurement distance an optical fibre is used. The measurement setup is illustrated in Figure 60.

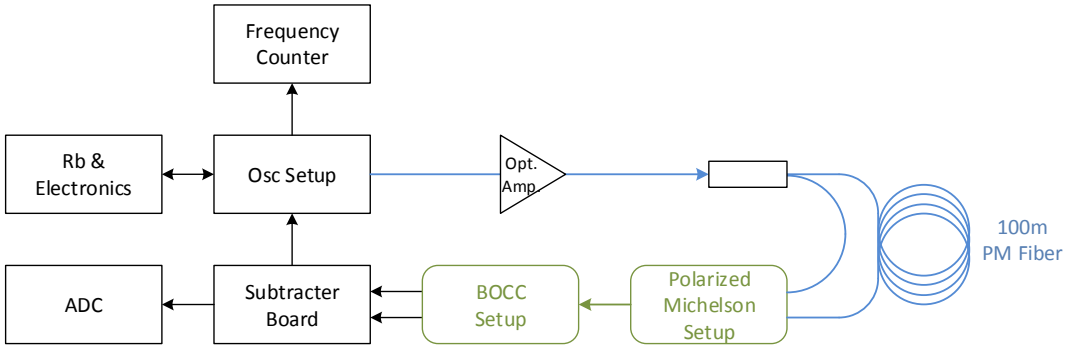

Figure 60: Using the BOCC signal to lock the oscillator on the length of the fibre

Since the BOCC system can handle relative distance changes, the absolute distance must be calculated in advance. The FDDM method results in a multiple factor of $n = 42$.
The BOCC system for stabilization is only applicable, when the pulses are overlapping. Therefore the length is defined by the multiple of the oscillator length. In this case the distance can be calculated to about $D_{opt} = 159.313\,\text{m}$. Applying the refractive index results in a fibre length of $D_{fiber} = 110.060\,\text{m}$.

After determination of the fibre length, the BOCC stabilization should be activated to lock the oscillator frequency to the fibre length. Therefore the translation stage is moved that the intensity of the forward and backward SHG pulses are equal. The difference of random signal and stabilization signal can be seen in Figure 61. The signal is measured by an ADC and recorded by a LabView software.

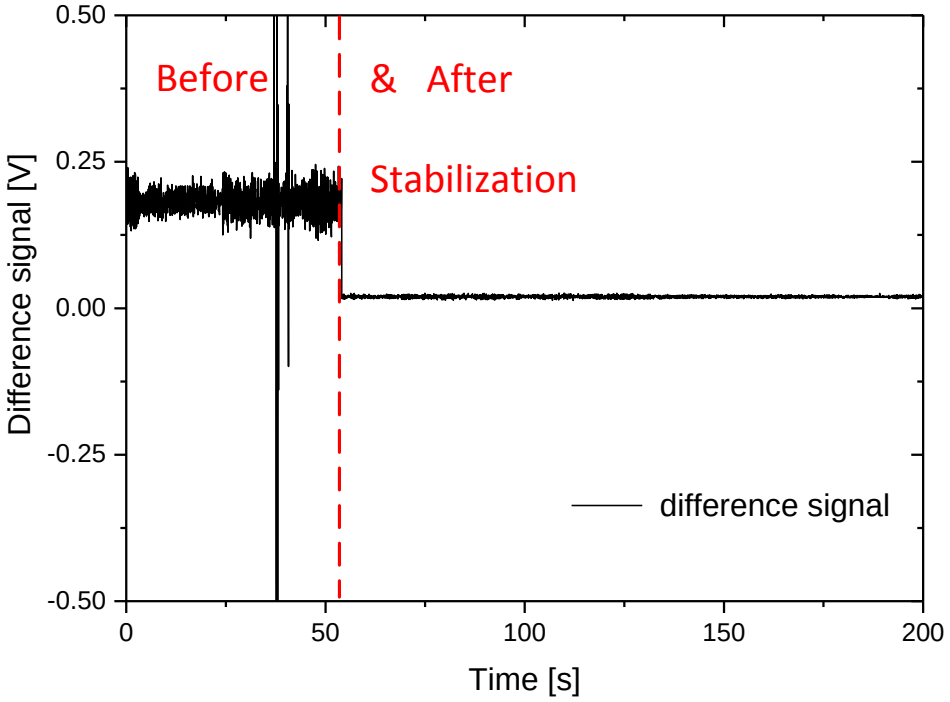

Figure 61: Starting the BOCC loop to stabilize the oscillator on the length of the fiber [50]

When the stabilization loop is closed, the signal is stabilized to the zero crossing point. The oscillator frequency is then locked on the length of the fibre.

The BOCC noise before stabilization is characteristic for the optical setup, especially for the optical fibre. Due to continuous vibrations in the laboratory (even on a vibration damped optical table) and the thermal noise of the fibre the signal has amplitudes of $U_{noise} \approx 10\,mV$ which is about $\Delta s = 64\,\mu m$. The peak at $t = 30\,s$ is a perturbation due to touching the fibre. The measurement system is accordingly sensitive.

After stabilization the repetition rate is connected to the fibre length and to its length noise. The signal is recorded with an measurement rate of 1500 S/s. Higher rates would be possible (up to 48 kS/s) but not necessary, because the noise would simply increase.
For data minimizing an average value over 30 values is created to enable measurements over longer timer ($t_{rec} > 10\,min$).

Since the laboratory temperature is not constant, the fibre has a length drift which is recorded by the repetition rate. The frequency in connection to the fibre is shown in Figure 62.

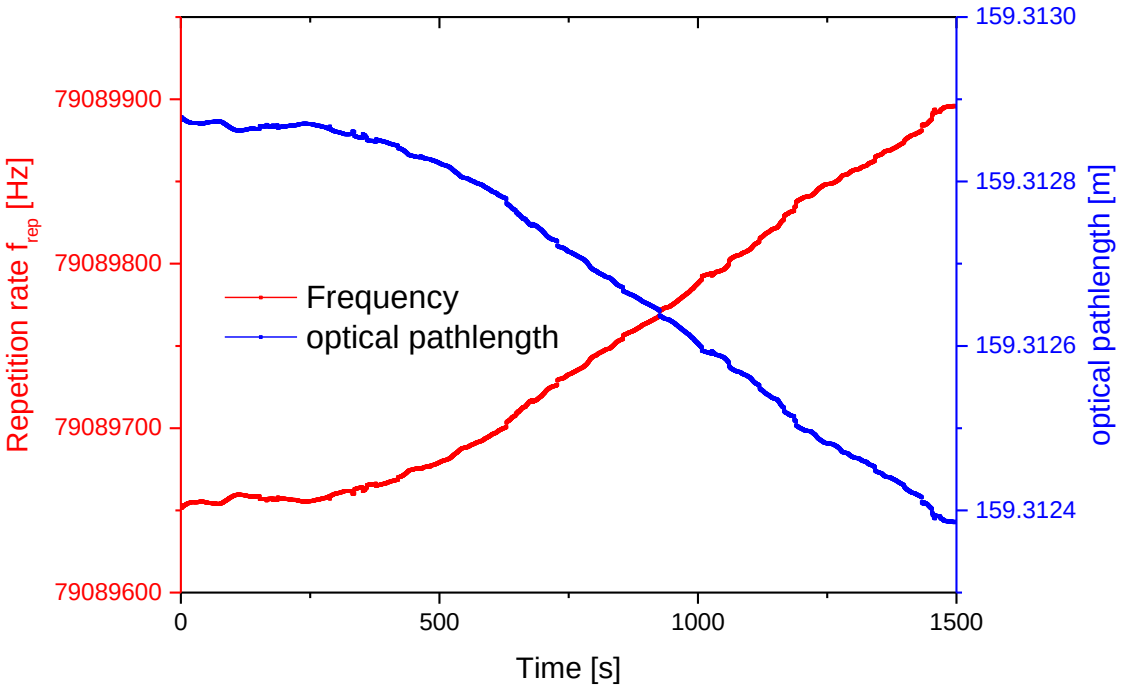

Figure 62: Correlation between oscillator frequency and locked distance [50]

The BOCC loop is active for more than 25 min. During the measurement time the optical path length has changed up to 500 μm, which is a oscillator length change of Δl_{osc} = 11.9 μm . The piezo within the SESAM oscillator has a total range of $\Delta l_{tot} = 2 \cdot l_{Piezo}$ = 12 μm. A longer stabilization time would not be possible.

The continuous measurement of the BOCC signal is related to a lengths of the oscillator. As long as the BOCC loop is active (which means that the BOCC signal is stabilized to the zero crossing point) the voltage is connected to the uncertainty of the length measurement. The higher the jitter, the higher the uncertainty. The slope is defined by a_s = 6.40 mV/μm or a_t = 1.89 mV/fs.
The recording can then be calculated to an Allan Deviation.
The Allan Deviation of the stabilization of the repetition rate to the fiber length is shown in Figure 63.

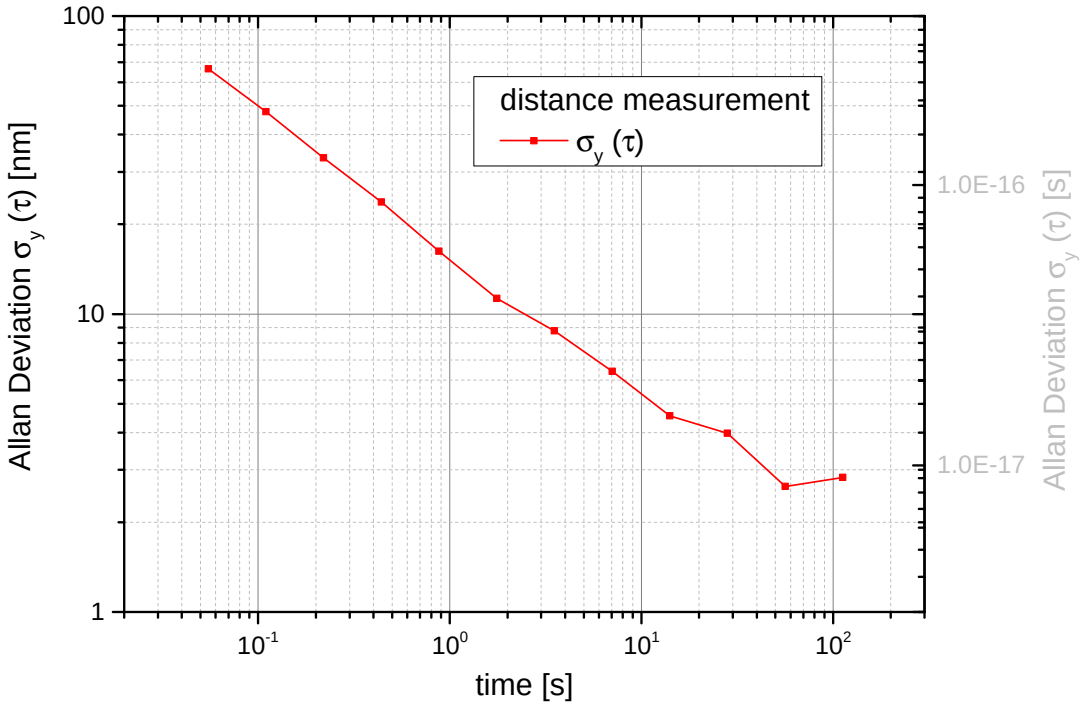

Figure 63: Distance resolution of the BOCC lock and the frequency stability [50]

The Allan Deviation shows with $\sigma_y(1\,\mathrm{s}) = 15\,\mathrm{nm}$ which correlates to a frequency stability of $\sigma_y(1\,\mathrm{s}) = 5 \cdot 10^{-17}$.
This performance is more than one order of magnitude better than any optical clock, for frequency stabilization or time distribution.

The measurement rate of about 50 Hz is limited since averaged values are taken for data limitation.

In summary an optical oscillator is locked with the BOCC on a fibre length for about 25 min. A continuous readout of the repetition rate results in an absolute fibre length with a resolution of $\Delta s < 20\,\mathrm{nm}$ at 1 s measurement time.
This results also in a possible frequency stabilization of $\sigma_y(1\,\mathrm{s}) = 5 \cdot 10^{-17}$ which is more than one order of magnitude better than current performances of optical clocks.

4.2.3 BOCC Fibre Stabilization

For time distribution the absolute and precise knowledge of the target distance is essential. The possibility is verified using the FDDM method in combination with a BOCC setup. Within the prior section the fibre distance is monitored by recording the repetition rate. The length itself changes by laboratory environmental variations.

An additional application for a BOCC system is to stabilize longer fibre distances. Fibre stabiliza-

tions are done commonly with CW laser interferometry [52] with great success. Frequencies are synchronized over long distances (D $>$ 920 km) with performances at $\sigma_y(1\,s) \approx 10^{-15}$. Nevertheless, these fibre stabilizations are used 'only' for frequency transfer. A time transfer is not possible since the absolute distance is not known precisely enough to create a time link.

A possible update is hereby the fibre stabilization using the BOCC setup. To stabilize an optical fibre to the repetition rate locks the fibre lengths to a multiple of the oscillator length. Since the length is kept constant (absolute) a time distribution between two spots is possible.

For the fibre stabilization the prior optical setup is updated with a Piezo strecher. The setup can be seen in Figure 64

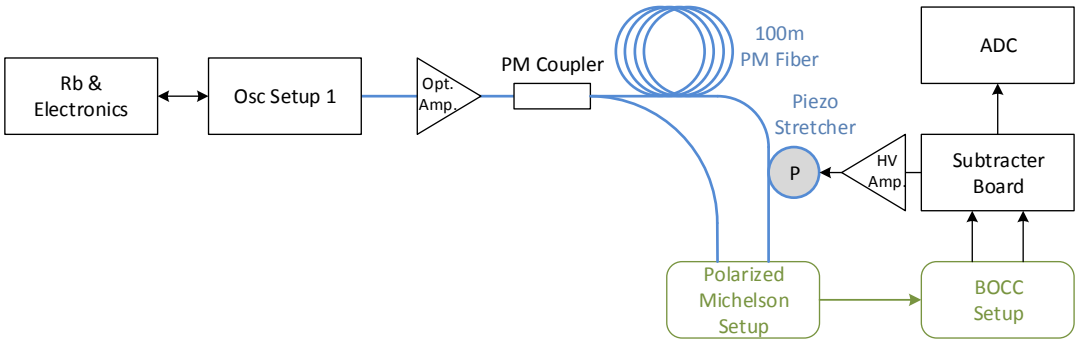

Figure 64: Updated setup with a Piezo strecher to change fibre length

The Piezo Stretcher is a Piezo Tube with a furled PM fibre. Using high voltage the Piezo Tube expands and stretches the optical fibre. The Piezo Stretcher has a total stroke of about 140 μm in the optical area.

The output of the Subtracter Board $U_{out} \in [0\,V, 5\,V]$ is amplified by an additional HV amplifier to $U_{HV} \in [0\,V, 150\,V]$. The Piezo Tube is capable of handle with voltages up to 1000 V. The here used HV Amplifier is limited to 150 V.

The procedure to start the stabilization is equal to the frequency lock on the fibre length.
The time offset between the pulses is modified to dt = 0 that the SHG intensity of the forward and backward pulses are equal. Then the output of the Subtracter Board is connected to the HV amplifier. As long as the lengths change of the fibre is within the stroke of the Piezo Stretcher the stabilization is working.
The according Allan Deviation of the fibre stabilization can be seen in Figure 65

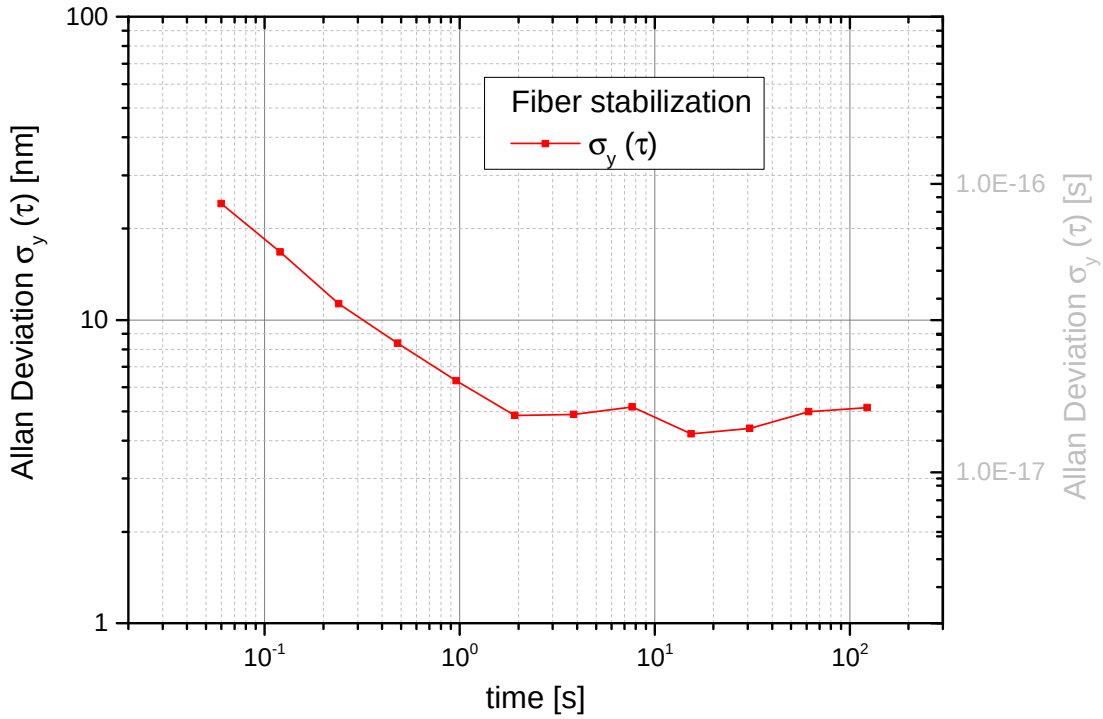

Figure 65: Fibre stabilization of a 100 PM fibre with time and length resolution [50]

The fibre stabilization is maintained for about 15 min. The laboratory environment varies that the stroke of 140 μm is reached after that time.
Nevertheless the fibre stabilization reached $\sigma_y(1\,s) = 6\,nm$ which correlates to a frequency stability of $\sigma_y(1\,s) = 2 \cdot 10^{-17}$. This is about two orders of magnitude better than current optical clock standards.

4.2.4 BOCC within Dynamic Systems

The BOCC setup is capable of highly precise distance measurements and for highest performance time and frequency distribution at static systems.
But what happens at dynamic systems? A theoretical approach should focus on this issue.

In Section 4.2.1 a stabilization range of $l_{stab} = 2.4\,\mu m$ is characterized. The system itself has a modulation frequency $f_{mod} = 1\,kHz$ which is defined by the HV amplifiers. Within this modulation time the system can adjust itself without falling out of the BOCC loop. This results in a maximum velocity of

$$v_{max} = l_{stab} \cdot f_{mod} = 2.4\mu m \cdot 1000\,Hz = 2.4\,mm/s$$

The system is capable of lock on targets with relative velocities up to 2.4 mm/s.
In Section 2.4.3 it is already discussed, that velocities between two neighboured satellites in the same orbit with $v_{rel} > 10\,m/s$ occur. Additionally, the modulation frequency lowers due to large distances ($D \approx 2 \cdot 10^7 m$) to $f_{mod} = 2 \cdot D/c \approx 30\,Hz$ which results in a maximum relative velocity of $v_{max} = 720\,\mu m/s$.
Referring to Section 2.4 this would result in a time window of $t_{synch} < 2\,s$ to synchronize two neighboured satellites (same orbit). This time would also include precise distance determination. In total a very challenging theme even in the simplest scenario.

BOCC Summary

The BOCC setup is capable for highest precision in distance resolution with $\Delta s(1\,s) = 15\,nm$.
Also a fibre stabilization is possible using the same signal. The first stabilization of a 100 m fibre results in a distance stability of $\Delta s(1\,s) = 6\,nm$ which corresponds to $\sigma_y(1\,s) = 2 \cdot 10^{-17}$ as a possible time and frequency synchronization between two spots. Nevertheless a focus lies on the control of the pulse power, since non adjusted pulse power results in a pulse broadening (diffluence) that minimizes the performance of the BOCC system.
Using the BOCC within dynamic systems results in a highly challenging setup.
The handling of the BOCC requires some effort since the dimension of the used crystal requires high precision optical setup. The usage of polarization maintaining fibres simplifies the optical setup significantly.

A possible application of the BOCC setup for time and frequency distribution is within optical fibres in static systems.

4.3 FDDM CC Verification

The FDDM and BOCC setup are characterized and first performance measurements are done.
The FDDM CC promises to be a combination of the simplicity of the FDDM and the performance of the BOCC.

There is no known system which would be similar to the FDDM CC system.

In Section 4.3.1 the first measurements and characterizations of the new system are shown.
Afterwards in Section 4.3.2 the CC signal is taken for frequency synchronization.
The FDDM CC signal is then used for a fibre stabilization described in Section 4.3.3.
And finally the combination of the two applications is shown in Section 4.3.4.

4.3.1 FDDM CC Proof of Concept

For the characterization of the FDDM CC signal, the FDDM signal must be generated for $dt \in [0, 1]$. In the prior chapters a Michelson Setup is used with a translation stage to vary the 'dt' value. As for this measurement setup a second optical oscillator is available with equivalent values of pulse length, repetition rate and pulse intensity which is used by frequency shift like a translation

stage. The setup for any measurement is then easier to implement, since no free-beam parts are necessary. The setup is created as can be seen in Figure 66.

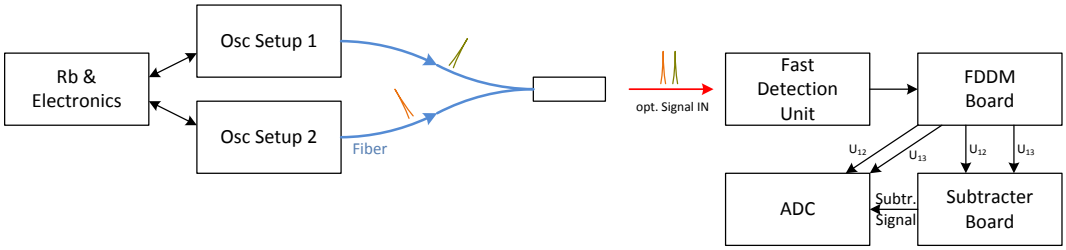

Figure 66: Setup to characterize the the FDDM CC signal with two oscillators

Both oscillators are PM fiber coupled. The overlap of the pulses is done by a fibre coupler. In this setup, the coupler is polarization maintaining. Since the FDDM method is independent of polarization also a single mode coupler could have been used.

The pulses reach the fast detection unit, which creates the multiple harmonics in the frequency domain. The FDDM Board separates the 1^{st}, 2^{nd}, 12^{th} and 13^{th} harmonic. Afterwards the Subtracter Board creates the subtracted signal between the 12^{th} and 13^{th} harmonic. The signal output of the FDDM Board and the Subtracter Board are monitored with an analogue digital converter.

Without stabilization the two oscillators have random repetition rates, which result in an oscillating FDDM signal. If both oscillators have the same repetition rate, the FDDM signal would be constant and the phase shift between both oscillators would define the 'dt' value.

To control the 'dt' value both oscillators are stabilized with the Synthesizer Board on the Rb Standard at a frequency of 79 106 500 Hz. With the control of the frequency, the FDDM signal can be measured precisely. A frequency mismatch of about 12.5 mHz is created. With this frequency offset the complete FDDM CC signal is characterized within 80 s which can be seen in Figure 67. The signal is recorded by a LabView software.

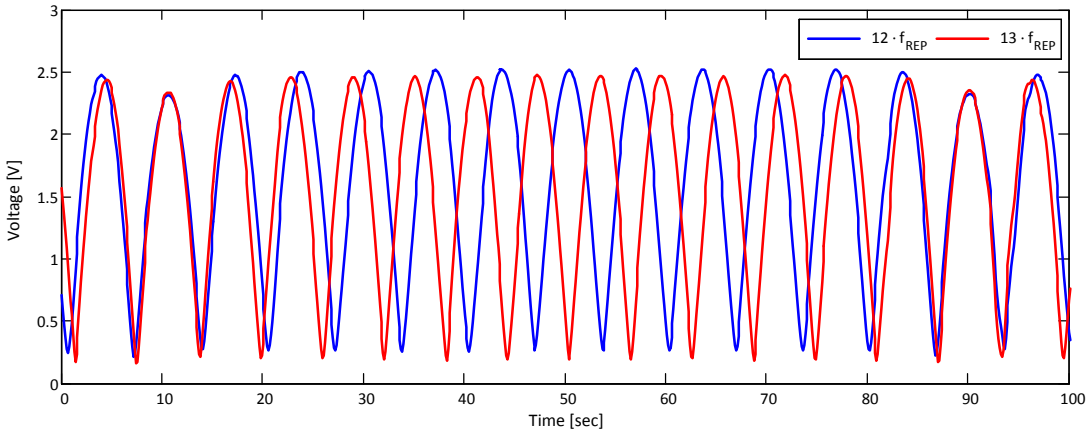

Figure 67: Measurement of the 12th and 13th Harmonic created by two oscillators

The Figure shows the 12th and 13th harmonic dependent on passing time which is correlated with a time offset 'dt'. The pulses are overlapped at $t_{meas} \approx 10\,s$ and pass through its characteristic until $t_{meas} \approx 90\,s$. The signal has a voltage offset of about 200 mV which depends on the used ADC. For the CC measurement the Subtracter Board returns the required signal. Since in section 2.6.1 the signal is always defined in a relative voltage 'dU', the measured values are normalized by the recording software. Using the measured input of the harmonics a theoretical signal can be created witch is then compared with the measured values. This can be seen in Figure 68.

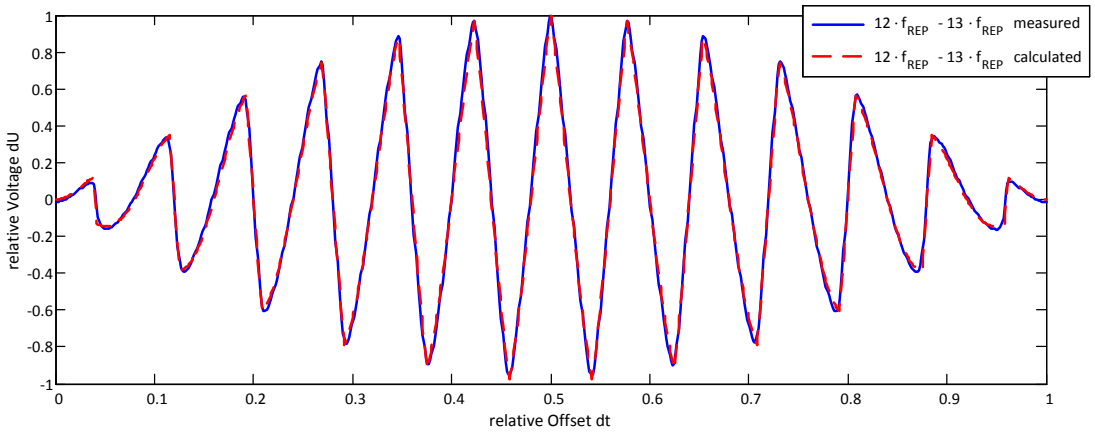

Figure 68: Comparison between measured FDDM CC signal and theoretical values

The normalized values (adapted by LabView Software) fits the predicted values of Section 2.6.1. Thus the FDDM CC signal is working which creates an additional signal for high precise measurements or high performance stabilization.

An important characteristic of the system is the slope for stabilization, as defined in Section 2.6.3.

The general slope 'dU/dt' is defined in Section 2.6.1 for the 12th and 13th harmonics in the Equation 14. Adapted to the oscillators used for this measurements (f_{REP} = 79 106 500 Hz).

Compared to the lock-in range (or stabilization range) of the BOCC setup (l_{stab} = 2.4 μm) the FDDM CC has a higher range with 1/25th of the oscillator length ($l_{stab} \approx$ 152 mm, mean value). And every slope which has the required algebraic sign can be used for stabilization. Even if the lock jumps out of loop, the system stabilizes itself again. Therefore using the FDDM CC system for stabilization loop can be activated by 'simply' starting it. The time offset between the pulses is then automatically stabilized.

The Signal of the Subtracter Board is also measured by the ADC and recorded by LabView, illustrated in Figure 69.

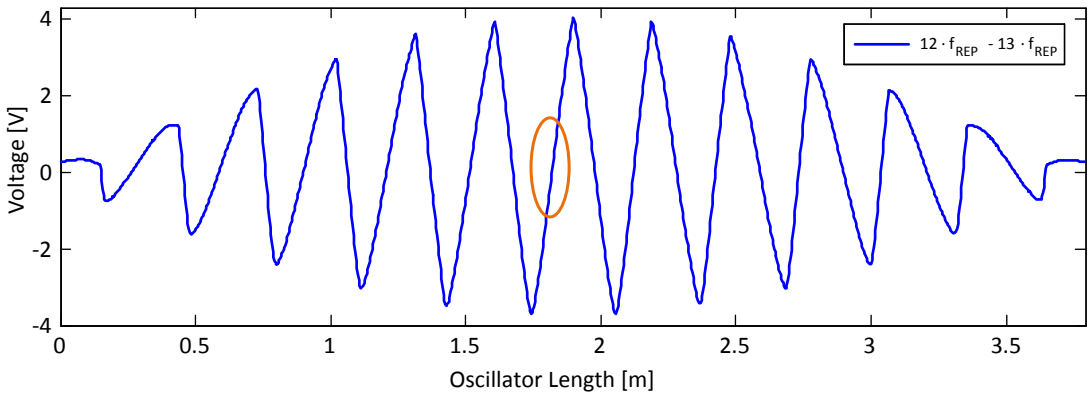

Figure 69: Non normalized FDDM CC signal created by Subtracter Board

The CC signal has a complete amplitude of $\pm$4 V. The x-axis of the CC signal is here defined by the oscillator length. As can be seen in Figure 69 compared to Figure 68 the signal of the Subtracter Board is different from the LabView program. In Section 14 it is mentioned, that different absolute amplitudes of the harmonics relates to an displacement shift of the CC signal. This can be seen by the CC signal at the right or the left end of the graph in Figure 68. The amplitudes have a correlation of $\frac{U_{12}}{U_{13}}$ = 1.05. This is caused by imperfection of the electronic devices of the FDDM Board and the Subtracter Board.

The amplitude of the CC signal is about $\pm$4 V which increases the slope. The fine resolution of one zero crossing point (at dt = 12/25 $\widehat{\simeq}$ 1.82 m) can be seen in Figure 70.

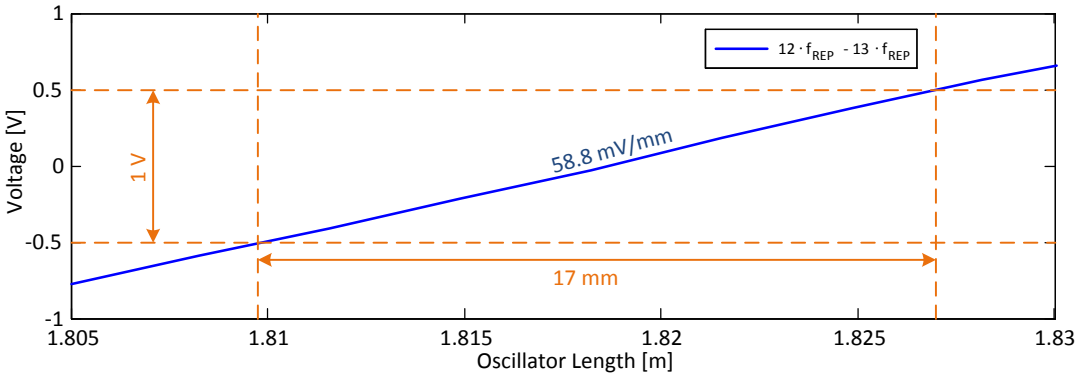

Figure 70: Magnified FDDM CC signal for slope determination

The slope of the chosen dt_{zc} is measured to 58.8 V/m (58.5 mV/mm).

The record of the CC signal shows no jitter of the voltage. Mentioned in Equation 20 in Section 2.6.3 the voltage of the CC signal can be used to define the stabilization possibility of the optical oscillator. This is already done in Section 4.2.1 but should be confirmed with the FDDM CC signal as well.

With the Electrical Spectrum Analyser the repetition rate peak of the Fast Detection Unit is measured. The required information about the SNR is then used to calculate the theoretical limit of the CC stabilization unit. This is very important, to see if the used electronic is capable of dealing with the stabilization signal.
The peak is illustrated in Figure 71.

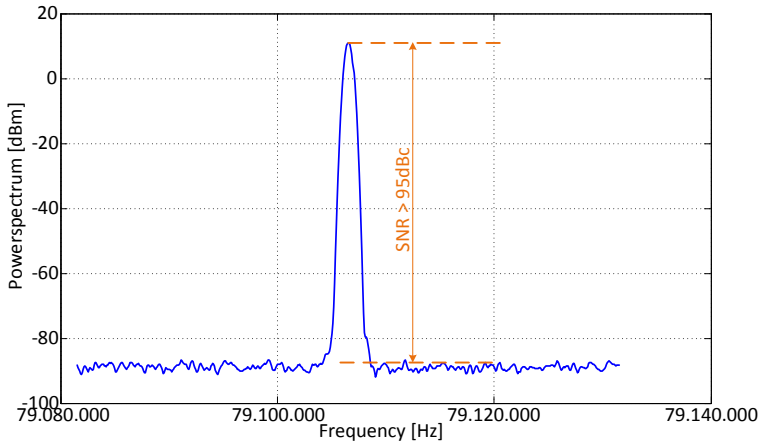

Figure 71: Oscillator peak at 79.106 MHz with integration time 1 s

The SNR of the repetition rate is measured to $>$ 95 dBc. With $P \propto U^2$ this equals to

$$\Delta U = \sqrt{SNR} \cdot U_0$$
$$\xrightarrow{U_{CC}=\pm 4\,V} \Delta U = 10^{-95/(2\cdot 10)} \cdot 4\,V < 100\,\mu V$$

The slope is evaluated to $a_s = 58.8\,mV/mm$. Using Equation 20 in Section 2.6.3 the theoretical limit of stabilization can be calculated to

$$\sigma_y(1\,s) = \frac{\Delta U}{a_s c \cdot 1\,s} < \frac{10^{-4} V}{58.8\,V/m \cdot c \cdot 1\,s}$$
$$\sigma_y(1\,s) < 10^{-14}$$

This value is smaller than current H-Maser stabilities. This theoretical value shows, that this setup is already capable for frequency and time distribution using current HF-Standards without further modifications.

The used electronic of the FDDM Board and the Subtracter Board contains low noise devices which correlates to low voltage noise. If the SNR of the optical oscillator is lower than the Electrical Spectrum Analyser is capable of measure, the slope of the CC signal can even be amplified without reaching the limit of the electronic system.

Since the electronic is limited to $\pm 5\,V$ any amplitudes above/below this voltage create saturation. This lowers the freedom to determine at any 'dt' value the absolute distance because there 'U_m' values outside the $\pm 5\,V$ boarders are not measurable.
Since stabilization loops try to reach any zero crossing point of the FDDM CC signal, the saturation of the electronic is not important. In contrary, the higher the slope, the better the stabilization possibility to the target. The limiting factor of measurement of the signal is the ADC with its sample rate of 48 kS/s/Channel and a resolution per channel of 14 bit. In the data sheet a resolution limit of 4 mV per measurement is defined [53]. Recording only the CC signal during stabilization limits the voltage resolution to $< 20\,\mu V/s$.

Equation 14 in Section 2.6.3 determines the slope at each voltage value. The slope a_t is calculated by the equation directly, whereas $a_s = a_t \cdot c$. In Table 8 U_{CC} is correlated to different slopes and the limit using the ADC of the measurement setup.

Table 8: Examples for time/lengths resolution limited by used ADC at 12th zero crossing point

U_{CC} Amp [V]	± 1 V	± 5 V	± 10 V	± 100 V
a_t [mV/ps]	4.25	21.26	42.53	425.28
a_s [mV/mm]	12.76	63.79	127.58	1275.82
$\Delta t_{ADC\,noise}$[fs]	4.30	0.86	0.43	0.04
$\Delta s_{ADC\,noise}$[μm]	1.29	0.26	0.13	0.01

As can be seen in Table 8 at $U_{CC} = \pm 5\,V$ time resolutions of $\Delta t_{ADC,noise} < 10^{-15}$s at 1 s measurement time can be reached without saturation of the used electronics. This is at the region of performances of current optical atomic clocks.

To reach equal distance resolutions like the BOCC setup, U_{CC} would have to be increased to 100 V which implies a loss of information since the electronic would be in saturation.
Nevertheless, the FDDM CC signal has multiple zero crossing points at the dt axis, whereas the BOCC system has only one signal when the pulses are overlapped ($dt \in \{0, 1\}$).

Calculating the requirements to the ground noise of the electronic measurement system would result in a SNR $> 140\,dBc$ which requires ultra low noise electronic.

4.3.2 Oscillator Stabilization using FDDM CC Signal

After verification and characterization of the FDDM CC signal, the setup is modified to use the CC signal for stabilization of the oscillator. The new setup is illustrated in Figure 72.

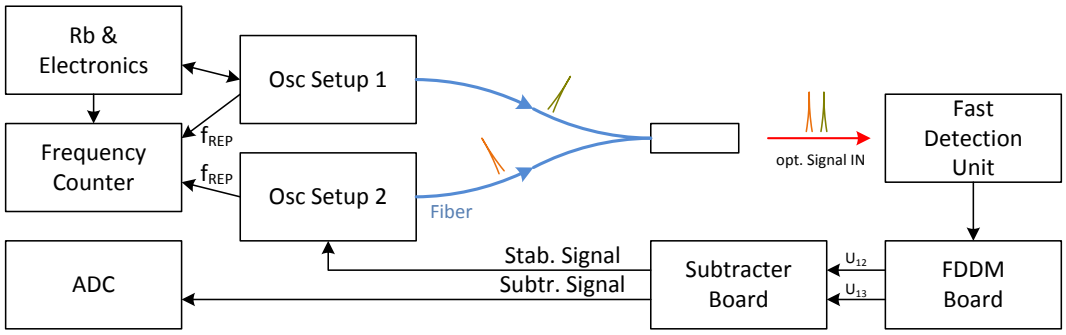

Figure 72: Characterized CC signals for oscillator stabilization

With the prior setup in Section 4.3 the CC signal is characterized. Using the Stabilization Signal output of the Subtracter Board for the oscillator setup creates a stabilization loop which locks the second oscillator to the first oscillator. When the stabilization loop is activated the voltage of the failure signal results in the stabilization performance. The voltage is recorded with the ADC.

Since the Subtracter Board contains a PI-Unit and a unit to control offset and gain for the output, the stabilization signal can be modified to reach the requirements of the oscillator setup ($V_{stab} > 0\,V$).
When the stabilization loop is active the repetition rate of oscillator 1 and 2 should be equal. Therefore their repetition rates are recorded by a Frequency Counter with two inputs [54].

The CC signal in Section 4.3.1 has an amplitude of $U_{CC} = \pm 4\,V$. To use the full potential of the Subtracter Board, the harmonics are electronically amplified to reach $U_{CC} \approx \pm 5\,V$ as can be seen in Figure 73.

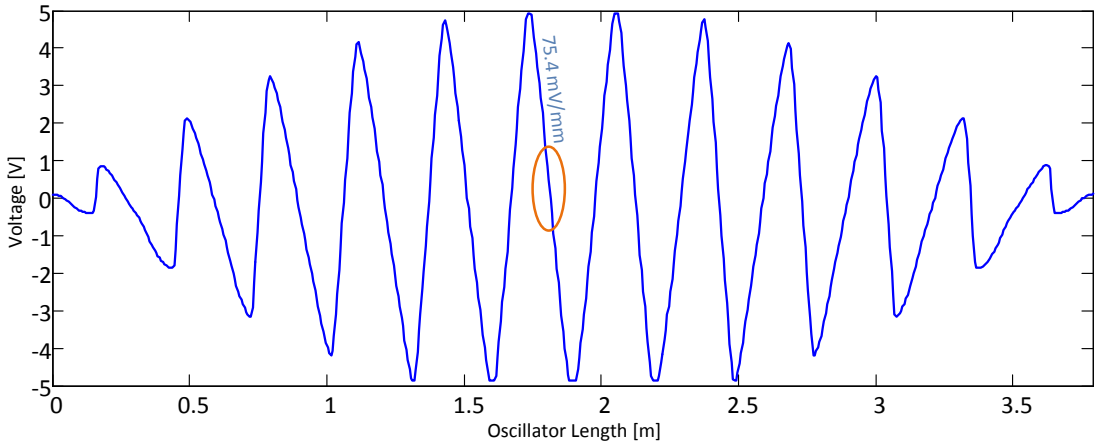

Figure 73: Characterized CC signals for oscillator stabilization

The CC signal nearly fits the electronic limit of $U_{CC} \approx \pm 5\,V$. Nevertheless a saturation can be seen at $U_{CC} = -5\,V$. The x-axis is normed to the oscillator length of 3.79m ($f_{REP} = 79\,106\,500\,Hz$) and the slope is measured to $a_s = 75.4 mV/mm$ ($a_t = 25.1 mV/ps$) at the 12^{th} zero crossing point.

After closing the stabilization loop, the CC signal is recorded by the ADC with a measurement rate of 48 kS/s. To reduce data, the measured values are averaged over 480 values, which results in a measurement rate of 100 Hz. The voltage measurement accuracy reaches then $\Delta U < 0.2\,mV$ per measurement point. The lowest stability which can be measured with the ADC is then

$$\Delta U_{ADC\,limit}(100\,Hz)/a_s = \frac{0.2\,mV}{75.4\,mV/mm} < 2.8\,\mu m$$
$$\Rightarrow \sigma_{ADC\,limit}(0.01\,s) < 10^{-14}$$

The stabilization limit dependent on the ADC measurement accuracy is limited to a stability of $\sigma(0.01\,s) \approx 10^{-14}$. Even when the stabilization has a better performance, the ADC would not be able to record it.

The measured CC signal for stabilization of the second oscillator is shown in Figure 74.

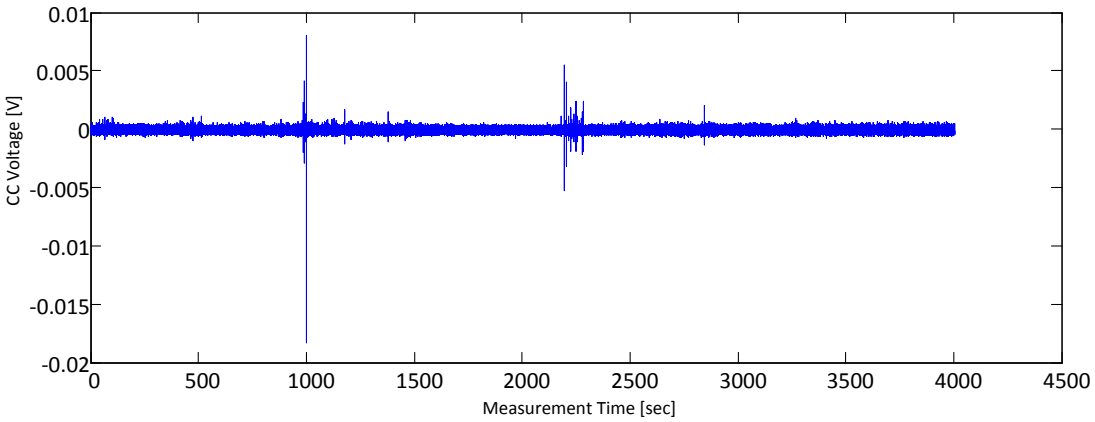

Figure 74: CC signal of the oscillator stabilization

The CC signal stays constant at '0' when the loop is activated. The CC signal shows no drift during the stabilization time of $t_{stab} > 1$ h.

The two mayor spikes at about 1000 s and 2200 s were created by a neighboured setup on the optical table. During measurement some hardware modification at the neighboured setup were done, which results in a shock impact on the table. Nevertheless, the system records the shocks but continues with the stabilization.

By using the slope of a_t = 25.1 mV/ps (a_s = 75.4 mV/mm) the deviation of the measurement can be calculated to an Allan Deviation which is shown in Figure 75.

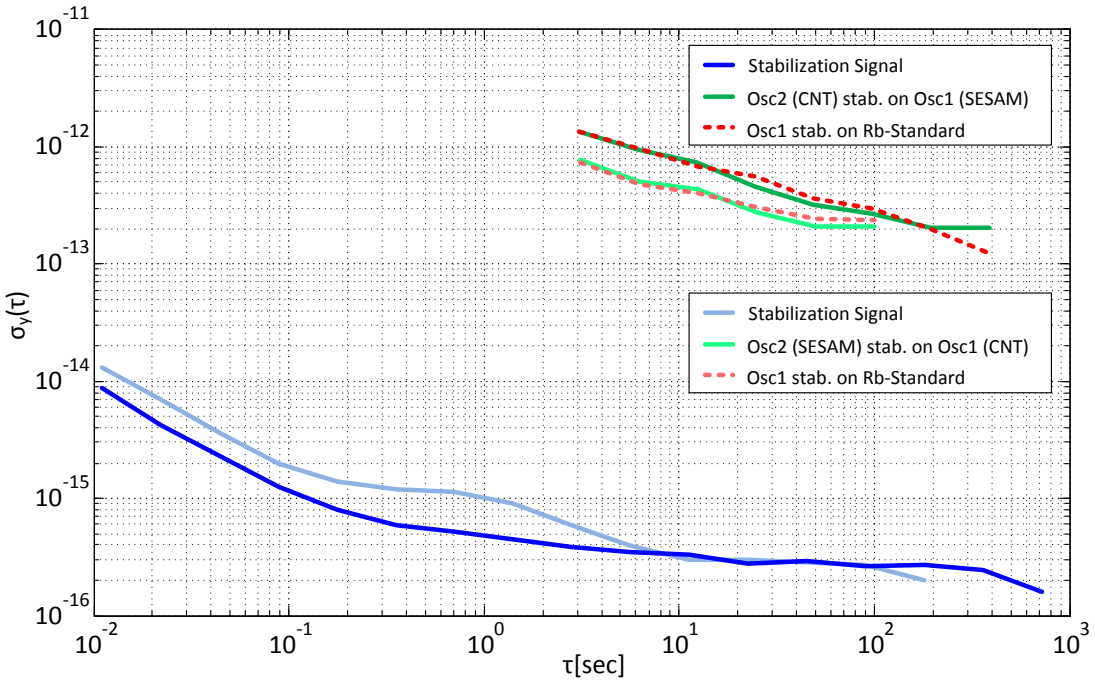

Figure 75: Stabilization of Osc.System1 on Osc.System 1

Two measurements are shown:

1) The curves with deep colours demonstrate when the SESAM oscillator is locked on the Rb-Standard and the CNT oscillator is stabilized on the SESAM oscillator. The CC signal shown in Figure 74 correlates to this Allan deviation.

2) The curves with bright colours demonstrate when the CNT oscillator is locked on the Rb-Standard and the SESAM oscillator is stabilized on the CNT oscillator.

to 1):

The Allan Deviation shows at 1 s measurement time already an Allan Deviation of $\sigma_y(1\,s) = 5{\cdot}10^{-16}$ which is enough to stabilize two optical oscillators with the performance of a Rb-Standard. There is accordingly no loss of stabilization between oscillator system 1 and oscillator system 2. The repetition rates of oscillator 1 and oscillator 2 are measured and their Allan Deviation is illustrated in the same figure. The frequency of oscillator 2 shows no difference to oscillator 1.
The SESAM oscillator shows stronger jitter on pump power of the laser diode than the CNT oscillator. Therefore the Allan deviation is $\sigma_y(1\,s) \approx 2 \cdot 10^{-12}$. Nevertheless the CNT oscillator follows any fluctuations of the SESAM oscillator.

to 2):

For the second measurement the two oscillator systems are transposed. The system should work

properly for both scenarios.
The CNT oscillator can be stabilized to $\sigma_y(1\,s) \approx 1 \cdot 10^{-12}$ since it is less sensitive to pump power fluctuations. Surprisingly the SESAM oscillator shows equal performance as the CNT oscillator. The frequency stabilization using the CC signal can handle jittery oscillators better than the Synthesizer Board.
The stabilization signal shows a rising instability at 1 s measurement time which results to a lower performance compared to the first scenario.

Both stabilization links start with $\sigma_y(0.01\,s) \approx 10^{-14}$ which is the measurement limit of the ADC. It is expected, that the stability of the link is even lower than the measured values.

It must be mentioned again, that a link between two clocks can never be better than the clock on which the stabilization system is based on. The Allan Deviations showed with this link is only a theoretical value. The system would be capable of create a link between two oscillators with the limit of $\sigma_y(1\,s) < 10^{-15}$. For real validation a time standard with these performances would be necessary.

In summary, with the FDDM CC stabilization method a new type of frequency stabilization is created. With a link between two oscillators of $\sigma_y(1\,s) < 10^{-15}$ the performance is at the same region as current optical atomic clocks. The system is based only on electronic devices and has an easier handling compared to the BOCC setup.

4.3.3 Measurement of larger Distances using FDDM and the CC signal

In Section 4.1.1 it is shown, that the FDDM method is capable of measure distances over 100 m of a fibre. This method is used a second time with the FDDM CC signal. Also the fibre length is increased and modified with an additional fibre coupler at the largest distance. This is later used, to split the pulse power for a distant frequency stabilization.
The setup with fibre is shown in Figure 78.

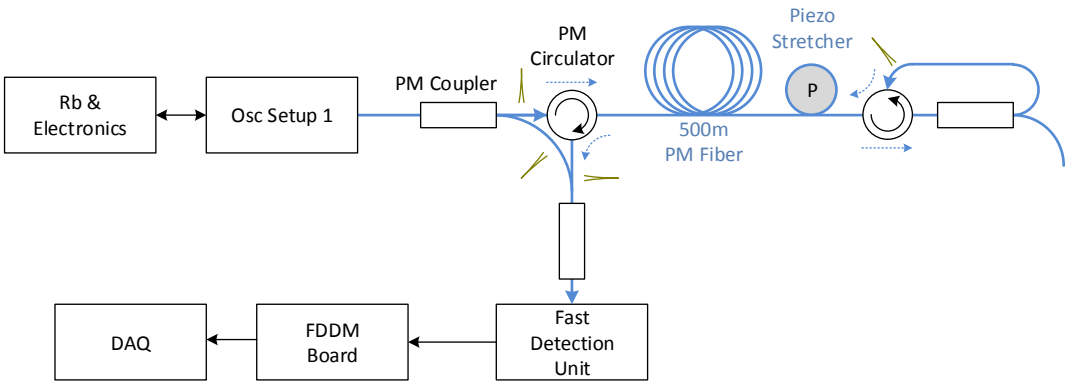

Figure 76: Measurement of the first and second harmonic shifting the repetition rate

The pulses from the (SESAM) optical oscillator are split into two paths. One part propagates through an optical circulator, a 500 m fibre, a Piezo Stretcher another optical circulator and a coupler. The loop is closed, that after the second coupler the pulses go back to the connected circulator. After propagating through all the fibre back, the pulses from the first coupler are heterodyned after the first circulator. All fibre components are polarization maintaining, but also non-polarization maintaining setups could be used.

The frequency must be shifted again to calculate the multiple factor 'n' to determine the absolute distance. In the previous Section 4.1.1, the frequency is shifted by temperature changing of the oscillator housing. In this case, the slip stick driver of the oscillator is used, to create in shorter time larger frequency shifts ($>$ 180 kHz, see description in Section 3.1.1).
Before and after the frequency shift, the oscillator is frequency stabilized to a Rb-Standard. During the shift, the harmonics start to oscillate. The oscillation is recorded by the ADC. The start and end points can then be used for calculations. All recordings are done by a LabView software. The content of the program is illustrated in Figure 77.

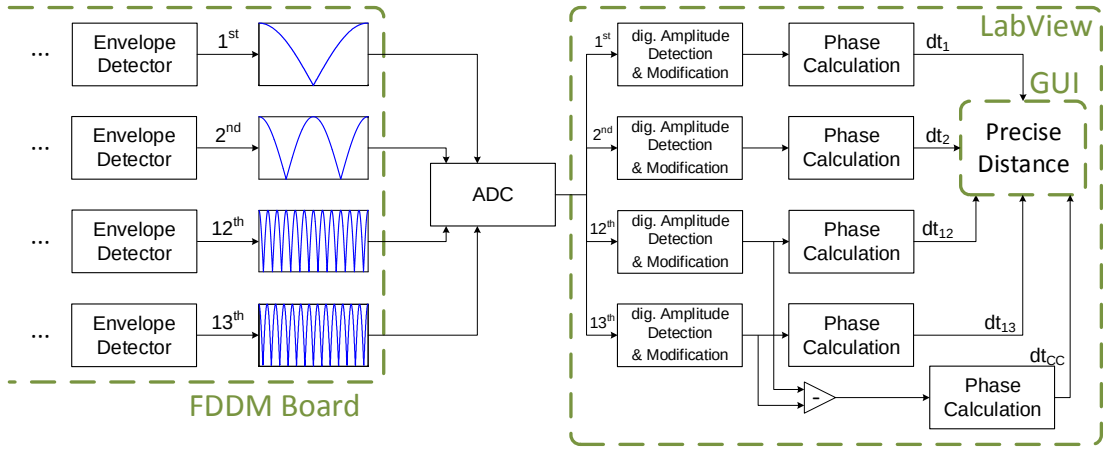

Figure 77: Software for automated length calculation

In Figure 78 the measurement data of the first two harmonics can be seen.

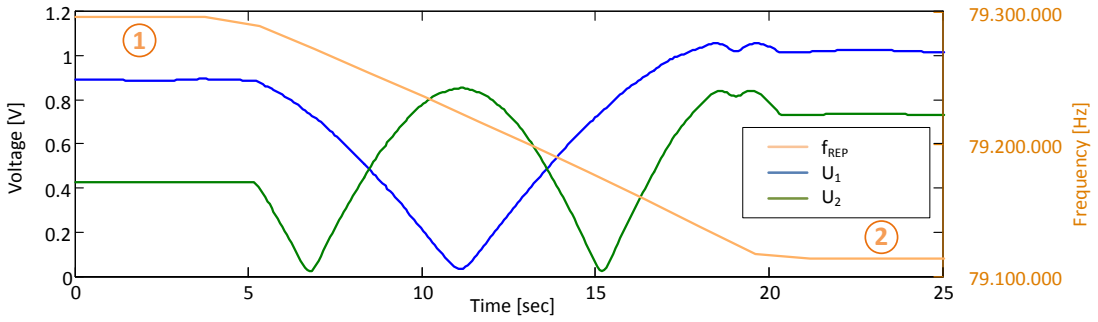

Figure 78: Measurement of the first and second harmonic shifting the repetition rate

At the start of the measurement (Point 1 in Figure 78) the frequency is at about 79 300 000 Hz and lowers within 15 s to about 79 120 000 Hz (Point 2 in Figure 78). The first and second harmonic are passed through their dt = 0 point at about 18 s. The dent at this point results from the saturation of the electronic amplification, since all harmonics have their maximum.

The amplitudes of the first and second harmonic are not equalized, which is not necessary for calculations. The amplitudes are measured before the start of the measurement of each path (reference and target path).
The voltage values of the harmonic 1 and 2 at Point 1 and Point 2 are recorded.

With the measurement of the reference and target path, theoretical values can be created and compared with the measurement. Figure 79 illustrates the theoretical deviation of the harmonics.

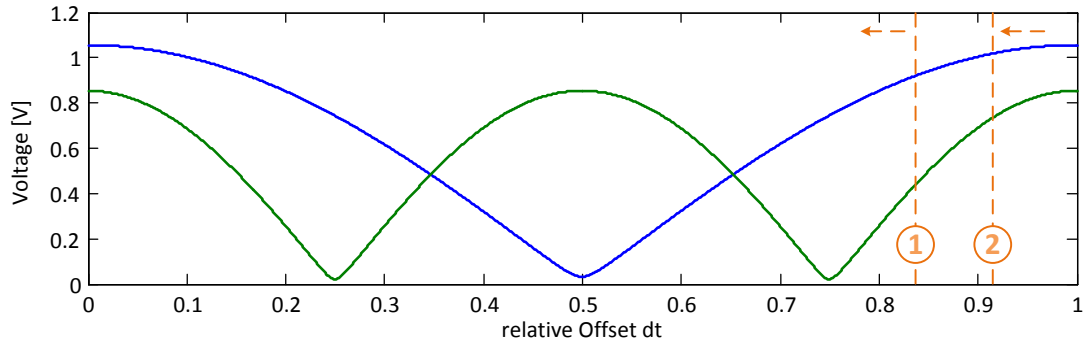

Figure 79: Simulated values using the individual amplitudes of the harmonics

The created deviation of the harmonic 1 and 2 fits the measured values. The comparison of the values of Point 1 and Point 2 shows where the start and end points are located. The first two harmonics are not used for precise measurement. The calculated points are hints for the higher harmonics.

The same measurement is done for the 12th and 13th harmonic. Figure 80 shows the record.

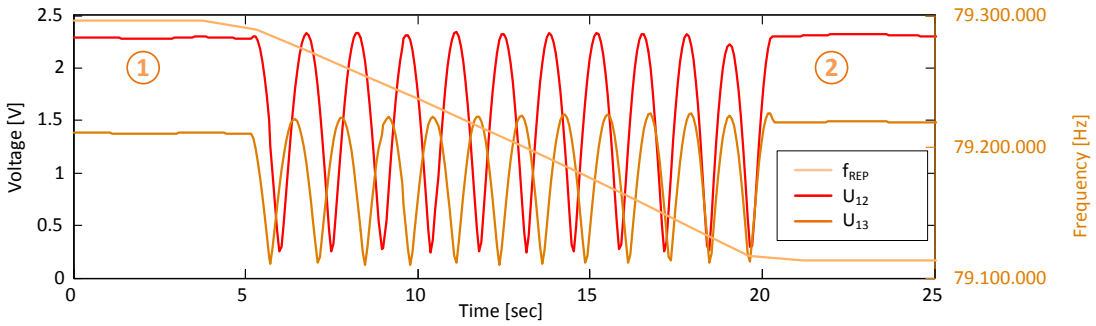

Figure 80: Measurement of the 12th and 13th harmonic shifting the repetition rate

The 12th and 13th harmonics show as expected a higher oscillation which helps for more precise resolution. As mentioned before at about 18 s measurement time, the dt=0 point is reached. This can be seen, as the amplitudes of the harmonics are lower due to saturation of the electronic amplifier.
Also the amplitudes are not equal. The noise floor and the harmonics for reference and target path have to be measured again, to create the theoretical values.
The measurement at Point 1 and Point 2 are taken to define the start and end values.

Important for the measurement is that, at Point 1 and Point 2 in Figure 80 the voltage is jittering and decreases the measurement accuracy. This depends on the jitter of the used SESAM oscillator.

With the measured values, the theoretical deviation of the harmonics can be regenerated, which is illustrated in Figure 81.

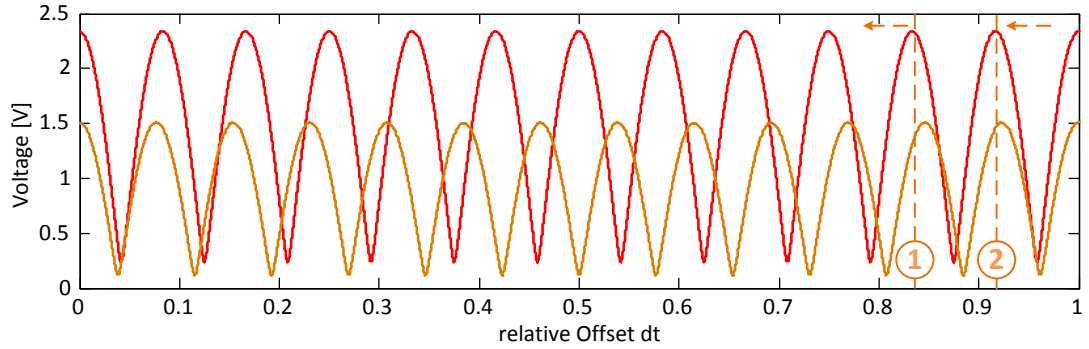

Figure 81: Simulated values using the individual amplitudes of the higher harmonics

The amplitudes and the offset of the theoretical values fit the deviation of Figure 80. The measurement of the first and second harmonic is hereby used to define the starting point, since the 12^{th} and 13^{th} harmonics are periodic in $dt_n = \frac{n}{2m+1}$ (see Section 2.6.1).

Starting Point 1 and ending Point 2 can be measured more accurate. This is like the measurement principle as in Section 4.1.1. Nevertheless, the accuracy is lowered compared to the prior measurement with the Electrical Spectrum Analyser, since the oscillator jitter is still present and prior observed harmonics had with 15^{th} and 18^{th} a higher number.
Compared with the first try, the readout is simpler since everything is done by a computer program.

For the first time, the FDDM CC signal is used for distance estimation. The same principle of measurement used before for the harmonics is now applicable for the CC signal. The measured values during the frequency shift can be seen in Figure 82.

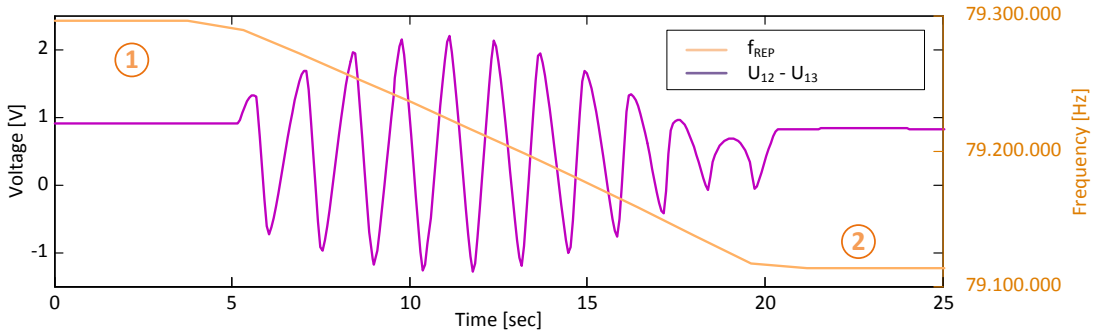

Figure 82: Measurement of the CC signal shifting the repetition rate

Since the amplitudes of the 12^{th} and 13^{th} harmonics are not equal and have different offsets, the CC signal shows the behaviour as mentioned in Section 2.6.1. The measured values at Point 1 and Point 2 in Figure 82 are again taken for precise distance measurement.

Interesting to know, that the jitter of the oscillator caused voltage jitter for the 12^{th} and 13^{th} harmonics. Since for the CC signal, both jitters are subtracted from each other, the jitter measured with the CC signal is lower correlated to the harmonics amplitudes.

The theoretical values can be calculated by using the amplitudes of the 12^{th} and 13^{th} harmonics. The values are shown in Figure 83.

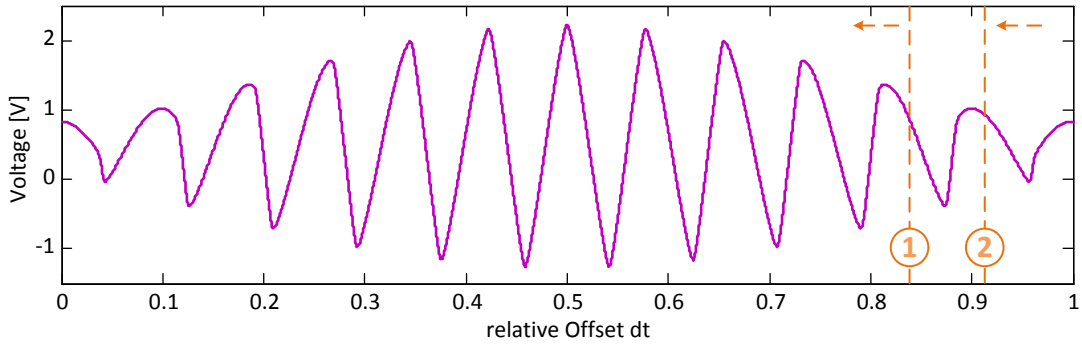

Figure 83: Simulated values of the resulting CC signal

The deviation of the FDDM CC signal and offset fit the measured values of Figure 82. The values to generate the FDDM CC signal are taken from the prior measurement of the 12th and 13th harmonics Point 1 and Point 2 in Figure 82.

A new advantage can be seen at this measurement method. Calculating the FDDM CC signal, each spike has its own voltage maximum. If the frequency is shifted that U_{CC} passes one of the spikes, the 'dt' value can be calculated instantaneously. The value is unique within the area within dt $\in [0, 0.5]$ or dt $\in [0.5, 1]$.
Therefore the CC signal implies advantages of the absolute value of 'dt' and the high precise resolution of higher harmonics.

With these values, the absolute optical distance can be calculated.

dt_1 =	0.83641	dt_2 =	-0,08842
f_1 =	79 295 864 Hz	f_2 =	79 112 979 Hz
$\Rightarrow$ m =	400	n_{ref} =	1.4475 [48]
$\Delta D_{1,opt}$ =	758.2421 m	$\Delta D_{2,opt}$ =	758.2414 m
$\Delta l_{fiber,1}$ =	523.828 m	$\Delta_{fiber,2}$ =	523.828 m

The here calculated values are the optical distance within the fibre which means, calculated without a refractive index. The accuracy of this measurement is $\Delta s < 1$ mm. The accuracy of the system described in Section 4.1.1 showed an accuracy of $\Delta s < 1$ cm.

The measurement accuracy with $\Delta s < 1$ mm is also the limit to measure the fibre length. Assuming a dependency of refraction index of temperature with $\partial_T n_0 = 6.25 \cdot 10^{-6}$/K [55] even a change of $\Delta T < 0.5$ K results in a lengths change of $\Delta s < 1$ mm. Since the fibre can not be temperature stabilized this is defined as the resolution limit.

In summary, the FDDM CC method increases the resolution of the absolute distance measurement. The measurement with a software program creates a direct output of the distance. The

resolution of the system is limited by the change of refraction index due to temperature.

4.3.4 Frequency Synchronization over Stabilized Fibre

In Section 4.3.2 the FDDM CC signal is used to lock the frequency of two optical oscillators.
In Section 4.3.3 a larger distance is measured using the FDDM CC signal.

To stabilize an oscillator over a larger distance the stabilization path itself must be stabilized to guarantee a loss free transport of information. If the length of the path is known and stabilized, it also can be used to transport the information of time from one point to another.

The combination of the prior sections allows the frequency synchronization over long distances and a time transfer between both oscillators.

The optical setup is updated which can be seen in Figure 84.

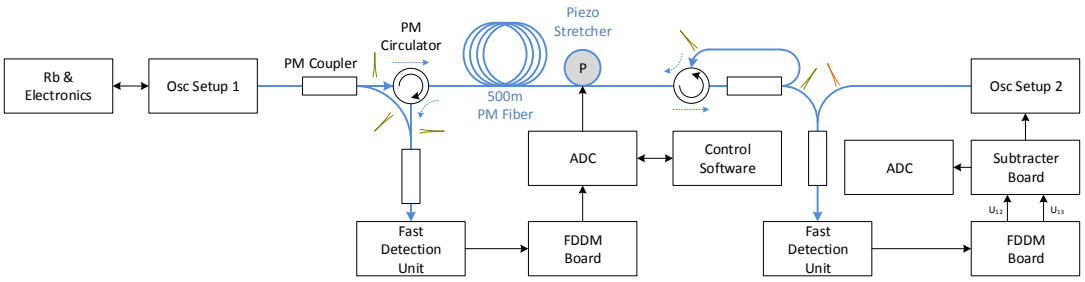

Figure 84: Setup to stabilize fibre and frequency transmittance

The pulses from oscillator 1 are still propagating through the fibre and back and are overlapped with the reference path. The CNT oscillator shows lower jitter in the output spectrum and is therefore used for the fibre stabilization.

After the detection unit, the FDDM Board is still connected to the ADC. The measurement of the harmonics is done as in the prior section. The software received an update, that an PID controller is included to create a stabilization output. The update can be seen in Figure 85.

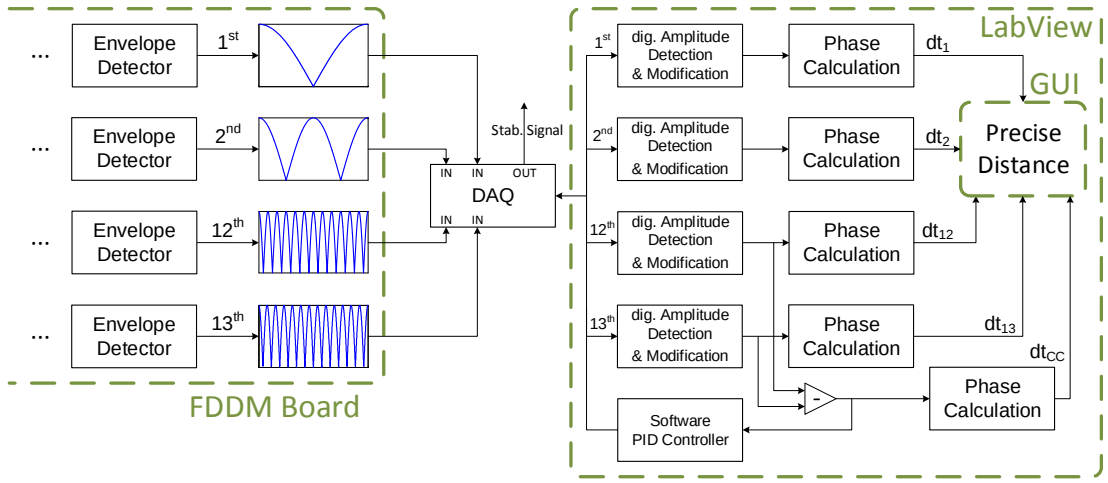

Figure 85: Updated software to create an output for length stabilization of the fiber

The ADC is capable of create a voltage output $U_{out} \in [0\,V, 5\,V]$. This output is amplified with factor 30 using high voltage amplifier. The high voltage is then used to control the Piezo Stretcher.
The harmonics are recorded with total 40 kS/s which results in 10 kS/s/channel. The last 8 kS/s are reserved for the output of the ADC.

A software PID controller creates the stabilization output which varies the Piezo Stretcher to modify the fibre length. The advantage of a software solution is, that any voltage point of the CC signal can be used as a starting point. The hardware is bounded to stabilize the CC signal to one prior defined point (to '0').

Important is that with the electronics, the amplitudes of the 12^{th} and 13^{th} are modulated to have similar voltage output. This is used to create the norm CC signal. The resulting zero crossing points are calculated as defined in Section 2.6.1 in Equation 13. With this input, the absolute distance to the second oscillator can be clearly calculated.
Pulse broadening due to group velocity mismatch of the pulse spectrum has therefore no influence on the FDDM CC signal. The adaption using the software avoids several issues using a hardware setup.

To stabilize the second oscillator a part of the pulses from oscillator 1 is separated by a coupler and then overlapped with the pulses from oscillator 2. The setup is afterwards the same used in Section 4.3.2. A second FDDM Board and a second ADC of the same type are used.
The electronic signal is amplified to create a higher slope for the CC signal.

The measurement of the CC signal is measured for characterization. The results can be seen in Figure 86.

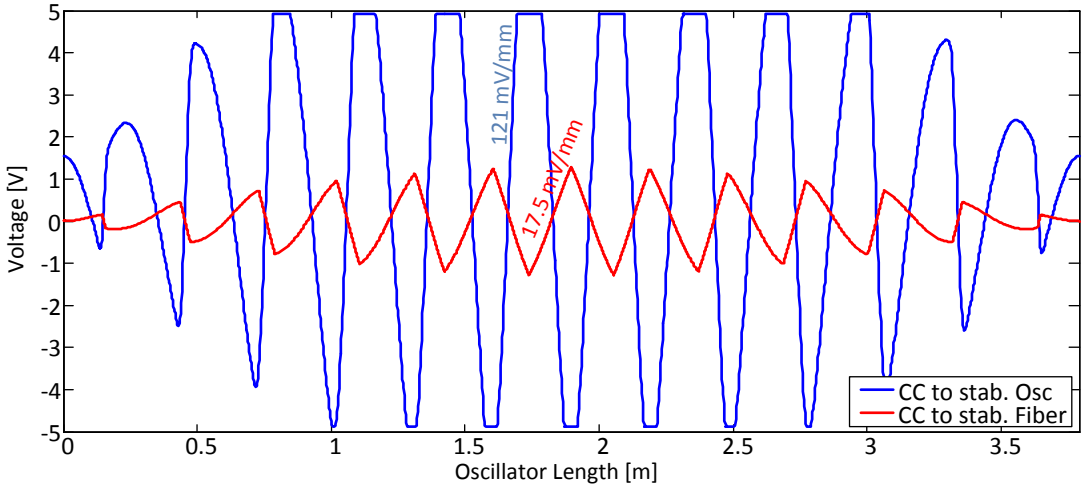

Figure 86: Characterized CC signals for fibre stabilization and oscillator stabilization

The slope for oscillator stabilization is with a_s = 121 mV/mm (a_t = 36.3 mV/ps) higher than within prior setups. This is caused by the new generated FDDM Board which is designed to create higher voltage outputs. Also the Subtracter Board is modified to create higher voltages. Thus information is lost, if it's used for absolute distance detection. Since this setup is used for frequency stabilization, saturation of the voltage is no disadvantage.

The slope for the fibre stabilization is measured to a_s = 17.5 mV/mm (a_t = 5.25 mV/ps). Since the whole signal processing is done electronically, the slope is not essential since the software PID controller can be modulated to create the necessary output.

The total hub of the Piezo Strecher is defined to 300 μm (2 · 150 μm) [50] which is not enough to create a long state ($t_{stab} > 1$ h) stabilization but results in the possible performance of this kind of stabilization.
Therefore the frequency stabilization of the second oscillator is activated first, because its performance is independent of the stabilized fibre. During the stabilization the CC signal is measured with the second ADC with its full performance of 48 kS/s.
Afterwards the software stabilization is activated. For the start vale the current CC voltage value is taken as set value for the PID controller. As long as the control loop works within its limits of $U_{stab} \in [0\,V, 150\,V]$ the stabilization is activated. If the signal it outside of its lock-in range, the recorded CC signal has a random drift.

In Section 4.3.2 it is mentioned, that the ADC is used only to record the hardware based CC stabilization signal. For record this signal, only one channel is necessary with the calculated limit of $\sigma_{ADC\,limit}(0.01\,s) \approx 10^{-14}$.
For the software based stabilization, four channels are used and the measurement rate is limited to 10 kS/s/channel. With the CC slope of a_s = 17.5 mV/mm the ADC creates a stability limit of $\sigma_{ADC\,limit}(0.01\,s) \approx 10^{-13}$. There is a performance difference of one order of magnitude between

hardware and software stabilization, because of the used ADC.

In Figure 87 the stabilized fibre and oscillator signals are illustrated.

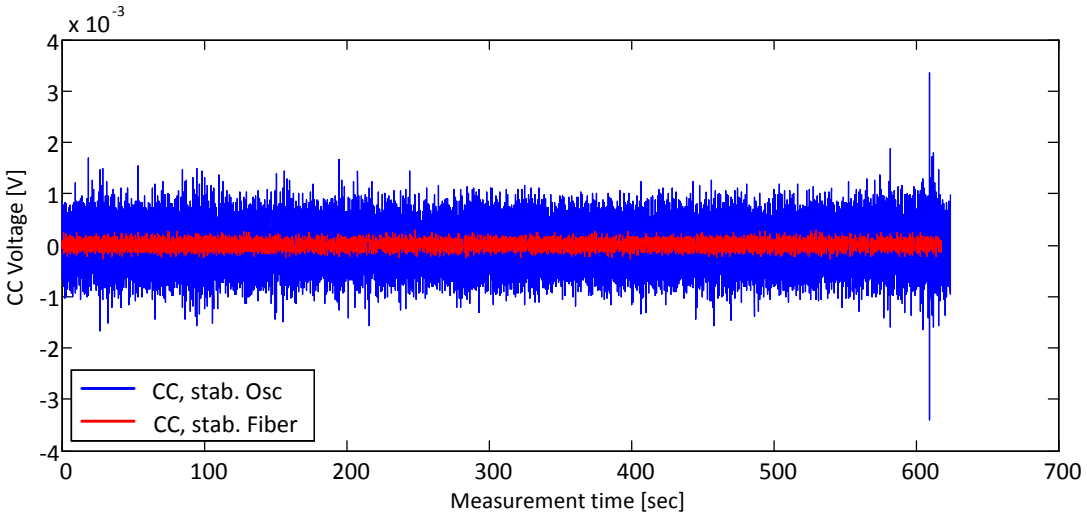

Figure 87: CC signal of the fibre and oscillator stabilization

The stabilization of the fibre is maintained for $t_{stab} > 10\,\text{min}$ and in parallel the frequency stabilization of the second oscillator. The offset voltage of the fibre signal is subtracted for illustration.

The failure signal of the oscillator stabilization is higher since the slope of $a_s = 121\,\text{mV/mm}$ ($a_t = 36.3\,\text{mV/ps}$) is doubled compared to the slopes of prior setups.

The digital stabilization shows the same characteristic as the hardware setup. But the handling is easier since the software can handle the U_{CC} value at each 'dt' value, not only on dt_{zc} (like the hardware). Also, the PID controller can be fitted automatically with the slope input. To receive low jitter performances of the CC failure signal, the PID controller must be adapted to the slope of the CC signal. This can be programmed automatically.

The measured values result in an Allan Deviation which is shown in Figure 88

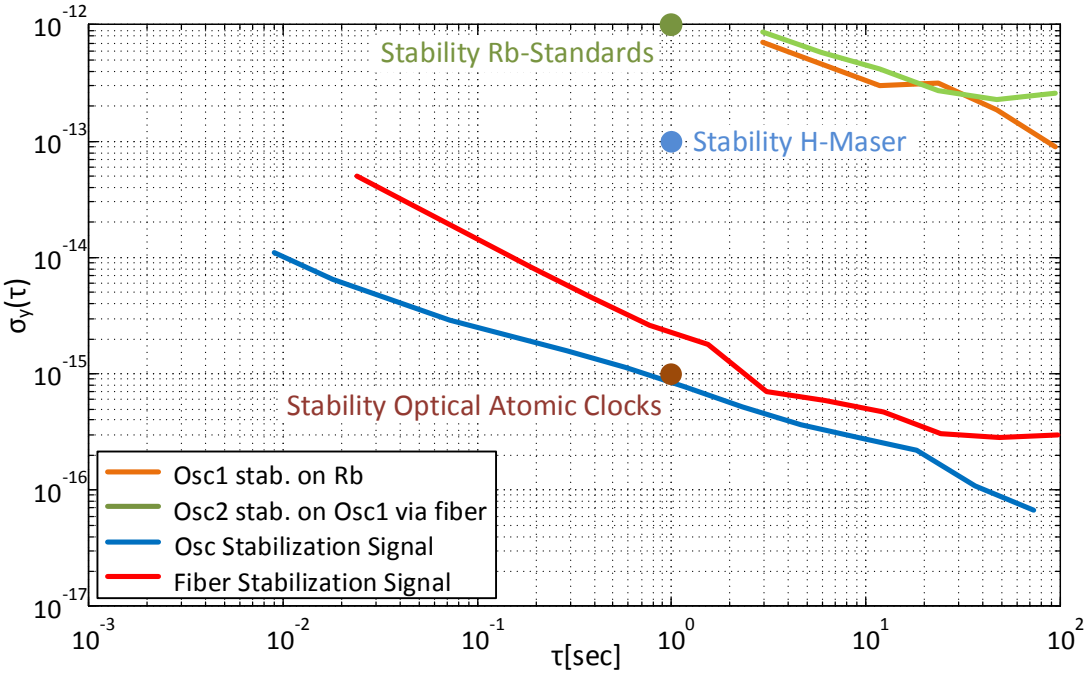

Figure 88: Complete system stabilized over a 500 m fibre connection

The frequency of the oscillator 2 (SESAM) follows again the repetition rate of oscillator 1 (CNT), which in turn is stabilized on the Rb-Standard.
The fiber is stabilized with $\Delta s < 1\ \mu m$ at 1 s measurement time. This results in a time stabilization $\sigma_y(1\,s) = 2 \cdot 10^{-15}$ which is more than 2 orders of magnitude better than the used clock standard. Also the oscillator stabilization has with $\sigma_y(1\,s) < 10^{-15}$ the possibility to create a stabilization between two optical clocks, without loss.

As mentioned before, the used ADC for software stabilization is a stabilization limiter with $\sigma_{ADC\,limit}(0.01\,s) \approx 10^{-13}$. But the stabilization software itself reaches already this predefined limit. Thus it can be expected, that with a faster ADC the performance can also be lowered to reach $\sigma_y(1\,s) < 10^{-15}$.

The digital system promises then a huge advantage compared to the analogue setup:

1) The amplitudes of the 12th and 13th harmonics can be adjusted with software dependent amplitude modification to receive the norm CC signal.
2) The stabilization point can be defined at any dt value.
3) The input for the PID controller can automatically be adapted to the occurring slope of the CC signal.

Also the electronic setup can be created comparatively simple when an FPGA is used. Then a higher measurement rate with higher voltage resolution promises stabilizations $\sigma_y(1\,s) < 10^{-15}$ without effort.

4.3.5 FDDM CC within Dynamic Systems

A theoretical approach should evaluate the possible performance of a highly dynamic scenario using FDDM CC. Since the stabilization ranges are higher than the BOCC system, a higher performance is expected.

The FDDM CC stabilization range of $l_{stab} \approx 152\,mm$ is characterized. The system itself has a modulation frequency $f_{mod} = 1\,kHz$ which is defined by the HV amplifiers. Within this modulation time the system can adjust itself without falling out of the stabilization loop. This results in a maximum velocity of

$$v_{max} = l_{stab} \cdot f_{mod} = 152\,mm \cdot 1000\,Hz = 152\,m/s$$

The system would be capable of lock on targets with relative velocities up to 150 m/s. This value is sufficient for velocities which occur in the scenario of neighboured satellites in the same orbit ($v_{rel,max} \approx 10\,m/s$, see Section 2.4.2). But the distance ($D_1 \approx 2 \cdot 10^7 m$) lowers the modulation frequency to $f_{mod} = 2 \cdot D/c \approx 7.5\,Hz$ which results in a maximum relative velocity of $v_{max} = 1.14\,m/s$. Therefore even with the larger lock-in range of the FDDM CC method, the system would not be able to lock on the target continuously. Nevertheless the time window to lock on the target would be $t = 26\,min$ where the system could be used with its characterized performance.

Using the system within different orbits would result in a time window of $t < 3\,s$ ($D_2 = 6 \cdot 10^6 m$). Implementing this system with these performances would be very challenging.

FDDM CC Summary

The FDDM CC system is capable of stabilize a $l_{fibre} > 500\,m$ whereas in parallel the CC signal can be used for frequency adaption of a second oscillator system. When the fibre is stabilized, the fibre length is exactly known ($\Delta s < 1\,\mu m$ at 1 s measurement time) which can then be used, for time transfer between the two oscillators.
Until now, the system shows no show stopper for stability synchronization with $\sigma_y(1\,s) < 10^{-15}$.

The handling is easier compared to the BOCC system since the lock-in range of the stabilization is automatically done, by the deviation of the FDDM CC signal itself. Also no complex optical system is required to receive similar performances than the BOCC setup.

The FDDM CC method is already applicable for the Galileo scenario with neighboured satellites within one orbit. The time window for measurement and synchronization is with $t_{syn} = 26\,min$ sufficient. Issues occur to measure/synchronize two satellites within two different orbits. Either the velocity is to high, or the distance which decreases the modulation frequency of the system.

4.4 Application for Space Missions

The purpose of the FDDM CC system is the application in space, especially for GNSS. Future developments are focused on the development of a possible 'world time' outside the earth using GNSS: A system which can stabilize itself using every available clock within the satellites. This possibility is studied in the OCTAGON2 project [56].
Best performance time distribution from ground to satellite reaches a timing jitter of less than 10 ps after a integration time of t $>$ 100 s [57]. Using the FDDM CC method or the BOCC system promises the advantage of inter-satellite communication due to time distributions with sub fs performances. Both systems are adequate to serve for a system with optical atomic clocks.

For distance resolution the BOCC system shows a performance which is more than one order of magnitude better than the FDDM CC system. As mentioned before, the distance resolution relates on the detection system and the used optical standard. This is a basic principle of any measurement systems. Therefore the measurement accuracy has its limit with the used frequency standard. Also time distribution is limited by this factor. Figure 89 illustrates the correlation between distance resolution and absolute distance.

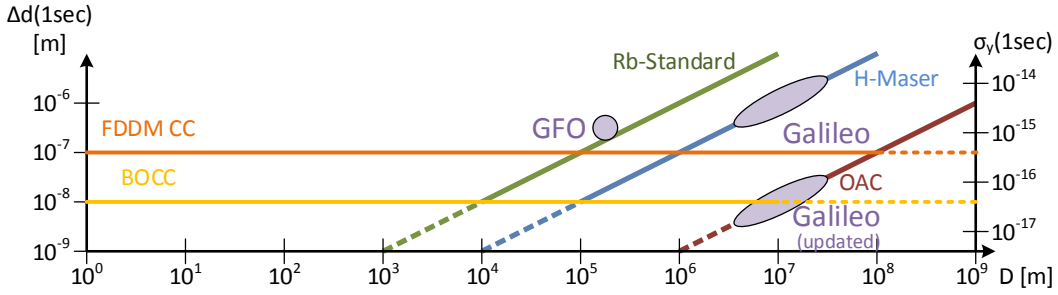

Figure 89: Correlation between CC systems, used time standard and absolute distance resolution

For satellite formation flights like GFO both systems would be sufficient for an application. For Systems like Galileo with an H-Maser as a time standard, both systems would result in the same performance, since the time standard itself is then the limiting factor. This means the current Galileo system would profit of each CC already.
If an optical atomic clock would be installed in a GNSS (Galileo updated), the BOCC system would be in advantage dependent on distance resolution. But since the time distribution with both system is limited by the clock of $\sigma_y(1\,s) = 10^{-15}$, there would be no total advantage for the BOCC system.

Regarding time and frequency distribution within Galileo, both systems have issues with dynamic scenarios, since the velocities are too high for their possibility to lock on the target. At least the FDDM CC method would be able for time and frequency distribution within the same orbit.

A solution for both scenarios would be if the system is installed in both satellites: Primary and

Secondary principle. The pulses from a primary satellite would be detected on the secondary satellite and send back. This has several advantages:

1) The modulation frequency of the optical pulse lasers does not depend on the distance
2) The relative velocity has no influence on the locking performance between two systems
3) The locked pulses of the secondary satellite are equal to an optical amplification

to 1):

The pulse laser of the secondary satellite is synchronized with the incoming pulses of the primary satellite. It is not necessary that the pulses propagate the distance between the two satellites. therefore there is no time delay dependent on time of flight between the satellites. The modulation frequency of the pulse laser to lock on the incoming pulses depends on the hardware of the pulse laser itself. With the parts used in this thesis, the HV amplifier for the Piezos with its limiting frequency of f_{mod} = 1 kHz would be the limiting factor.

to 2):

A relative velocity between two satellites results in a frequency shift of the repetition rate (see Section 4.1.3). The frequency shift is also present in the secondary satellite. If the relative velocity would stay constant, the shift is a constant in the secondary satellite. The pulse laser in the secondary satellite has to adapt its repetition rate once to the incoming pulses. This would be the same scenario shown in Section 4.3.2 where the secondary oscillator is locked on the primary oscillator, with the given performances. The secondary satellite must only adapt its repetition rate to velocity changes (accelerations) between the two satellites.
Acceleration values are a $< 1.5\,mm/s^2$ within the same orbit and a $< 5\,m/s^2$ between different orbits.
The BOCC system with full modulation frequency ($f_{mod,max}$ = 1 kHz) is capable of lock on targets with accelerations up to $a_{BOCC} < 2.4\,mm/s^2$. The BOCC system would then be able to be used for inner-orbit time and frequency transfer, but not for inter-orbit synchronizations.
The FDDM CC system with full modulation frequency could lock until accelerations $a_{FDDMCC} < 152\,m/s^2$. This would be sufficient for time and frequency transfer in any scenario.

to 3):

The propagation through long distances results in an attenuation of the optical power of the pulses. When the second oscillator is locked on the primary oscillator, these pulses are equal to the primary pulses. The pulses of the second oscillator could be send back (amplified) to the primary satellite. The pulses must travel the distance only once.

Using the updated scenario, the FDDM CC method is capable of handle all scenarios of the GNSS mission. Also the singular propagation with an additional amplification at the secondary satellite is an additional advantage.

An algorithm can be created for time and frequency synchronization (including Doppler Shift) after precise distance determination. The application of the FDDM CC system has its advantages in simplicity of the data handling. The Algorithm is described in more detail in Appendix E.

5 Summary

Within this dissertation a new method of time and frequency transfer and an included precise distance measurement between two points is presented.

The Frequency Domain Distance Measurement (FDDM) method is capable of absolute distance measurements with resolution limits defined by the based reference clock itself.
The Frequency Domain Distance Measurement Cross Correlation (FDDM CC) includes all advantages of other known equivalent methods but with increased simplicity in handling, complexity and robustness (see Appendix F).

During the thesis several electronic devices are created:

- Compact synthesizer board with frequency resolution $\Delta f_0 < 1\,\text{mHz}$ and stabilities $\sigma_y(1\,\text{s}) = 2 \cdot 10^{-13}$ (Section 3.2.1)
- Frequency comparator for fine frequency resolution with measurement accuracy dependent on synthesizer board (Section 3.2.2)
- FDDM Board for harmonics separation and measurement (Section 3.2.3)
- Subtracter Board to create CC failure signal and control loop for stabilizations (Section 3.2.4)

All electronic boards include low noise parts which are also available for space applications. The electronic is therefore already adaptable for next space relevant developments.

The FDDM method is clearly verified in Section 4.1.1. At the first try the system is already capable of distance resolutions $\Delta s < 1\,\text{cm}$.
The length of an optical fibre is measured in Section 4.1.2 with the resolution limit of the FDDM method. Therefore the origin application of the FDDM method is validated.
As shown in Section 4.1.3 the FDDM method is also capable of measure velocities with $v_{rel} > 10\,\text{km/s}$ with resolutions $\Delta v_{rel}(1\,\text{s}) < 1\,\text{cm/s}$ using an automated LabView software.

A Balanced Optical Cross Correlator (BOCC) is created in Section 4.2 with the background of the FDDM system and its applicability in space for GNSS systems. The setup is capable of distance resolutions of $\Delta s(1\,\text{s}) < 10\text{nm}$.
It is also shown that frequency transfers with $\sigma_y(1\,\text{s}) < 10^{-16}$ are possible with the BOCC system. A fibre with $l_{fibre} > 100\,\text{m}$ is stabilized to $\Delta s(1\,\text{s}) < 10\,\text{nm}$.
The BOCC as a distance measurement system is already proofed by multiple publications. The setup created in this thesis is defined to compare performance, handling, compactness, simplicity and robustness with the new FDDM (CC) method. It is also tested for special requirements for space applications in Galileo or GFO.

Section 4.3 contains validation, characterization and application of the FDDM CC method.

First measurements in Section 4.3.1 are a proof-of-concept. The result suits the theoretically prediction prepared in Section 2.6.1. Using a software program modifies the CC signal to its norm

form without loss of information. The advantage of the digital method is that amplitude variations of the FDDM CC signal can be avoided which cause dt_{zc} shifts (time/lengths shifts).

After characterization the FDDM CC signal is used for frequency lock between two oscillators, which is shown in Section 4.3.2. The frequency of one oscillator is synchronized with a second oscillator without loss of stability. The lock between the two oscillators with $\sigma_y(1\,s) < 10^{-15}$ is sufficient for frequency synchronization between two optical clocks.

Since the FDDM CC signal is characterized to have a higher distance resolution, in Section 4.3.3 the length of an optical fibre ($l_{fibre} > 500\,m$) is measured with accuracies limited by optical characteristics of the fibre to $\Delta s < 1\,mm$. The calculation of the lengths is done automatically using a LabView software.

After determination of the fibre lengths, in Section 4.3.4 the fibre is stabilized with a Piezo Stretcher and a LabView software to guarantee the exact optical length between two distant points ($\Delta s < 1\,\mu m$). A second oscillator is frequency stabilized at the other end of the optical setup. The stabilization of the fibre and the oscillator transpose the frequency from one point to a distant point ($D > 500\,m$) without loss of stability. The limit of the stability is caused by the speed limit of the used measurement and control hardware. There is no show stopper to reach stabilities $\sigma_y(1\,s) < 10^{-15}$ which is suitable to synchronize optical atomic clocks (time and frequency) over large distances.

The FDDM CC method has no criterion for exclusion that performances equal to the BOCC setup are possible. The new system would be capable of handle dynamic systems for ground and space applications with same performances including simple optical setup and easy electronic efforts.

With the first try, the FDDM CC system has already proofed performances to full fill all requirements for applications in space (see Section 4.4). The simplicity of the setup results in low power consumption, low volume and high robustness. Also all electronic devices necessary to create these performances are available with space qualified hardware.

6 Outlook

Further developments for FDDM CC would include concentration on automation of signal evaluation and automation of the system. The next project (ADAM&EVA2) will include the theoretical concept of real time synchronization of a simulated GNSS scenario.

The target should be to create a network between three optical setups. Each of the setups simulates a satellite, with own time standard (Rb Standard), OFC and stable HeNe-Laser. The next step is to design each system for automatic function and communication between the systems. Since an optical link is necessary to use any optical measurement system, the link could also be used for data communication.

In Appendix E an algorithm is described how communication between the satellites which is necessary for calculation and Doppler Shift compensation. This information could be done by digital optical transmission by a slightly different wavelength as the optical oscillator.

The time transfer between two systems is handled theoretically within this thesis. The proof-of-concept should be done in the next phase. A possibility for time transfer is coding a single pulse and define it as 't_0' to be transmitted from a primary oscillator to a secondary oscillator. Since the FDDM CC system is capable of $\sigma_y(1\,\mathrm{s}) < 10^{-15}$ frequency synchronisation the time distribution should be able with the same performance.

With the next steps a complete setup between multiple systems would be created and can define the real performance of the FDDM CC method. A complete setup is illustrated in Figure 90

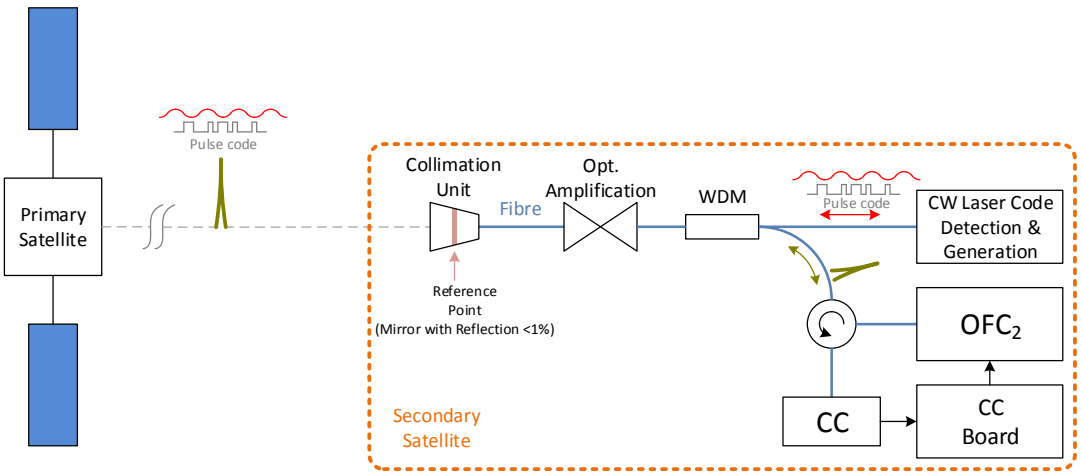

Figure 90: Possible setup for a satellite system

Coded pulses propagate from a primary satellite to a secondary satellite with information about velocity and distance. Since the secondary oscillator is locked automatically to the primary satellite its output can be seen as an amplification of the pulses which are sent back to the primary

satellite. An outcome of this thesis is that for FDDM CC a special polarization of the pulses is not necessary. A fibre setup with multi-mode fibres would increase simplicity of handling.

This first proof-of-concept shown in this thesis presents the various possibilities of the FDDM CC system. Until now, the main focus is on applications for GNSS or GFO, but ground applications would be interesting as well. An important aspect is an optical link between two points outside of the laboratory, for distance measurements or time distribution as well.
A measurement shows frequency transfer over optical fibre without high effort. Most institutions or universities would profit of a time distribution system in a local area. Also the ground application using optical fibre over large distances ($D > 100\,\text{km}$) would be interesting.

List of Abbreviations

ADAM & EVA	Absolute Distance Accurately Measured and External Vehicle Adjustment
ADC	Analogue Digital Converter
BOCC	Balanced Optical Cross Correlator
CC	Cross Correlation
CEO	Carrier Envelope Offset Frequency
CNT	Carbon Nano Tube
DFG	Differential Frequency Generation
FDDM	Frequency Domain Distance Measurement
FFT	Fast Fourier Transformation
FPGA	Field Programmable Gate Array
FWHM	Full Width Half Maximum
GFO	GRACE Follow On
GNSS	Global Navigation Satellite System
GRACE	Gravity Recovery and Climate Experiment
HF	High Frequency
H-Maser	Hydrogen Microwave Amplification by Stimulated Emission of Radiation
HV	High Voltage
OAC	Optical Atomic Clock
OFC	Optical Frequency Comb
PLL	Phase Lock Loop
PID	Proportional Integral Derivative
PM	Polarization Maintaining
Rb	Rubidium
RMS	Root Mean Square
SAW	Surface Acoustic Wave
SESAM	Semiconductor Saturable Absorber Mirror
SHG	Second Harmonic Generation
SNR	Signal to Noise Ration
VCO	Voltage Controlled Oscillator
WDM	Wave Division Multiplexer

Appendix

A Lattice and Single Ion Optical Atomic Clocks

To see the complexity of the an optical atomic clock, the optical transitions necessary for function should be shown. Transition stages of two different optical clocks are shown in Figure 91 to have an overlock of the required laser systems.

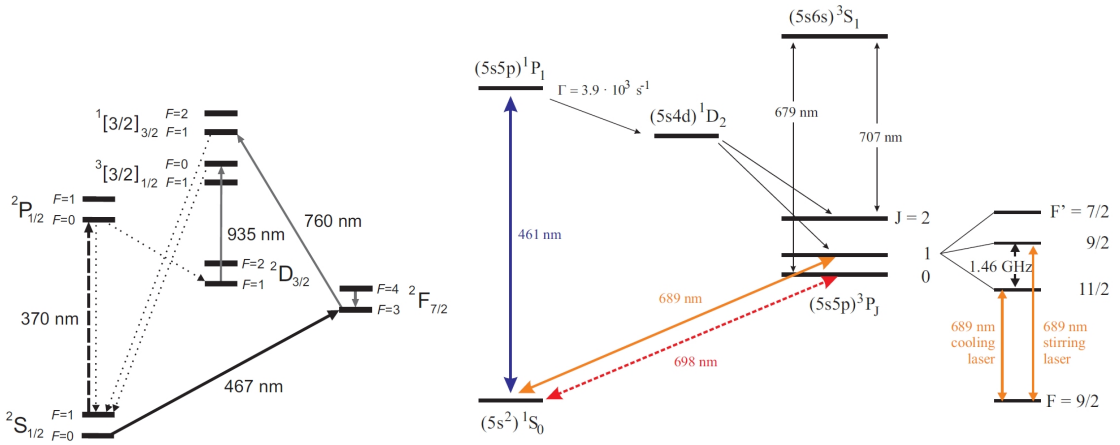

(a) Partial level scheme of $^{171}Yb^+$ [8]

(b) Partial level scheme of ^{87}Sr [58]

Figure 91: Examples for Clock, Cooling and Repumping transitions

The correspondent laser systems are listed in Table 9

Table 9: Example of used light during Yb^+ or Sr OAC operation [8] [58]

Lasers Yb Single Ion Clock	Wavelength
Cooling stage	369 nm
Repumper	936 nm
Repumper	760 nm
Octupole Clock	467 nm
Photoionization	399 nm
(Quadrupole)	(411nm)

Lasers of Sr Lattice Clock	Wavelength
First cooling stage	461 nm
Second cooling stage	689 nm
Stirring and spin polarization	689 nm
Repumper	679 nm
Repumper	707 nm
Lattice	813 nm
Clock	698 nm

Two optical clock types are shown in Figure 91: single ion clock and neutral atom (lattice) clock. Each clock type has its advantages and disadvantages. The main criteria for comparison is the amount of laser system which are required for functionality of an optical atomic clock. Also each laser type requires itself high stability to work properly, e.g. the second stage cooling laser of the Sr Lattice Clock requires a line-width at $\Delta f \approx 10\,\text{kHz}$ [58] which correlates to $\sigma_y(1\,\text{s}) \approx 4 \cdot 10^{-11}$. Thus an additional laser stabilization is required to receive performances in this area (highly stable

External Cavity Diode Lasers).

A.1 Lattice Clocks

The lattice clock is equal to the HF Standards mentioned before. Multiple atoms (about 10^6) are excited with one 'clock laser' or 'clock microwave' the same time.
To receive a large amount of neutral atoms the physics package of a lattice clock works mostly with cooling laser and a magneto optical trap. Also a continuous particle flux is necessary because the investigated particles are cleared out of the magneto optical trap when the investigation is finished.
In Figure 92 a setup of a physics package of a Lattice Clock is illustrated.

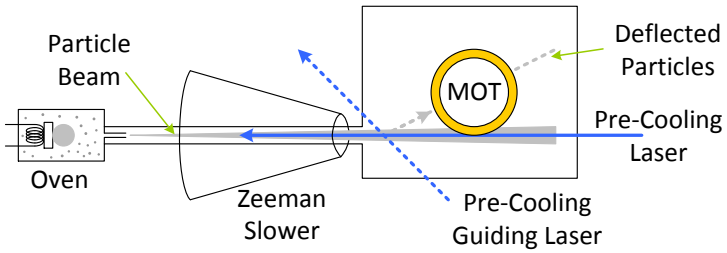

Figure 92: Schematic setup of the physics package of a Lattice Clock [20]

The particle beam distributed from a particle oven is cooled down in counter direction using the Zeeman Effect [59] to cool the particles from hundreds of Kelvin to less than 1 Kelvin. To select a specific amount of particles and provide particle colliding, a guiding laser (cooling laser) deflects some particles to a magneto optical trap (MOT). The MOT with its coils controls the inner magnetic field using Maxwell coils. A schematic setup can be seen in Figure 93.

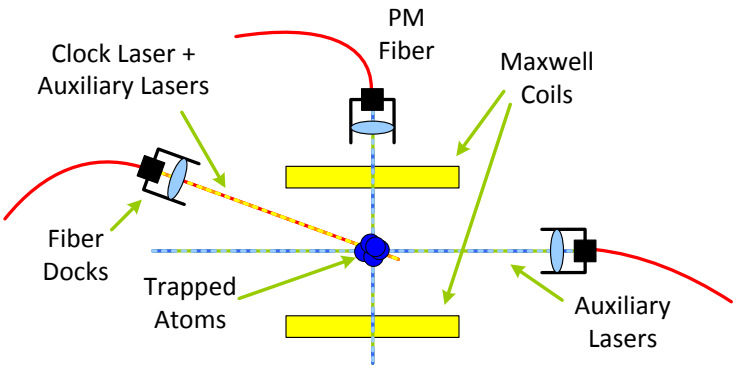

Figure 93: Schematic setup of a MOT for Lattice Clocks

Within the MOT the particles are trapped using first and second stage cooling laser combined

with repumping laser. A special laser system is also in use, which gives the name for the clock type: the lattice laser. The lattice laser with its 'Magic Wavelengths' is a standing wave across the particles. The Stark Shift [59] induced by the lattice laser is equal for ground and excited state of the clock transition. With a standing wave the particles are arranged to a lattice since they are 'trapped' within the low potential of the standing wave. Dependent on the used lattice laser setup, 1D, 2D or even 3D lattices can be created [20]. Even one standing wave is challenging to create regarding the requirements of the laser and the optical setup. Higher dimension lattices are even more challenging. The advantage of the lattice formation is that the particle are prevented of collision and movement. Collisions broaden the narrow transition frequency as well as their movements. Also a higher amount of particles can be investigated when the particles are trapped within a lattice laser. This results in a statistical advantage and therefore a lower Allan Deviation. When the particles are cooled and trapped with the lattice laser, the investigation can be done. Therefore highly stable lasers are required.
The Lattice Clocks promise highest performances but imply also highest requirements on technology and complexity. It has do be mentioned, that accuracy values are only theoretically since a long time comparison (t $>$ 1h) between two optical time standards is not yet achieved (for now). Also a geopotential difference of Δh $\approx$ 1 cm on earth surface would create a frequency shift (red shift) of the transition frequency higher than the accuracy of the clock [20]. Therefore measurements of this accuracy are challenging to implement on earth.

A.2 (Single) Ion Clocks

The (single) ion clock is different only in the physics package compared to the before described Lattice Clock. 'Single' is kept in brackets because most Ion Clock types are concentrated using only one ion. But the physics package could be modified to create traps for multiple ions. When quantum logic clocks are used, basically two ions are within the trap.

The physics package of a Single Ion Clock is schematically shown in Figure 94

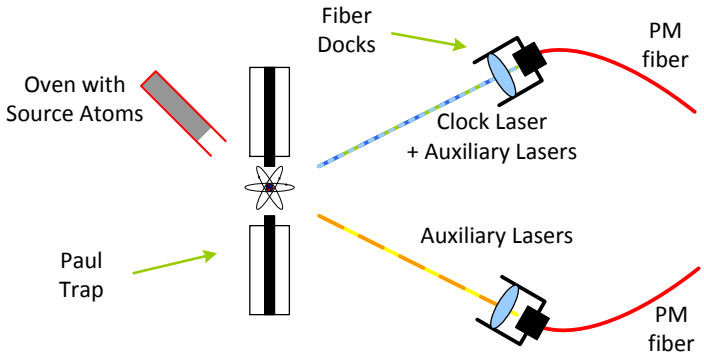

Figure 94: Schematic setup of physics package of a Single Ion Clock [20]

The element is concentrated within an oven. The hot oven dispenses the particles in direction of the Paul Trap centre. Using two level ionizing the particles lose one electron and are then trapped

by their electronic load within the fluctuating field within the Paul Trap. When a particle is trapped the oven is deactivated that no further particles could accidentally collide with the trapped ion. This is the largest difference between the Lattice Clock and the Single Ion Clock: The particle stays trapped within the trap and is not exchanged after investigations.
The particle is cooled down and repumped until lowest temperatures in micro-Kelvin scales are reached. Then the particle is ready for investigation.

Single Ion Clocks have similar performances than Lattice Clocks. Even when the handling is 'simpler' compared to Lattice Clocks, the accuracy values are still theoretically caused by the same limitation as mentioned in the prior section.

Interesting to know, that this trapping type is 'similarly' used for quantum computing using multiple ions within one trap. A quantum logic clock can not only be used as reference clock but represents also a quantum computer with two qubits.

A.3 Optical Atom Clock Setup

In the prior two Sections, the physics package of both clock types is described.
The complete clock setup includes also the handling of the Clock Laser and the auxiliary lasers. Auxiliary lasers contain any laser type except the clock laser.
The Clock Laser is locked by Pound-Drever-Hall stabilization to an ultra highly stable cavity. The cavity is a 'simple' crystal tube (ultra low expansion glass) with coated mirrors. This setup contains highest requirements on mechanical robustness, thermal stabilization and crystal/coating properties. The laser created with these cavities have the highest available performance.

The optical interaction within an OAC is roughly illustrated in Figure 95.

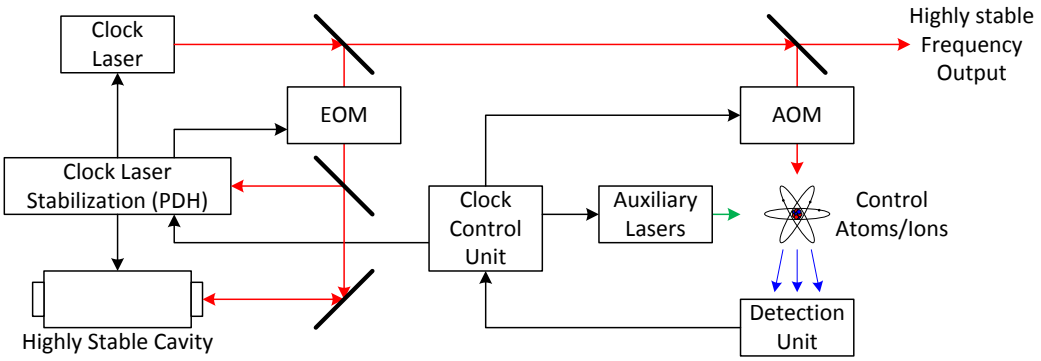

Figure 95: Schematic setup of the laser interactions

The highly stable clock laser locked on the cavity would drift like any oscillator without a norm. The norm are the atoms or ions which are for investigation. Using the Ramsey Method [60] for precise transition detection controls the Clock Laser to provide any frequency drifts. The output is

then an absolute highly stable laser at the optical area which can be used as a new time standard.

B Frequency Comb and its Interaction with Optical Clocks

B.1 CEO Definition and Handling

Within the optical area, an additional effect defines the output of a short pulse laser: the Carrier Envelope Offset Frequency (CEO).
The CEO is caused by the output pulses of the oscillator and the non-perfect mode lock of the oscillator. The pulse length itself is defined by the length of the envelope of the pulse. But within the pulse the mode is shifted by a special phase, which defines the CEO. Figure 96 illustrates the shift.

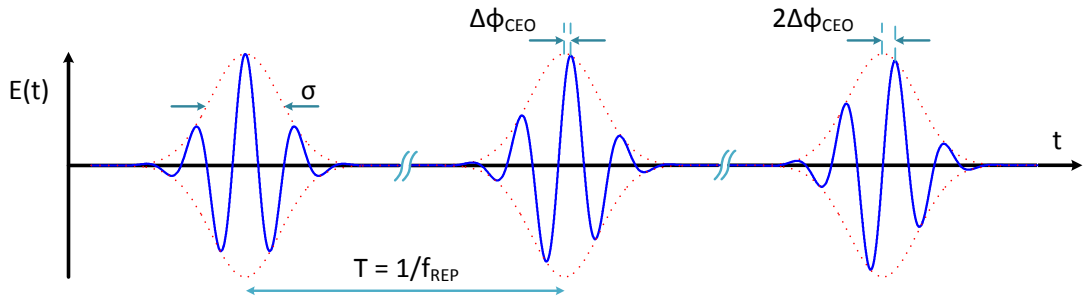

Figure 96: Illustration of the phase shift from pulse to pulse [20]

In Figure 96 all necessary information of the physics of an OFC is illustrated. The time offset between two pulses defined by the oscillator length, the phase shift from one pulse to another and the correlation between pulse lengths and repetition rate ($1/f_{REP} >> \sigma$).

If optical atomic clocks are used, CEO stabilization or termination is essential. Using f2f-interferometry or CEO free combs are two ways to handle with the CEO.
Both systems require super continuum and non-linear crystals with focus on second (second harmonic generation) or third order effects (sum and difference frequency generation).

A super-continuum for CEO detection requires at least one octave of frequency span. A highly non-linear optical medium with focus on third order non-linearity can be used to create a super-continuum (e.g. non-linear optical fibre) . When the octave spanning continuum is created, Second Harmonic Generation (SHG) of the lower frequency must be done, see Figure 97. A more precise description of SHG is given in Section 2.6.2.

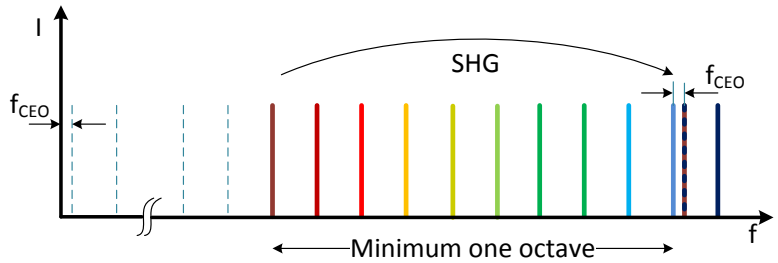

Figure 97: Illustration of the f_{CEO} detection due to second harmonic generation

A part of the super-continuum is frequency doubled and overlapped with itself. The result is the measurable CEO frequency. This technology is used since the beginning of OFCs [61]. The results of this setup are two frequencies (f_{REP}, f_{CEO}) which can be modified to change the optical output of an OFC.

Another approach is to 'delete' the CEO [62].
The third order non-linearity allows sum and difference frequency generation. An even larger super-continuum is required, with increasing issues of handling. The pulses with super-continuum pass a crystal with third order effect, for differential frequency generation. The principle is illustrated in Figure 98.

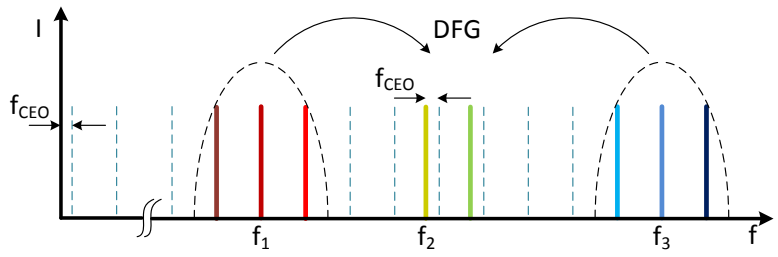

Figure 98: f_{CEO} termination due to differential frequency generation

Two parts of the super-continuum interact within the crystal to create a 'middle' frequency.

$$f_3 = f_2 + f_1 \quad \Rightarrow \quad f_2 = f_3 - f_1 = i \cdot f_{REP} + f_{CEO} - j \cdot f_{REP} - f_{CEO} = k \cdot f_{REP}$$

The differential frequency generated pulses contain no CEO. Therefore stabilization is not necessary.
This technique seems most promising, but the handling of super-continuum of this size is challenging and requires a distinguished balance between pulse duration and pulse power. Also, the possibility of delete f_{CEO} can also be seen as loss of a degree of freedom.

Both types of OFCs enable to measure a random optical frequency with precisions $\Delta f/f_0 < 10^{-16}$.

This is necessary if the random frequency is the output of an OAC. It is essential that the performance of an OFC is better than an OAC. Otherwise the performance of an OAC would be lowered. Since OFCs are already commercially available with sufficient performance values this is not a show stopper. Also first applications for space are in development status.

B.2 Frequency Comb Interaction with Optical Atomic Clocks

The purpose of an OFC is not only to measure laser frequency very precisely. To lock the OFC to a laser source enables to transform the laser stability to the electronically measurable HF area indicated by the stability of the repetition rate. The OFC is therefore a connection between the HF area and the optical area.

The stabilities described in Section 2.2 can be adapted to the OFC. The interference frequency Δf is detected and/or controlled. The OFC-OAC-interaction is illustrated in Figure 99.

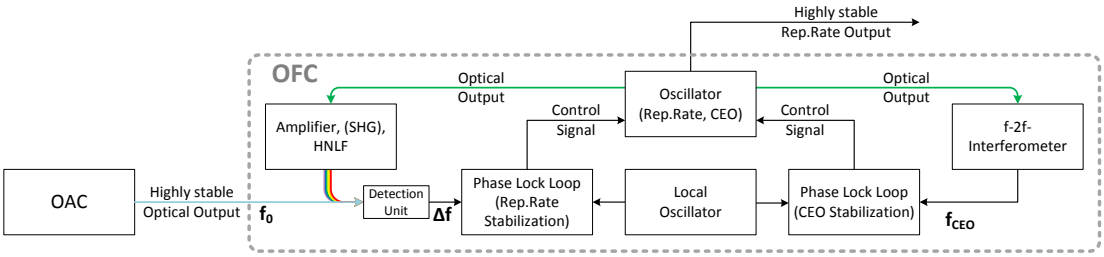

Figure 99: Schematic setup of an OFC stabilized to an optical standard with CEO stabilization

In this example, the OFC contains a CEO detection and stabilization unit. The highly stable input of the OAC is overlapped with the optical output of the OFC. The interference frequency Δf is stabilized with a PLL. A stable local oscillator serves as frequency input for the CEO and Δf stabilization. The repetition rate is locked to the optical frequency of the OAC.

The setup is similar with CEO free OFCs as can be seen in Figure 100.

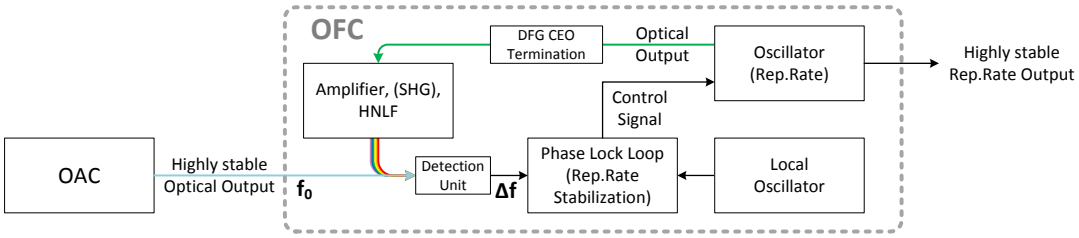

Figure 100: Schematic setup of an CEO-free OFC to an optical standard

The CEO-free OFC profits of a single frequency stabilization. However the complexity of the management of a CEO-free spectrum is challenging. When Δf is stabilized to a local oscillator, the

repetition rate takes over the stability of the optical standard.

The repetition rate contains the high stability of the optical clock. This high stability is to be transferred to other systems for synchronization or comparison, in static or dynamic systems. This is an essential requirement for the methods presented in this thesis.
Situational the repetition rate must be modified (e.g. Doppler Shift). Adjusting the CEO or Δf results in the required frequency adjustment of the repetition rate. Adjustment in sub-mHz area is possible and sufficient for any frequency shifts.

The optical output of an OFC must cover the optical output of an OAC for interference. The optical output of an OFC is defined by its amplification element:

Erbium: 1560 nm [20] Ytterbium: 1040 nm [63] Ti-Sapphire: 780 nm [64]

Pulses of these wavelengths can then be optically broadened to create super-continuum. However handling of Ti-Sapphire pulse lasers requires free-beam optic which is challenging compared to possible in-fibre setup using Erbium or Ytterbium. Also the characteristic of Ytterbium results in longer pulse durations which imply issues handling the CEO or creating Differential Frequency Generation for CEO-free OFCs. The element of choice for OFCs (especially for space applications) is Erbium, since technological development using space applicable in-fibre technology is in advance compared to the other two element setup [20].

But the centre wavelength of Erbium at 1560 nm is too far away from required optical areas of OACs (e.g. see Table 9). The solution is to enlarge the optical spectrum of an Erbium OFC. Figure 101 shows some examples of OAC optical areas and the correlation with Erbium doped OFCs.

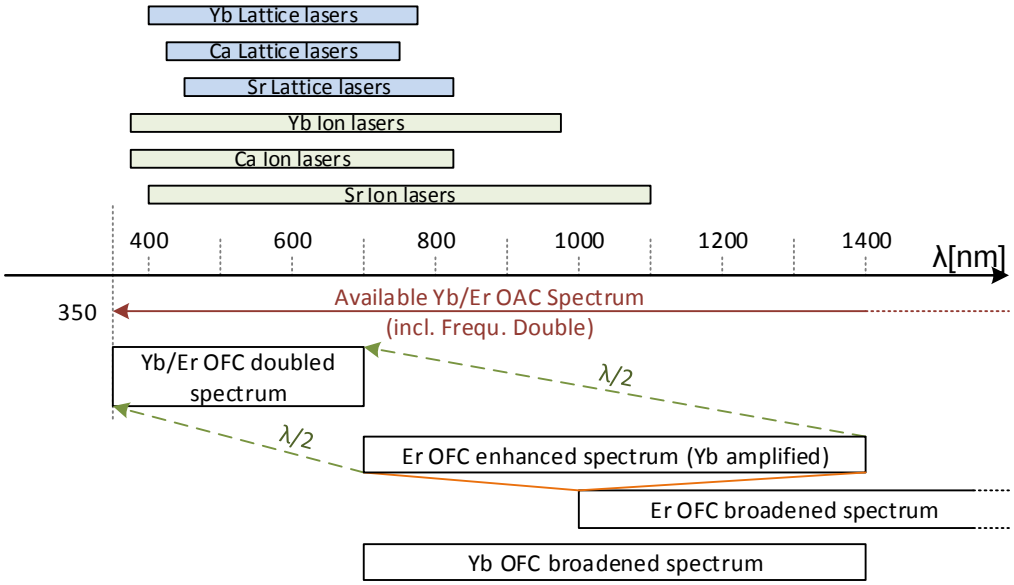

Figure 101: Optical spectrum of OFC and OAC examples

The enlargement of the Erbium optical spectrum would be a possibility to handle the optical output of OACs with Erbium OFCs.

C Synthesizer Board

The simplified overview of the Synthesizer Board is shown in Figure 102

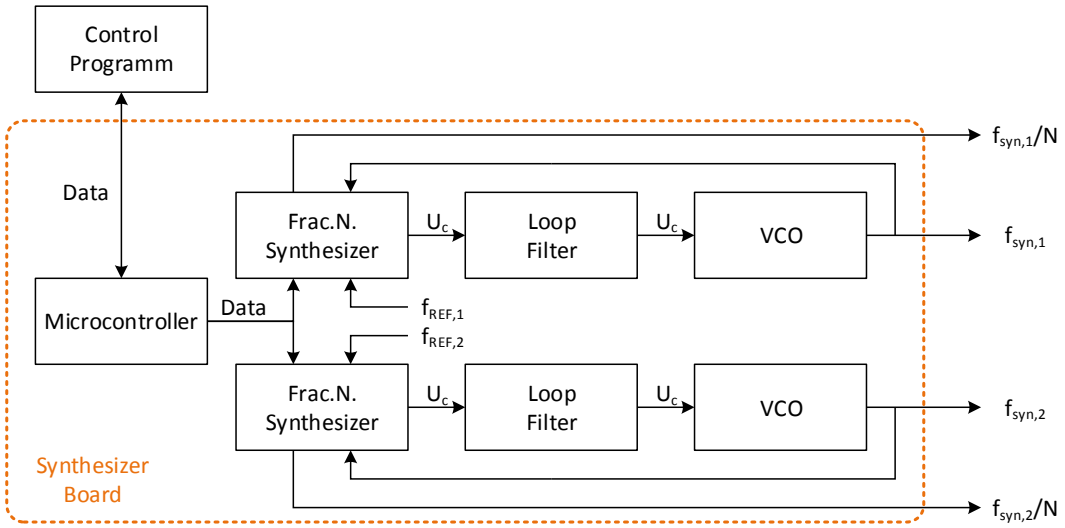

Figure 102: Schematic setup of the designed synthesizer board

The loop filter is special designed for each VCO since the properties of each VCO are different. For the design a special dedicated software is used programmed by the same company which designed the fractional N-Synthesizer [65].
The software considers four phase noise sources and create a simulated phase noise output. An example of a 100 MHz VCO is shown in Figure 103.

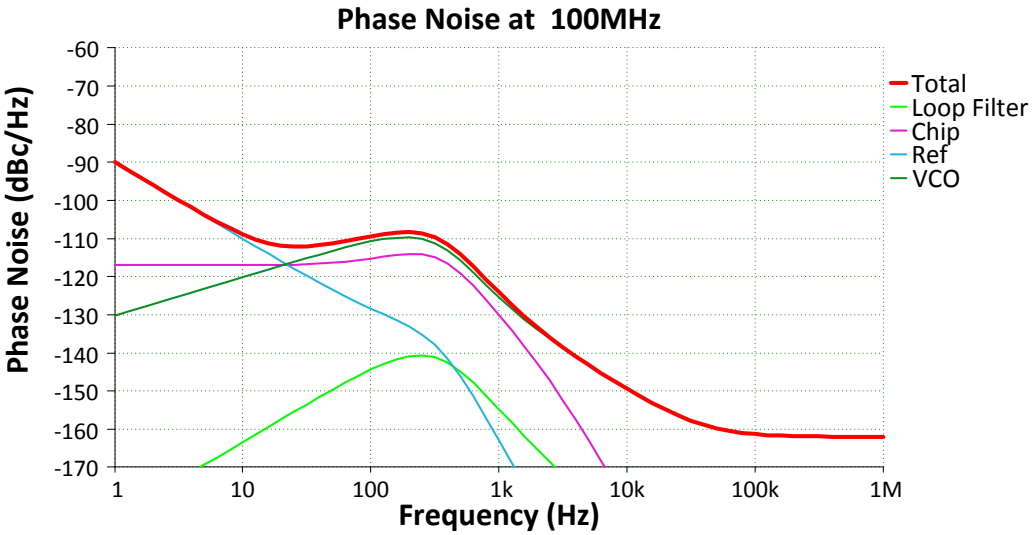

Figure 103: Example of a simulated loop filter with different noise floors and the overall noise

Every source has its phase noise behaviour and must be considered.
Generally data sheets of VCOs and Reference Oscillators are available and can be added to the program. The software itself contains already the phase noise of the used synthesizer.
The software suggests a loop filter which must be adapted. Every change of the loop filter has strong influences on every phase noise. The target is to minimize the overall noise of the loop.

The synthesizer board is designed by this simulation. Nevertheless the real setup results in a different phase noise as can be seen in Figure 104.

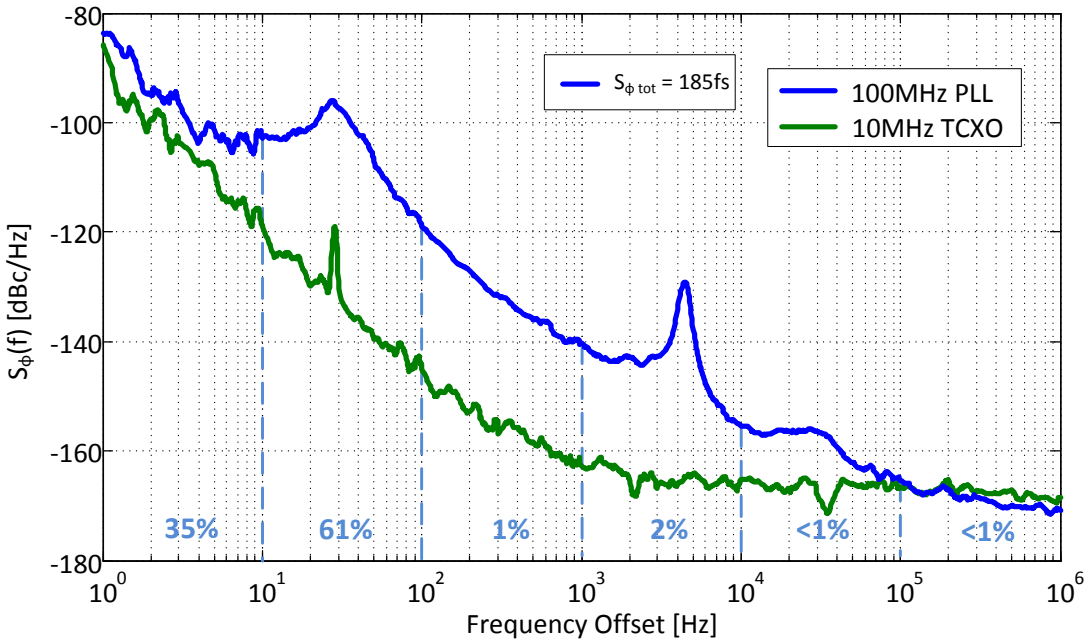

Figure 104: Example of a real noise measurement of a 100 MHz synthesized frequency

An Electrical Spectrum Analyzer is locked on a H-Maser with an internal 10 MHz thermal stabilized ultra low noise oscillator (TCXO) as reference. The phase noise of the synthesizer board is then measured.
The characteristic of the VCO at 100 MHz is clearly different as the design. Nevertheless the integrated phase noise is with $\int_{1\,Hz}^{1\,MHz} S_\Phi(f)df$ = 185 fs ($\sigma_y(1\,s) < 2 \cdot 10^{-13}$) sufficient for Rb-Standard.

Also shown in Figure 104, the integrated phase noises within several frequency areas (separated in decades). The largest part of the phase noise (61%) is within 10 Hz and 100 Hz. This is the area where the frequency control loop has its limit of the modulation frequency of the VCO. Any modulation over 30 Hz have less influence on the oscillator stability as below 30 Hz.

To verify the stability output of the synthesizer board, the board must be connected to a frequency standard with highest stability. For verification a H-Maser is used with the setup illustrated in Figure 105.

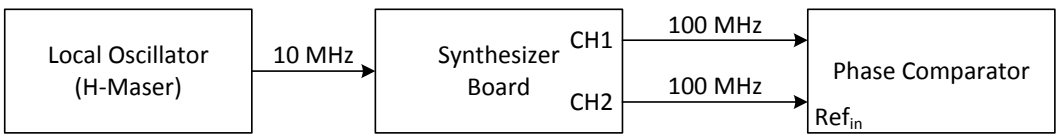

Figure 105: Schematic setup to verify the best performance created by the synthesizer board

The Synthesizer Board multiplies the 10 MHz reference of the H-Maser two times. One of the outputs is then used as reference. The second output as the measurement frequency. This implies that the measurement results in the VCO with the lowest performance.
The phase comparator itself has a defined stability limit at $\sigma_y(1\,s) < 2 \cdot 10^{-14}$ [43]. This is enough for this measurement since the H-Maser has its limit at $\sigma_y(1\,s) \approx 8 \cdot 10^{-14}$.
The synthesized stability of the synthesizer board for a 100 MHz oscillator is shown in Figure 106.

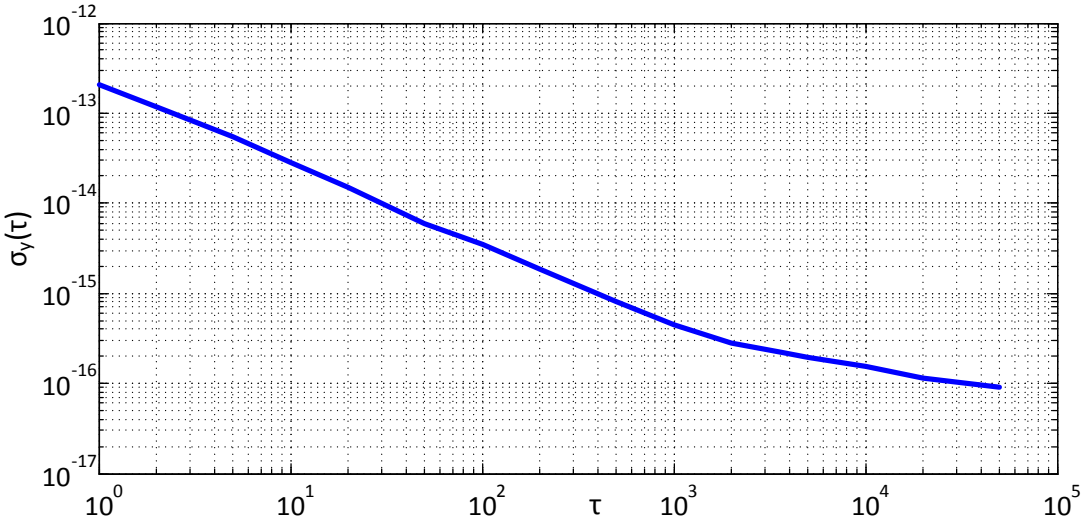

Figure 106: Measured stability of the synthesizer board

As can be seen in Figure 106, the synthesizer board has the possibility to create signals with stabilities at $\sigma_y(1\,s) = 2 \cdot 10^{-13}$ and fits the estimated phase noise of $S_y = 185$ fs. The stability limit of the synthesizer board is therefore sufficient for any measurements with Rb-Standards which have stabilities at $\sigma_y(1\,s) \approx 10^{-12}$.

The synthesizer is characterized only at 100 MHz since the frequency comparator allows only frequency inputs of 100 MHz $\pm$ 10 mHz [43].

D FDDM Board Harware Setup

For the setup of the FDDM Board exist three essential targets:
– Separate the harmonics from each other
– Adapt the output voltage to have similar/equal amplitudes
– Create high SNR

The schematic setup is shown in Figure 107

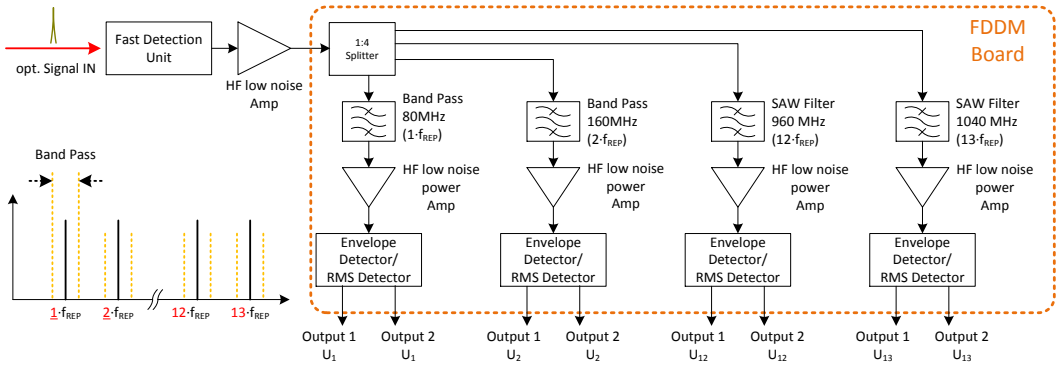

Figure 107: Schematic setup of the FDDM board for harmonic separation and detection

The frequency splitter has a frequency dependent characteristic. Also a low noise splitter is needed to add as less noise on the SNR as possible. The used splitter has a frequency linearity which varies between -6.7 dB at 50 MHz to -7.6 dB at 1 GHz.

There are several bandpass filter used in the circuit. For the first and second harmonic a self designed Chebichev bandpass filter in 5^{th} order is sufficient for separation of the frequency. For the 12^{th} and 13^{th} harmonic Surface Accustic Wave (SAW) filters are used. SAW filter are special filters with the property of a narrow band pass at higher frequencies. Mostly used also in GNSS or mobile phone applications to separate neighboured carrier frequencies.
A disadvantage of the SAW filter is that their attenuation is quite different to each frequency: -3 dB at 960 MHz and -5 dB at 1040 GHz. Also not any arbitrary frequency is available since the production of SAW filters comply with their application on different mass markets (GNSS). This is also the reason, why the 12^{th} and 13^{th} harmonics are chosen. These frequencies are available with affordable prices and are in a frequency area which is still manageable dependent on frequency properties above 1.5 GHz.

Every filter contains attenuation as well as the splitter. The fast detection unit is limited to +5 dBm per harmonic. Higher amplitudes of the harmonics would create saturation and distort the signal. After the filter, the lower amplitudes receive an attenuation of total -7 dB to about -2 dBm. The 12^{th} harmonic received an attenuation of about -10 dB to -5 dBm and the 13^{th} harmonic with -12 dB attenuation to about -7 dBm.

The Envelope detectors can handle inputs until +17 dBm (without loss of linearity). Thus the lower frequencies are amplified by a low noise amplifier with +15 dB whereas the higher frequencies receive an amplification of +20 dB. Nevertheless there is already a difference of 2 dB between the 12^{th} and 13^{th} harmonic which must be considered for further amplitude modifications.

The envelope detectors have an output for envelope detection and for Root Mean Square (RMS) value of the reference signal. Since the modulation frequencies ($f_{mod} < 10\,kHz$) of the harmonics are below the origin purpose of the envelope detector ($f_{mod} > 10\,MHz$) the RMS output can also be used for FDDM detection. The correlation between input power and output voltage is shown in Figure 108

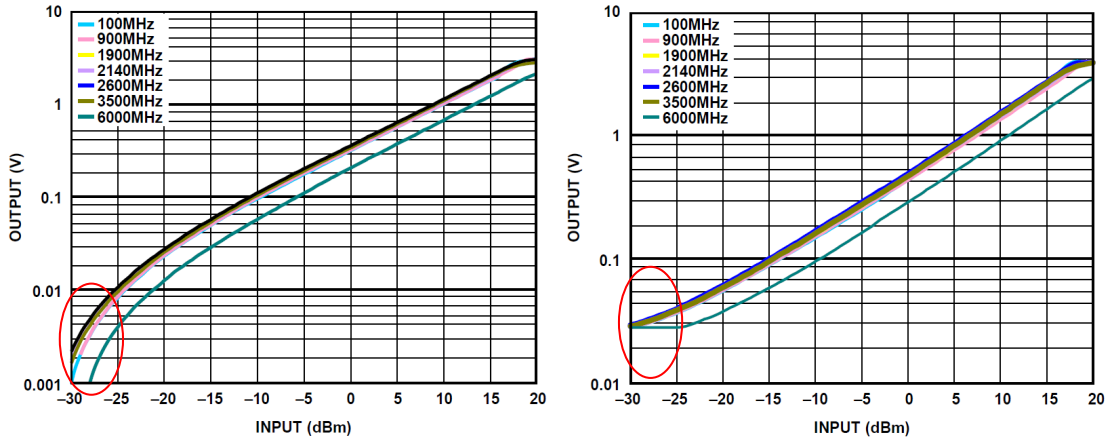

Figure 108: Correlation between input and output voltage of U_{ENV} (left) and U_{RMS} (right) [66]

Both outputs have a linear correlation between input power and output voltage within $P_{in} \in [-20\,dBm, +17\,dBm]$. Important is hereby the behaviour of each output at $P_{in} \to 0$:
$U_{ENV} \to 0$ whereas $U_{RMS} \to 30\,mV$ (see red circled areas in Figure 108).
The voltage offset of U_{RMS} results in a limited SNR of

$$\frac{\Delta U}{U_0} \leq \frac{0.03\,V}{3\,V} = 10^{-2} \quad \Rightarrow SNR \leq 40\,dBc$$

The ground noise of the RMS output would limit the performance of any stabilization loop. Therefore only the envelope output should be used for exact measurements or stabilizations. Its noise floor is only limited by the general noise floor of the circuit board. Additionally since the neighboured harmonics receive an attenuation which results below -30 dBm, it can be used to terminate them.
The RMS output can be used for monitoring of the functionality.

E Algorithm for Time / Frequency Synchronization

The distance determination described in prior sections can be summarized in algorithm. The aim is the precise distance detection to track the target with BOCC or FDDM system, which includes also static systems.
The algorithm illustrated in Figure 109 presents a rough overview.

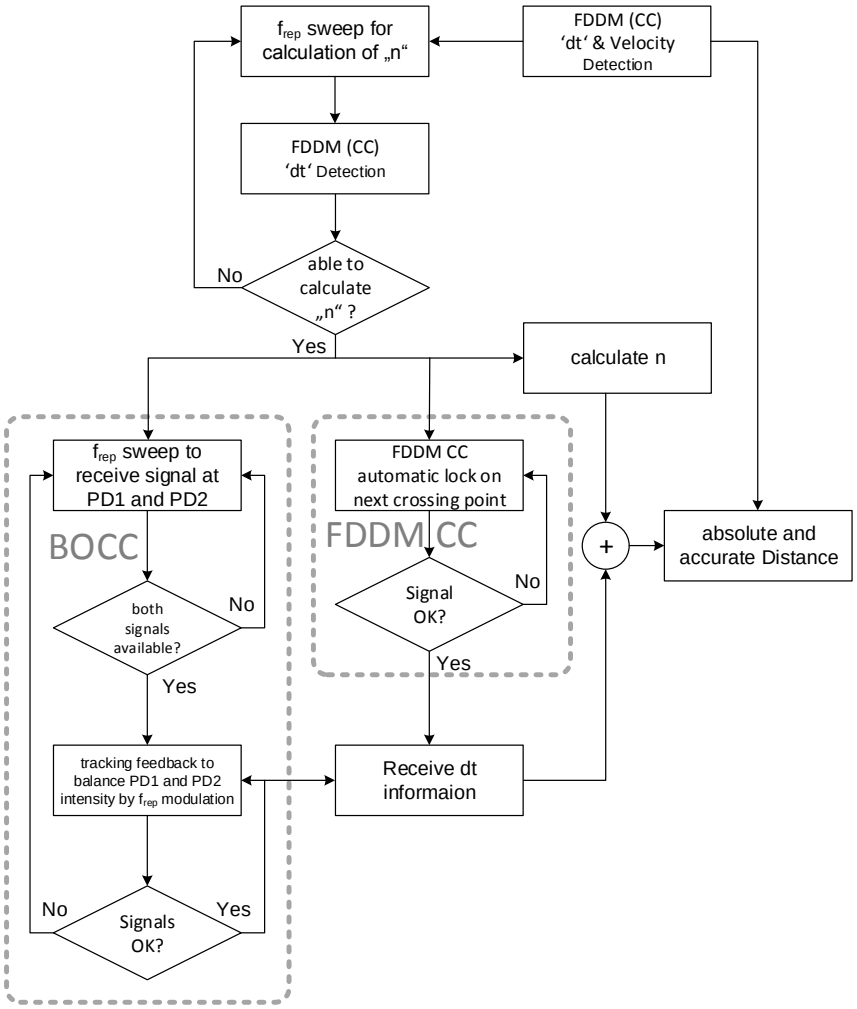

Figure 109: Algorithm for distance determination for both systems

The FDDM CC method is used to receive the primary ’dt’ value and the velocity of the target. Because distance calculation requires two point measurement, the repetition rate of the oscillator must be changed. If the pulse laser is connected to a HF-Standard, the repetition rate is directly modified. If an OFC is used which is locked on an OAC the optical interference between them (Δf, see Section 2.3) can be shifted.
During the frequency shift, the FDDM (CC) signal is continuously measured until the multiple factor ’n’ is calculable. As soon as the multiple factor is available, the target locking can be activated.

Two possibilities are available for target locking: BOCC or FDDM CC system.
In static systems both methods would be available. At dynamic scenario with velocities above $v_{rel} > 2.4\,mm/s$ (see Section 4.2.4) only the FDDM CC system can be used.

Before starting the BOCC loop the BOCC signal must be available, which implies a frequency shift of the repetition rate of the oscillator until forward and backward SHG signals are available with similar intensity. Afterwards the BOCC loop is activated and controls the repetition rate. The output signal can also be used for fibre stabilization.
The calculate the 'dt' value using the BOCC system (during lock) is simpler than the FDDM CC system. The zero crossing point of the BOCC failure signal is a multiple factor (n^{th}) of the oscillator length.
If the system is out of loop, it must be started again with the intensities of forward and backward intensities.

The activation of the FDDM CC loop is simpler compared to the BOCC loop. The 'zigzag' form of the FDDM CC signal with its multiple zero crossing points and their slopes allows an automatic lock to one of the zero crossing points. The 'dt' value is clearly defined by amplitude measurement. If an abrupt outer perturbation interrupts the loop, its automatic function guarantees an instant lock again.

This rough overview of the algorithm presents the simplicity of the administration of a precise distance measurement using FDDM CC compared to BOCC. Amplitude detection calculations of zero crossing points, slopes and velocity determination are not included since these are necessary for both systems.

For time and frequency transfer a second algorithm is created which implies only the FDDM CC system. It is illustrated in Figure 110.

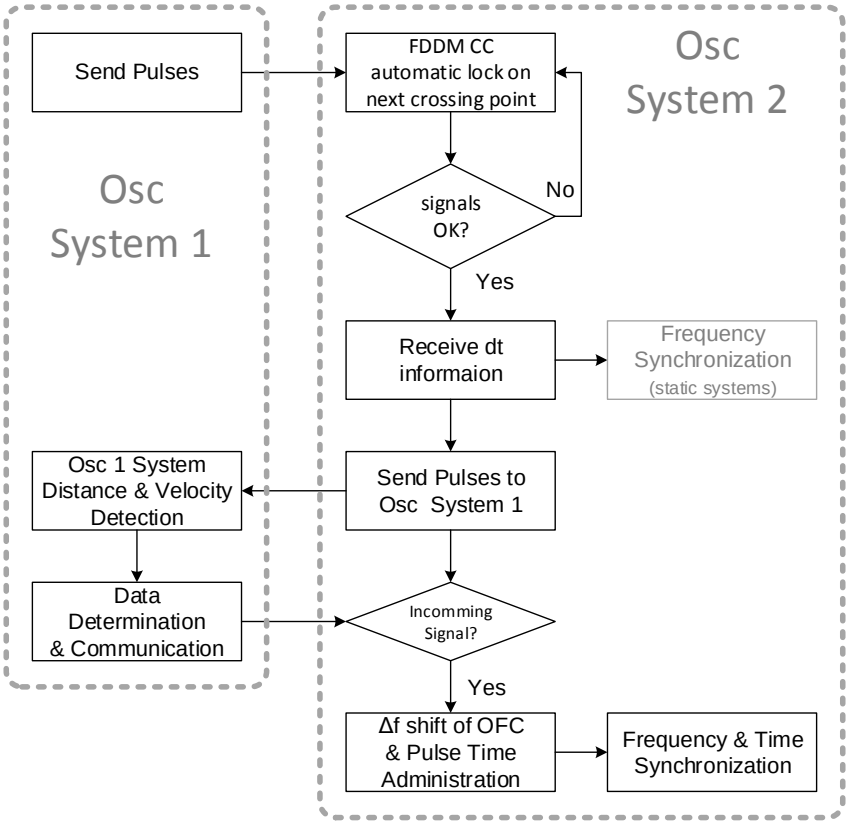

Figure 110: Algorithm for frequency transfer with FDDM CC

The interaction between two oscillator systems is required for a dynamic synchronization. The primary system is responsible for precise velocity and distance detection. The precise velocity implies the information of the Doppler shift. The velocity detection is directly connected with the absolute distance, which can be used to create a time synchronization between System 1 and System 2.

System 2 receives the pulses from System 1 and locks to its pulses with the FDDM CC method. For static systems, a frequency synchronization is already implied. The oscillator of System 2 is synchronized and sends parts of the pulses back to System 1. System 1 detects the pulses that starts a distance and velocity measurement. After all variables are available, the systems have to communicate to each other (electronically or optically).
As soon as the second system receives data of System 1 it can adapt possible Doppler shift due to relative velocity.

The data of System 1 includes also pulse codes to mark one specific pulse which transports after all calculation time 't_0' from System 1 to System 2.
After this procedure both systems are synchronized and the connection can be capped.

Until now, 'only' the proof of concept of the FDDM CC method is shown. Further developments should include data acquisition, data processing, data communication and more digitalization of all systems.
It is shown, that a digital system is capable of create equal performances with easier handling and more degrees of freedom compared to analogue techniques.

F Trade Off

There are several systems which have similar applications.
A trade off between the systems is listed in Table 10.

Table 10: Trade Off between different systems

	MSTAR [67]	Time-of-Flight [49]	Michelson Interferometry [68]	BOCC	FDDM CC
Relative Distance Resolution Δd(1 s)	< 1 nm	< 1 mm	< 1 nm	< 10 nm	$< 1\,\mu$m
Absolute Distance measurement?	yes	yes	no	no	yes
Dynamic applicable?	yes	no	yes	no	yes
Frequency Distribution?	no	no	yes	yes	yes
Transfer Stability σ_y(1 s)	—	—	$< 10^{-18}$	$< 10^{-16}$	$< 10^{-15}$
Time Distribution?	no	no	no	yes	yes
Optical link required?	yes	no	yes	yes	yes
Polarization dependent?	yes	no	yes	yes	no
Optical complexity	high	—	high	high	low
electronic complexity	high	high	medium	low	low

References

[1] E.Goebel, I.M.Mills, and A.J.Wallard. Bureau international des poids et mesures: The international system of units, 2006.

[2] Thomas E. Parker. Long-term comparison of caesium fountain promary frequency standards. *Metrologia*, 47:1–10, 2010.

[3] S.A. King, R.M. Godun, S.A. Webster, H.S. Margolis, L.A.M. Johnson, K. Szymaniec, P.E.G. Baird, and P. Gill. Absolute frequency measurement of the $^{2}s_{1/2} - {}^{2}f_{7/2}$ electric octupole transition in a single ion of ^{171}yb+ with 10^{-15} fractional uncertainty. *New Journal of Physics*, 14(1):013045, 2012.

[4] Audoin Claude and Guinot Bernard. *The Measurement of Time*. Cambridge University Press, 2009.

[5] W. Kester. Converting oscillator phase noise to time jitter. Technical report, Analog Devices, 2009.

[6] D.A. Howe D.B. Sullivan, D.W. Allan and EL. Walls, editors. *Characterization of Clocks and Oscillators*. National Institute of Standards and Technology, 1990.

[7] Analog Devices Inc., editor. *The Data Conversion Handbook*, volume Chapter 6.5, Sampling Clock Generation. Analog Devices, 2016.

[8] Huntemann N., Okhapkin M., Lipphardt B., Weyers S., Tamm Chr., and E. Peik. High-accuracy optical clock based on the octupole transition on $^{171}yb^{+}$. *Physical Review Letters*, 108:090801, 2012.

[9] Physikalisch-Technische Bundesanstalt (PTB), editor. *Viewpoint: Optical Atomic Clocks Could Redefine Unit of Time*. Fritz Riehle, 2012.

[10] Jefferts S.R., Heavner T.P., Parker T.E., and Shirley J.H. Nist cesium fountains - current status and future prospects. *SPIE*, 6673, 2007.

[11] Micalizio S., Godone A., Levi F., Francois B., Calosso C.E., Battisti A., Gioia M., and A.Borella. The pulsed optically pumped rb frequency standard: A proposal for a space atomic clock. *Metrology of Aerospace*, pages 384 – 388, 2015.

[12] Demidov N., Vorontsov V., Belyaev A., and Blinov I. Studies of a short and long - term stability of an active hydrogen maser with stand alone cavity auto tuning. *European Frequency and Time Forum*, pages 488 – 493, 2012.

[13] Ushijima I., Takamoto M., Das M., Ohkubo T., and Katori H. Cryogenic optical lattice clocks with a relative frequency difference of $1 \cdot 10^{-18}$. *Nature Photonics*, 9:185–189, 2015.

[14] J.Ye A.D.Ludlow. Progress on the optical lattice clock. *C. R. Physique*, 16:499–505, 2015.

[15] Safronova M., Jiang D., Arora B., Clark C., Kozlov M., Safronova U., and Johnson W. Blackbody radiation shifts and theoretical contributions to atomic clock research. *IEEE Transactions on Ultrasonics, Ferroelectrics, and Frequency Control*, 2010.

[16] Huntemann N., Sanner C., Lipphardt B., Tamm Chr., and Peik E. Single-ion atomic clock with $3 \cdot 10^{-18}$ system uncertainty. *Physical Review Letters*, 2016.

[17] Yao Jian, Yao Jianping, Wang Yong, Tjin Swee Chuan, Zhou Yan, Lam Yee Loy, Liu Jian, and Chao Lu. Active mode locking of tunable multi-wavelength fiber ring laser. *Optics Communications*, 191:341–345, May 2001.

[18] Anatoly Grudinin Oleg Okhotnikov and Markus Pessa. Ultra-fast fibre laser systems based on sesam technology: new horizons and applications. *New Journal of Physics*, 177(6), November 2004.

[19] Set Sze Y., Yaguchi Hiroshi, Tanaka Yuichi, and Jablonski Mark. Laser mode locking using a saturable absorber incorporating carbon nanotubes. *Journal of Lightwave Technology*, 22(1):51 – 56, January 2004.

[20] B. Eder. Time measurement with satellite based optical atomic clocks. Master's thesis, Technische Universität München, October 2012.

[21] M. Watkins B. D. Tapley, S. Bettadpur and C. Reigber. The gravity recovery and climate experiment: Mission overview and early results. *GEOPHYSICAL RESEARCH LETTER*, 31, 2004.

[22] S. Bettadpur B. D. Tapley, D. P. Chambers and J. C. Ries. Large scale ocean circulation from the grace ggm01 geoid. *American Geophysical Union*, 2004.

[23] National Aeronautics and Space Administration. Grace mission overview. Internet, February 2012.

[24] European Space Agency. Galileo fact sheet, April 2016.

[25] Urs Hugentobler. Optical clock technologies and their applications for globally optimized navigation. Technical report, Forschungseinrichtung Satellitengeodäsie, 2010.

[26] Urs Hugentobler. Optical clock technologies and their applications for globally optimized navigation - 2. Technical report, Forschungseinrichtung Satellitengeodäsie, 2013.

[27] L. Cacciapuotia, N. Dimarcqb, G. Santarellib, P. Laurentb, P. Lemondeb, A. Claironb, P. Berthoudc, A. Jornodc, F. Reinaa, S. Felthama, and C. Salomond. Atomic clock ensemble in space: Scientific objectives and mission status. *Nuclear Physics B*, 166:303 – 306, 2007.

[28] R. Schmidt, F. Flechtner, U. Meyer, K.-H. Neumayer, Ch. Dahle, R. Koenig, and J. Kusche. Hydrological signals observed by the grace satellites. *Surv. Geophys.*, 29:319 – 334, 2008.

[29] T. Rosenband et al. Frequency ratio of al^+ and hg^+ single-ion optical clocks; metrology at the 17th decimal place. *Science*, 319:1808 – 1812, 2008.

[30] S. Blatt et al. New limits on coupling of fundamental constants to gravity using 87sr optical lattice clocks. *Phys. Rev. Lett.*, 100:140801–1 – 140801–4, 2008.

[31] Sheard et al. Intersatellite laser ranging instrument for the grace follow-on mission. *Journal of Geodesy*, 2012.

[32] Daniel Schütze. Grace follow-on laser ranging interferometer. In *Quantum to Cosmos 5*, 2012.

[33] F. J. Tischer. Propagation-doppler effects in space communications,. *IEEE Journals & Magazines*, 48:570 – 574, 1960.

[34] P.T. Callahan, K. Safak, P. Battle, T. D. Roberts, and Franz X. Kaertner. Fiber-coupled balanced optical cross-correlator using ppktp waveguides. *Optics Express*, 22:9749–9758, 2014.

[35] F. Loehl, H. Schlarb, J. Mueller, J.W. Kim, J. Chen, F. Wong, and F.X. Kaertner. Sub-10 femtosecond stabilization of a fiber-link using a balanced optical cross-correlator. *IEEE*, 2008.

[36] Gowind P. Agrawal. *Nonlinear Fiber Optics*. Academic Press, 2001.

[37] R. W. Boyd. *Nonlinear Optics*. Academic Press, 2008.

[38] G.D. Boyd and D.A. Kleinman. Parametric interaction of focused gaussian light beams. *Journal of Applied Physics*, 39, February 1968.

[39] Sze Y. Set, Hiroshi Yaguchi, Yuichi Tanaka, and Mark Jablonski. Laser mode locking using a saturable absorber incorporating carbon nanotubes. *Journal of Lightwave Technology*, 22:51 –, 2004.

[40] Fumio Shohda, Takafumi Shirato, Masataka Nakazawa, Junji Mata, and Jun Tsukamoto. 147 fs, 51 mhz soliton fiber laser at 1.56 m with a fiber-connector-type swnt/p3ht saturable absorber. *Optical Express*, 16:20943–20948, 2008.

[41] Stefan Mayerhofer. Development and characterization of an erbium-femtosecond-fiberlaser based on carbon nanotubes. Master's thesis, Hochschule für Angewandte Wissenschaften München, 2016.

[42] Analoge Devices. *Integer-N/Fractional-N PLL Synthesizer, ADF 4155*, 2014. Data Sheet.

[43] TIMETECH. *TimeTech, Phase Comparator, 6 channels, 100 MHz with 5/10 MHz Option, Part No: 10265*, copyright 03/2006, timetech gmbh, 25th mar 2006 edition, 2013.

[44] Thomas Unterholzer. Construction and verification of an adaptive frequency counter to measure the frequency stability for high-precision distance measurements for space applications. Bachelor thesis, Technische Universität München, September 2015. Fakultät für Elektrotechnik und Informationstechnik.

[45] Reinhard Lerch. *Eletkrische Messtechnik*. Springer Verlag, 2010.

[46] Andreas Fischer. Measurement setup for absolute and dynamic distance measuring with the fddm method. Masterthesis, Technische Universität München, February 2016.

[47] Martin Hutterer. Absolute distance measurement using a stabilized optical oscillator. Bachelor thesis, Hochschule München, January 2015.

[48] C. Koos, P. Vorreau, T. Vallaitis, P. Dumon, W. Bogaerts, R. Baets, B. Esembeson, I. Biaggio, T. Michinobu, F. Diederich, W. Freude, and J. Leuthold. All-optical high-speed signal processing with siliconorganic hybrid slot waveguides. *Nature Photonics*, 2009.

[49] Joohyung Lee, Young-Jin Kim, Keunwoo Lee, Sanghyun Lee, and Seung-Woo Kim. Time-of-flight measurement with femtosecond light pulses. *Nature Photonics*, August 2010.

[50] S. Lindner. Balanced optical cross correlation for distance measurement in space. Master's thesis, Technische Univeristät München, 2015.

[51] J. A. Armstrong. Measurement of picosecond laser pulse widths. *Applied Physics Letters*, 10, 1967.

[52] K. Predehl, G. Grosche, S. M. F. Raupach, S. Droste, O. Terra, J. Alnis, Th. Legero, T. W. Hnsch, Th. Udem, R. Holzwarth, and H. Schnatz. A 920-kilometer optical fiber link for frequency metrology at the 19th decimal place. *Science*, 336:441–444, April 2012.

[53] National Instruments. *NI 6009, Low-Cost, Bus-Powered Multifunction DAQ for USB, 12- or 14-Bit, Up to 48 kS/s, 8 Analog Inputs*.

[54] Agilent Technologies / Keysight Technologies. *Agilent 53200A Series RF/Universal Frequency Counter/Timers*, 5990-6283enen edition, 2013.

[55] N. Lagakos, J. A. Bucaro, and J. Jarzynski. Temperature-induced optical phase shifts in fibers. *Appl. Opt.*, 20:2305 – 2308, 1981.

[56] Technische Universität München. Optical clock technologies and their applications for globally optimized navigation 2, dlr fkz: 50 na 1525. Technical report, Forschungseinrichtung Satellitengeodäsie, 2016.

[57] E Samain, P Exertier, C Courde, P Fridelance, P Guillemot, M Laas-Bourez, and J.M. Torre. Time transfer by laser link: a complete analysis of the uncertainty budget. *Metrologia*, 52:423432, 2015.

[58] Falke St., Schanth H., Vellore Winfred J.S.R., Middelmann Th., Vogt St., Weyers S., Lipphardt B., Grosche G., Riehle F., Sterr U., and Lisdat Ch. The ^{87}sr optical frequency standard at ptb. *Metrologia*, 48:399 – 407, 2011.

[59] Franz Schwabl. *Quantenmechanik*. Springer, 2002.

[60] I. Bloch. *Licht-Atom Wechselwirkung im Zwei-Niveau System*. Universitt Mainz, Feb. 2004.

[61] Th. Udem, S. A. Diddams, K. R. Vogel, C. W. Oates, E. A. Curtis, W. D. Lee, W. M. Itano, R. E. Drullinger, J. C. Bergquist, and L. Hollberg. Absolute frequency measuremtns of the hg+ and ca optical clock transitions with a femtosecond laser. *Physical Review Letters*, 86, No.22:2, 2001.

[62] Puppe Thomas, Sell Alexander, Kliese Russell, Hoghooghi Nazanin, Zach Armin, and Kaenders Wilhelm. Characterization of a dfg comb showing quadratic scaling of the phase noise with frequency. *Optics Letters*, 41:1877–1880, 2016.

[63] Ruehl Axel, Marcinkevicius Andrius, Andrius Marcinkevicius M. E. F., Fermann Martin E., and Ingmar Hartl. 80 w, 120 fs yb-fiber frequency comb. *Optics Letters*, 35(18):3015 – 3017, September 2010.

[64] Matos L., Kleppner D., Kuzucu O., Schibli T. R., Kim J., Ippen E. P., and Kaertner F. X. Direct frequency comb generation from an octave-spanning, prismless ti:sapphire laser. *Optics Letters*, 29(14):1683 – 1685, July 2004.

[65] Analoge Devices. *ADIsimPLL Design Tool*, 2015. Software.

[66] Analoge Devices. *DC to 6 GHz Envelope and TruPwr RMS Detector*, rev. b edition, 2014.

[67] O. P. Lay, S. Dubovitsky, R. D. Peters, J. P. Burger, S.-W. Ahn, W. H. Steier, H. R. Fetterman, and Y. Chang. Mstar: a submicrometer absolute metrology system. *Optical Letters*, 28, No.11:3, 2003.

[68] B.P Abbot et al. Observation of gravitational waves from a binary black hole merger. *Physical Review Letters*, 116, February 2016.